

AN EXPERIMENTAL INVESTIGATION OF POINT
DEFECTS AND MOTION OF CHARGE IN

Al O , MgO, AND SrO
2 3

By

BRYCE TODD JEFFRIES

Bachelor of Science
Central State University
Edmond, Oklahoma
1977

Master of Science
Oklahoma State University
Stillwater, Oklahoma
1979

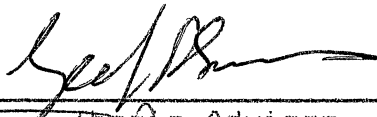
Submitted to the Faculty of the Graduate
College of the Oklahoma State
University in partial fulfillment
of the requirements for
the Degree of
DOCTOR OF PHILOSOPHY
July, 1985


Thesis
19850
J47e
cop. 2





AN EXPERIMENTAL STUDY OF THE ELECTRONIC
STRUCTURE OF DEFECTS AND MOTION OF
CHARGE IN Al_2O_3 , MgO , AND SrO
2 3

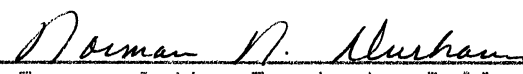
Thesis Approved:



Thesis Adviser








Dean of the Graduate College

TO
MY GOD

ACKNOWLEDGEMENTS

The author wishes to express his appreciation to his major adviser, Dr. Geoffrey P. Summers, for his guidance and help in completing this thesis. Thanks is also given to the doctoral committee.

Thanks are given to the Physics Faculty for their friendship and the many things taught to me.

Thanks is given to Pradip, Kish, and Joel for their friendship.

Special thanks is given to Linda, my wife, and to my children.

My best thanks are given to God who continually shows His love for me.

Finally appreciation is given to the Department of Energy, Oklahoma State University, and Conoco for the financial support provided.

TABLE OF CONTENTS

Chapter	Page
I. INTRODUCTION.	1
Introduction	1
Sapphire	1
MgO.	7
Statement of the Problem	9
II. THEORY.	11
Introduction	11
Optical Density.	11
Photoluminescence.	12
Photoconductivity.	17
Thermoluminescence	21
Fluorescence	23
MgO Theory	24
Sapphire Theory.	28
III. EXPERIMENTAL PROCEDURE.	29
Introduction	29
Sample Preparation	29
Optical Density.	31
Thermoluminescence	31
Photoconductivity.	33
Photoluminescence.	37
Excitation	39
IV. SAPPHIRE EXPERIMENTAL RESULTS AND DISCUSSION. . .	41
Introduction	41
Optical Density.	41
Photoluminescence.	47
Photoconductivity.	60
Thermoluminescence	77
Fluorescence	92
Analysis and Discussion.	94
V. MgO EXPERIMENTAL RESULTS AND DISCUSSION.	102
Introduction	102
Thermoluminescence	104
Luminescence Decay	107

Chapter	Page
Photoluminescence.	110
Excitation	132
Photoconductivity.	146
Analysis and Discussion.	157
BIBLIOGRAPHY	164
APPENDIX - SrO	166

LIST OF TABLES

Table		Page
I.	Moment Analysis of the Band Shape Function for the 3.0 eV Emission Band	54
II.	Temperature Dependent Moment Analysis.	57
III.	Characteristics of Thermochemically Colored MgO Samples.	103

LIST OF FIGURES

Figure	Page
1. Sapphire Structure.	2
2. Sapphire Oxygen Vacancy	4
3. F Center Model.	6
4. MgO Structure	8
5. Configuration Coordinate Diagram.	13
6. F Center Radial Charge Density.	26
7. MgO F Center CCD.	27
8. Thermoluminescence Apparatus.	32
9. Photoconductivity Apparatus	34
10. Sample Holder	35
11. Excitation System Spectrum.	36
12. Photoluminescence Apparatus	38
13. Excitation Apparatus.	40
14. Linde Optical Density	42
15. INSACO Optical Density.	44
16. CS Optical Density.	45
17. AM Optical Density.	46
18. Absorption Gaussian Curve Comparison.	48
19. CS Emission	49
20. Type I Emission	50
21. Emission Gaussian Comparison.	52
22. Bandwidth Temperature Dependence.	53

Figure	Page
23. Emission Shape Funtion.	56
24. Type I First Moment Variation	58
25. Photocurrent vs Electric Field.	61
26. Photocurrent vs Light Intensity	62
27. INSACO PC at 6 K.	63
28. INSACO PC at 77 K	64
29. INSACO PC at Room Temperature	65
30. AM PC at 77 K	66
31. AM PC at Room Temperature	67
32. CS PC at 77 K	68
33. CS PC at Room Temperature	69
34. CS PC at 77 K	71
35. CS PC at Room Temperature	72
36. Photoconductivity vs Optical Density.	73
37. Relative Temperature Dependent PC	75
38. Neutron Irradiation Temperature Dependent PC.	76
39. Thermoluminescence.	78
40. Leading Edge Plot	79
41. Leading Edge Plot	80
42. Type II TL Emission Spectrum.	81
43. Type I TL Emission Spectrum	82
44. Type I TL Peak.	84
45. Linde TL Peaks vs Bleaching	85
46. Linde TL Peaks vs Gamma Irradiation	86
47. Linde TL vs Anneal.	87
48. Linde Optical Density vs Anneal	88

Figure	Page
49. Linde Anneal Comparison	89
50. Linde TL vs Neutron Irradiation	91
51. Concentration Quenched Anneal Study	93
52. F center Model.	101
53. Thermoluminescence Peaks.	105
54. Thermoluminescence Peaks.	106
55. Thermoluminescence Peaks.	108
56. Luminescence Decay.	109
57. Second Order Lifetime, MgO 1.	111
58. Second Order Lifetime, MgO 2.	112
59. Second Order Lifetime, MgO 3.	113
60. Second Order Lifetime, MgO 6.	114
61. First Order Lifetime, MgO 1	115
62. First Order Lifetime, MgO 2	116
63. First Order Lifetime, MgO 3	117
64. First Order Lifetime, MgO 6	118
65. Temperature Dependent Photoluminescence MgO 1	120
66. Temperature Dependent Photoluminescence MgO 3	121
67. Temperature Dependent Photoluminescence MgO 6	122
68. Temperature Dependent Photoluminescence MgO 2	125
69. Temperature Dependent Photoluminescence MgO 2	126
70. MgO 2, F center Longlived Emission.	128
71. MgO 2, F+ side, Temperature Dependence.	129
72. MgO 5, Temperature Dependent Emission	130
73. MgO 5, Temperature Dependent Bleaching.	131
74. MgO 3, Temperature Dependent Bleaching.	133

Figure	Page
75. Temperature Dependent Photoluminescence, MgO 8. . .	134
76. MgO 1, Excitation Spectrum.	135
77. MgO 1, Fast Component Excitation Spectrum	137
78. MgO 1, F and F+ Fast Component Excitation	138
79. MgO 2, F+ Side Fast Component Excitation.	139
80. MgO 2, F Side Fast Component Excitation	141
81. MgO 3 Total Excitation Spectrum	142
82. MgO 3 Total Fast Component Excitation	143
83. MgO 5 Fast Component Excitation	144
84. MgO 7 Fast Component Excitation	145
85. Temperature Dependent Photoresponce, MgO 7.	147
86. MgO 7 5.0 eV Photoresponce Bleach	149
87. MgO 7 Bleached Component.	150
88. Dark Current, MgO 7	151
89. Dark Current Lifetime Plot.	153
90. Mgo 8, Temperature Dependent Photoresponce.	154
91. MgO 8, Temperature Dependent Peak Height.	155
92. MgO 8, Temperature Dependent Height, No Bleaching .	156
93. Model of F center and H ⁻ ion Interaction.	161
94. SrO TL Peak Spectral Dependence	167

CHAPTER I

INTRODUCTION

Introduction

The properties of color centers in single crystal insulators have been of interest to investigators for several decades. The crystals investigated in this work are the oxides Al_2O_3 , MgO , and SrO . The first two are studied in the main body of the dissertation and the third is studied in the appendix.

The color centers which are of interest in this dissertation are due to oxygen vacancies. An F type center results when one or two electrons are trapped at an oxygen vacancy forming an F^+ or F^- center respectively. An H^- ion can also be trapped in an oxygen vacancy. This effect is looked at along with F type centers in this study.

Sapphire

The crystalline form of sapphire, i.e. Al_2O_3 , is shown in Figure 1. Its crystal structure is rhombohedral but it is indexed on its hexagonal axis. It has a C_{3v} symmetry about this axis. In the figure the two triangles of oxygen ions are rotated 60 degrees with respect to one another. The aluminum atom is not equidistant between the two planes

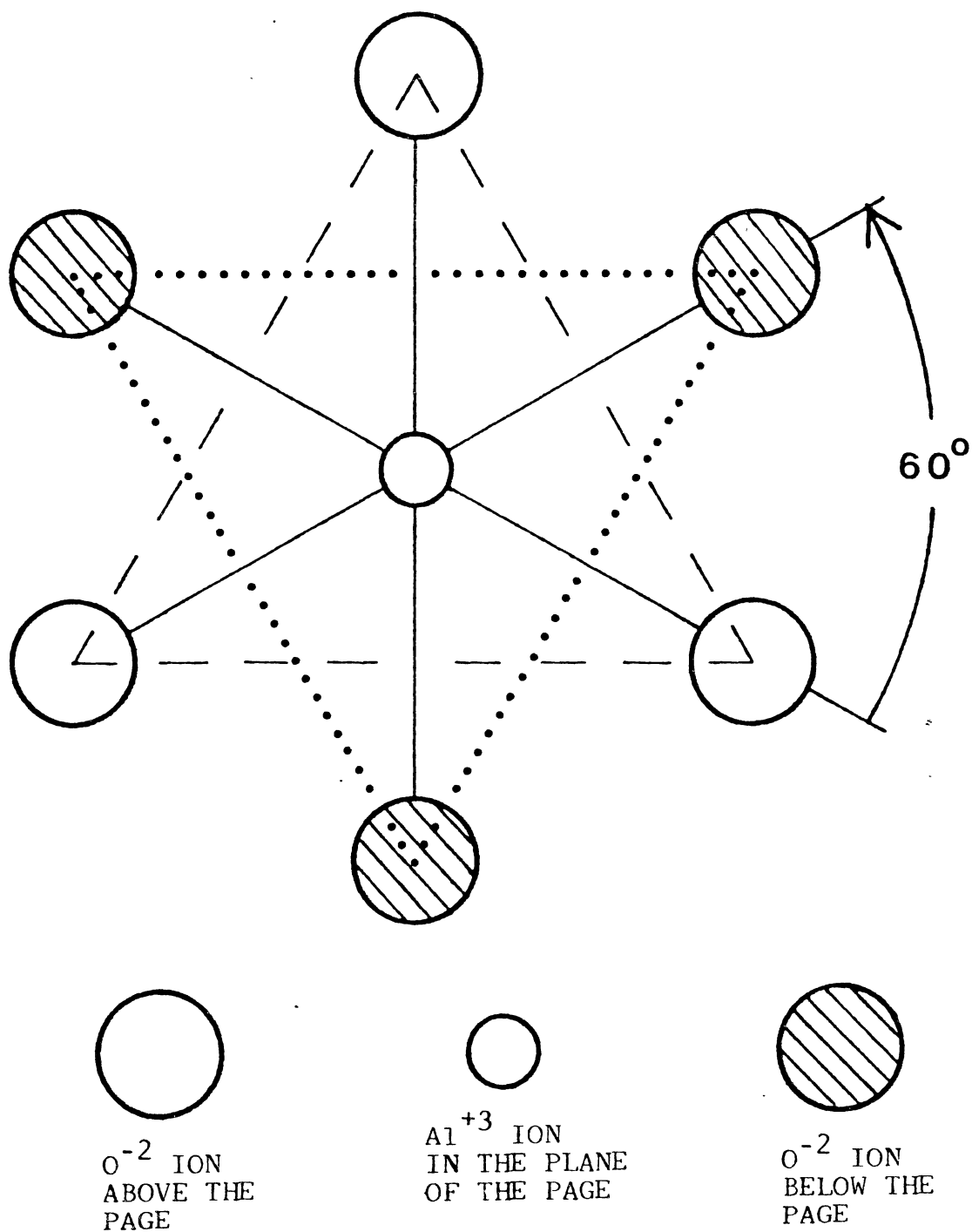


Figure 1. Sapphire Structure. Threefold Axis of Rotation

Source: Brewer (26)

of oxygen atoms. The C_2 site symmetry of an F type center is shown in Figure 2. The C_2 axis of the vacancy is perpendicular to the C_2 axis of the crystal.

Identification of the F type center in Al_2O_3 has been difficult because no satisfactory ESR identification has been made. Thus identification has come from comparing the experimental results with similar experiments on the alkaline earth oxides.

Arnold and Compton (1) showed that irradiation with electrons would produce a 6.1 eV absorption band in Al_2O_3 . The primary cause of the absorption band was shown to be oxygen vacancies by a set of experiments performed by Pells (2). They used H^+ , N^+ , and O^+ ions, and neutron particle irradiation to attempt to produce the 6.1 eV absorption band. All of the particles produced the absorption band except for the oxygen ions. This implied that the 6.1 eV absorption band is due to an oxygen vacancy.

Turner and Crawford (3) gamma irradiated an Al_2O_3 crystal and found absorption bands at 3.02 and 5.46 eV and an OH absorption band at 3316 cm^{-1} . The second band was found to be due to Cr^{+2} ions and the 3.02 band was thought to be due to a composite V center. They bleached into the 3.02 eV band and the 6.1 eV band was reduced appreciably. This implied that the 6.1 eV band was due to an electron trapping defect (4).

Thus the implication is that the 6.1 eV band is an F type center. Lee and Crawford (5) bleached into the 6.1 eV

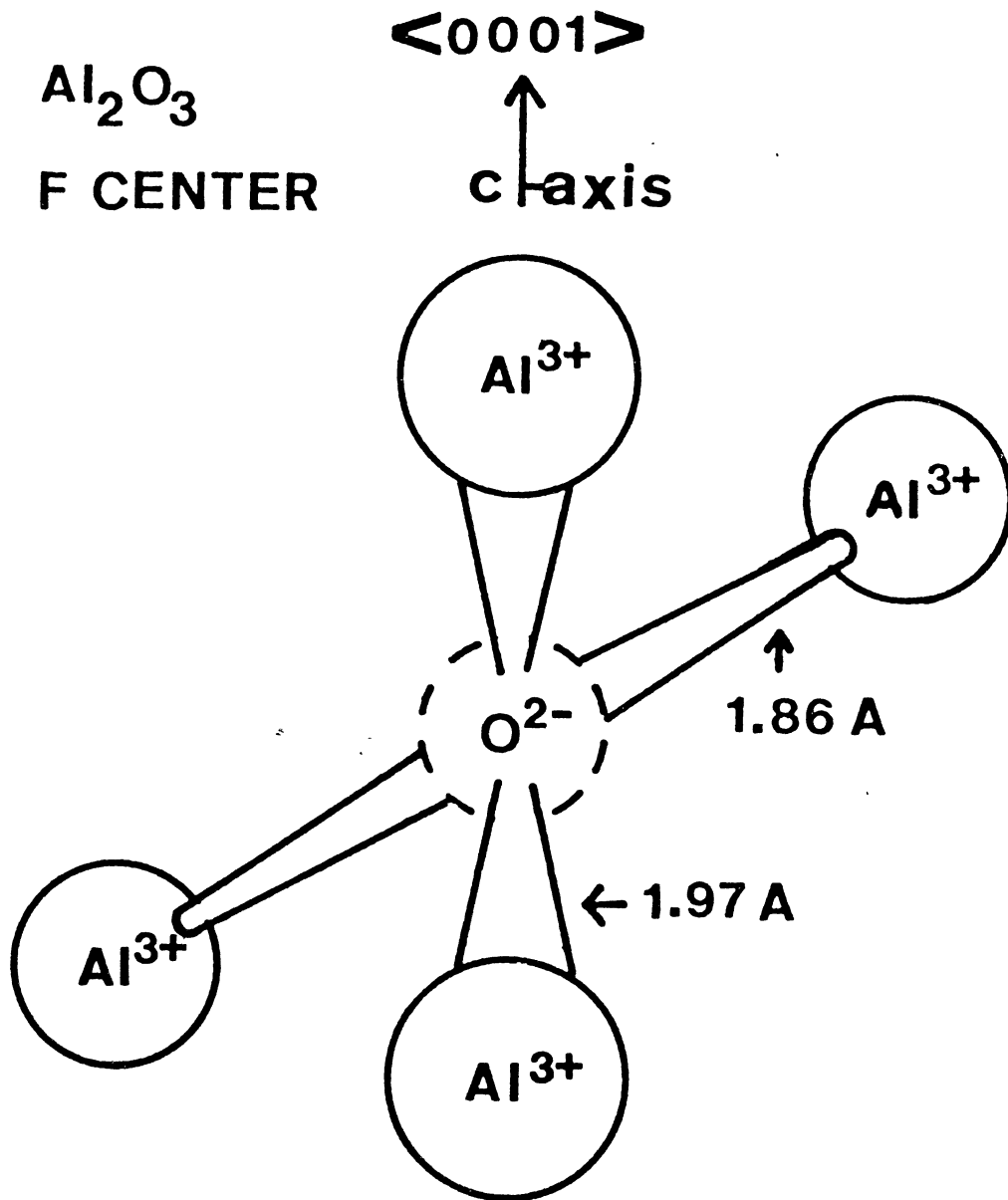


Figure 2. Sapphire Oxygen Vacancy. C Axis
of Rotation 2

Source: Brewer (26)

band and increased the absorption of the 4.8 and 5.4 eV bands in their crystals. This also increased the emission band at 3.8 eV. This implied that the 6.1 eV band is the F center absorption band, and that the 4.8 and 5.4 eV absorption bands belong to the F⁺ center with its emission being at 3.8 eV.

Draeger and Summers (6) observed a 3.0 eV emission band associated with the 6.1 eV absorption band and showed that the shape of the 3.0 eV emission band's excitation spectrum was similar to that of the 6.1 eV absorption band's.

La et al. (7) used a point ion model to calculate the energy levels of the Al₂O₃ F⁺ center. Their calculations showed an excitation from a 1A to a ¹p-like state. The state was split into three levels with 1A, 2B, and 2B characteristics. Evans and Stapelbroek (8) experimentally found the transition energies to be 4.8 eV for the 1A to 1B transition, 5.4 eV for the 1A to 2A transition, and 6.3 eV for the 1A to 2B transition. The emission was found to have a 1B to 1A transition at 3.8 eV. In a different experiment phosphorescence was detected in the emission near room temperature by Lehmann and Gunthard (9).

Brewer et al. (10) measured a two component luminescence below 55 K in the 3.0 eV emission band. They suggested emission for the F center occurs from a ³p-like state. The crystal symmetry splits this state into three components. This is shown in Figure 3 along with the associated energy spacings between the different states. They also noticed

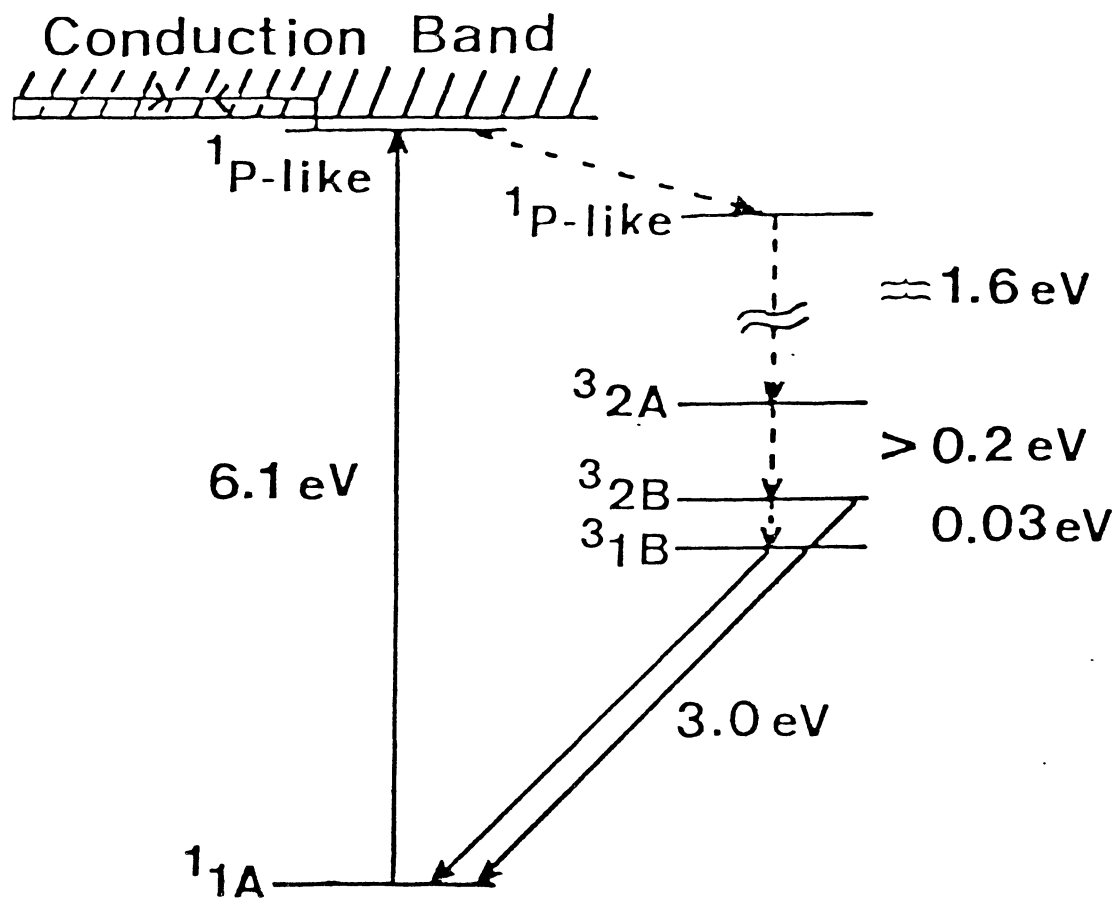


Figure 3. F Center Model. F Center in Al_2O_3

Source: Brewer (26)

a phosphorescence near room temperature and measured its thermal activation energy to be 0.72 eV.

MgO

The lattice structure common to the alkaline earth oxides is shown in Figure 4. The structure is face centered cubic and exhibits O_h symmetry. The identification of the F⁺ center was made by Henderson and King (11). They identified the F⁺ center EPR signal correlated with the optical absorption band near 5.0 eV in a neutron irradiated crystal. The 5.0 eV absorption peak was also observed by Chen et al. (12) but they did not see the EPR signal correlation. The crystals they used had been either additively colored or electron irradiated.

Wertz et al. (13) looked at the regeneration of the F⁺ center in additively colored MgO using ionizing radiation. Their work implied that both the F and F⁺ absorption occurs near 5.0 eV.

Two things have clouded the identification of the 2.3 eV emission band as belonging to the F center in MgO. The first is the presence of a long lived phosphorescence near room temperature which was first observed by Hughes and Henderson (14). This phosphorescence can have a lifetime ranging from less than a second to many seconds.

The second issue is that a model consistent with experimental evidence describing the F center had not been found previous to the recent work by Summers et al. (15).

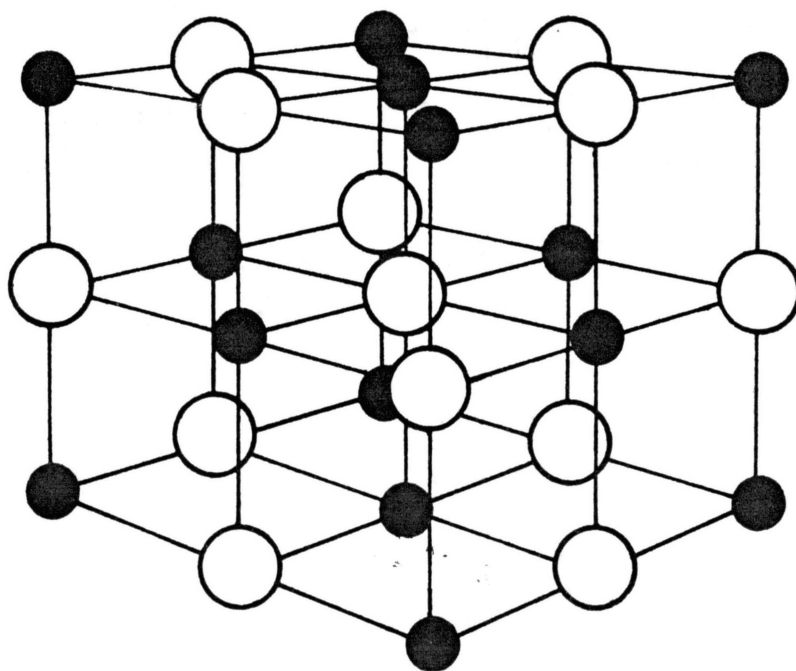


Figure 4. MgO Structure. Face Centered Structure

Previously Wilson and Wood (16) proposed a model based on the results for CaO. The emission occurred from an excited ${}^3T_{1u}$ to a ${}^1A_{1g}$ ground state. Since the states were loosely coupled to the lattice vibrations, vibronic structure on the emission band was expected along with a lifetime of several milliseconds. These characteristics were not present in the F center. Edel et al. (17) used ODMR techniques to show that the excited state in emission is not predominantly a triplet as suggested. They proposed a model where the phosphorescence is dependent upon the concentration of F centers which can interact with each other by exchanging an electron and producing an $F^+ F^-$ pair.

Recent infrared absorption experiments by Gonzales et al. (18) measured sharp absorption lines in MgO, CaO, and SrO which they suggest are the local modes of oscillation of H^- ions substituted into oxygen vacancies.

Recently, Summers et al. (15) have proposed a model which gives an emission transition from a ${}^1T_{1u}$ to a ${}^1A_{1g}$ state. This model predicts a short lifetime but predicts a much stronger coupling between the relaxed excited electronic state and the lattice vibrations.

Statement of the Problem

The above discussion concerning $Al^{2+}O^{2-}$ showed a lack of basic experimental and theoretical knowledge about the F center. Using the experimental techniques discussed in Chapter III, the following properties of the F center will

be looked at. The effect of and the identification of the electron traps active from 77 K to 300 K will be looked at. The relaxed excited state and its closeness to the conduction band will be looked at. A simple theoretical model will be used to measure the basic properties of the F center and relate the data to the model proposed by Brewer. And, the spatial extent of the relaxed excited state will be qualitatively looked at using the thermal bleaching of a crystal where concentration quenching is present. Also the interconversion between the F and F⁺ centers will be measured.

In MgO, the concentration of H⁻ ions present in the crystals will be related to the experimental results to help identify the cause of the 2.3 eV emission band, to determine the properties of the electronic structure of the F center, and to look at how the measureable quantities vary as the H⁻ ion concentration varies. Since the concentration of F and F⁺ centers will vary different inherent properties of each can be looked at.

CHAPTER II

THEORY

Introduction

The theory pertinent to the different experimental studies described in this dissertation is given in this chapter. The different experimental phenomena looked at were optical density, photoluminescence, photoconductivity, thermoluminescence, and fluorescence lifetime. Also, recent theoretical work on the F center in MgO, and the F and F⁺ centers in Al₂O₃ are reviewed.

Optical Density

The optical density of a material is defined by the relation,

$$OD = \log_{10} \frac{I_0}{I}$$

where

I_0 is the intensity of the incident light and

I is the transmitted light intensity.

The intensity of the transmitted light is given as,

$$I = I_0 \text{EXP}(-\alpha d)$$

where

α is the absorption coefficient, and

d is the crystal thickness.

combining these relationships gives

$$\alpha = 2.303 \left(\frac{OD}{d} \right)^{-1} \text{ cm}^{-1}$$

Photoluminescence

The configuration coordinate diagram (CCD) shown in Figure 5 allows the qualitative determination of several of the properties of F centers. Assuming the Franck-Condon principle applies, the Stokes shift and the absorption and emission band widths may be qualitatively obtained. The Franck-Condon principle assumes that the average separation of the ions does not change during transition of the system from one state to another. The Born-Oppenheimer assumption is also used in this model. This assumption states that the nuclear and electronic motion can be treated independent of each other. It also allows the separate calculation of the total system energy for the ground state and the excited state and for the discrete quantum vibrational states characteristic of each. With linear coupling between the electronic and phonon states, the parabolic curves representing the ground and excited states show the total energy for both the electronic and lattice energy. The curves are labeled with m and k corresponding to the electronic states and the horizontal lines represent the different electronic and vibrational energies of the total system. The most

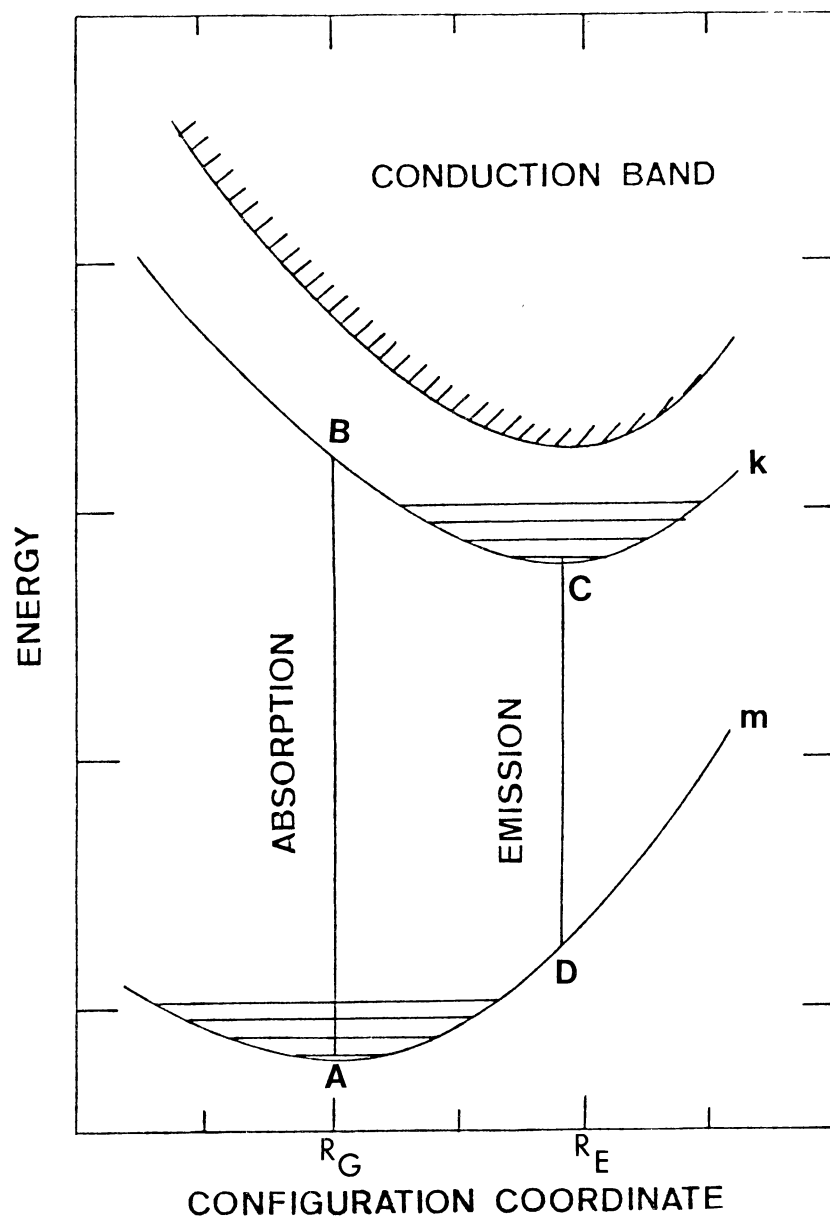


Figure 5. Configuration Coordinate Diagram

probable energy for absorption is E_{AB} and for emission is E_{CD} which occurs at configuration coordinate R equal to R_G and R_C respectively. The Stokes shift energy is defined as $E_{AB} - E_{CD}$. The F center states as shown in this diagram are assumed to be predominantly linked to one dominant mode of vibration of the crystal, for example the breathing mode of the centers nearest neighbor ions surrounding the defect.

The CCD can be used to describe semiclassically the broad-band characteristics of color centers (19). Two of these values are the oscillator strength, f , and Smakula's equation which are calculated to be,

$$f_{mk} = \frac{2m}{3h} \frac{|\bar{r}_{mk}|^2}{(\bar{R}_o)^2}, \text{ and} \quad (2.1)$$

$$N f_{A mk} = \frac{nmc}{2\pi e h} \left[\frac{E_o}{E_{eff}} \right]^2 \int u_{mk}(E) dE, \quad (2.2)$$

where r_{mk} is the electric dipole matrix element and u_{mk} is the generalized absorption coefficient. For a Gaussian bandshape Smakula's equation is written as

$$N f_{A mk} = 0.87 \times 10^{17} \frac{\text{cm}^{-3}}{(n+2)^2} \frac{n}{u_{mk}(\text{max})W_{mk}},$$

where W is the full width at half maximum, and n is the index of refraction at the peak energy.

In order to consider the F center emission line shape in detail the problem must be treated quantum mechanically. The following brief discussion outlines the calculation (20). Two nondegenerate electron states are used and

assumed to be linearly coupled to a normal coordinate, q , of the lattice. The Franck-Condon principle and the Born-Oppenheimer approximation are assumed. The resulting two potentials describing the electronic states are,

$$E_a = 0.5 M \omega^2 q^2, \text{ and}$$

$$E_b = 0.5 M \omega^2 q^2 + E_{ab} - A \hbar \omega (M \omega / \hbar)^{0.5} q.$$

A is a dimensionless constant which is a measure of the strength of the linear electron-lattice interaction. It is also a measure of the change in the equilibrium position of the vibrational mode after a transition occurs. The linear coupling results in ω (1) being the same for each state, and (2) the states having the same curvature. M is the effective mass and E_{ab} is the energy separation between the two states at q equal to zero. The quantum mechanical solutions for the lattice are harmonic oscillator wave functions.

The probability for an optical transition is proportional to the square of the electric dipole matrix element. This matrix element can be factored using the Born-Oppenheimer approximation, into two parts with the first being the dipole matrix element involving the electronic wave functions and the second being the vibrational overlap integral which then determines the optical line shape associated with the transition.

Letting $S = A^2 / 2$ gives the normalized transition prob-

ability as

$$W_{nm} = e^{-S} \frac{m!}{n!} S^{n-m} \left[\frac{L_{n-m}(S)}{L_n(S)} \right]^2,$$

where L is the Laguerre polynomial.

At $T = 0$ K, this reduces to

$$W_{n0} = \frac{S^n}{n!} e^{-S}.$$

If this model is extended to consider weak linear coupling to many modes, the line shape is the same. The normalized transition probability, or line shape, can be analyzed by computing its moments. For experimental data this is done as follows.

The emission of the crystal was calculated in watts/second over the energy range of the band. This intensity can then be written as

$$I = NEA$$

where N is the number of centers, E is the energy, and A is the Einstein coefficient for spontaneous emission. A can be written as

$$A = K E^3 g(E)$$

where K is a proportionality constant and $g(E)$ is called the shape function which in its normalized form can be then be written as

$$g(E) = I/E^4. \quad (2.3)$$

The moment analysis is then performed using $g(E)$. The zeroth moment is used to normalize the other moments. The

first moment about the centroid gives the mean value of the energy. The smallness of the first moment about the centroid shows the symmetry of the curve. The second moment about the centroid is used to calculate the Huang-Rhys factor, S , using the formula

$$S = \frac{\langle E^2 \rangle - \langle E \rangle^2}{(\hbar\omega)^2}.$$

The value for $\hbar\omega$ is obtained by plotting the half width energy, W , for the shape function as a function of the temperature. This is curve fitted to the equation which is valid for linear coupling;

$$W(T) = W(0) \coth(\hbar\omega/2kT). \quad (2.4)$$

The Stokes shift is then calculated from the relation

$$E = \hbar\omega(2S-1). \quad (2.5)$$

Photoconductivity

The electron in the relaxed excited state of an F center can be moved either optically or by phonons to a different energy level or to the conduction band. Associated with each of these processes is a probability per second which is the inverse of its lifetime. These probabilities per second can be combined in the relation (21)

$$\frac{1}{\tau} = \frac{1}{\tau_R} + \frac{1}{\tau_I} + \frac{1}{\tau_Q} \quad (2.6)$$

where τ is the total lifetime, τ_R is the radiative emission

lifetime, τ_I is the lifetime for thermal ionization, and τ_Q is the combined lifetime for all other processes. The probability per second for thermal ionization can be written as

$$\frac{1}{\tau_I} = \frac{1}{\tau_Q} \text{EXP}(-E/kT)$$

where $1/\tau_Q$ is the pre-exponential factor and E is the thermal energy for excitation into the conduction band. The quantum efficiency, n_I , of thermally exciting electrons into the conduction band is the probability of excitation divided by the total probability. If τ_Q is ignored this can be written as

$$n_I = \frac{1/\tau_I}{1/\tau_Q + (\tau_I/\tau_R) \text{EXP}(E/kT)} = \frac{1}{1 + (\tau_I/\tau_R) \text{EXP}(E/kT)} \quad (2.7)$$

This equation can be curve fitted to data which exhibits an increase in the quantum efficiency as the temperature is increased.

Photoconductivity in insulating crystals can be studied by looking at the photon or thermally induced transient currents. In the treatment of photoconductivity below several assumptions are made. Only electrons are considered. Only one type of electron producing defect is assumed. Only one type of trapping mechanism is assumed present in the crystal. All of the electrons travel the same same distance before becoming trapped. No charge enters or leaves the crystal through the electrodes. The

model also assumes the traps are uniformly distributed and that when a trap is encountered the electron is trapped. This model is simple but gives good qualitative results in many cases. In this model (22), a crystal of thickness d is placed between plane parallel conducting electrodes. A battery of voltage V and an electrometer are connected in series with the electrodes. In the geometry used in our experiments, the exciting light passes through one of the electrodes.

At time $t=0$ a pulse of light induces c_0 electrons into the conduction band and at time $t=t$ the number remaining is

$$c = c_0 \exp(-t/T)$$

where T is defined as the mean trapping time and is given by

$$T = 1/(D_{\text{av}} v_t)$$

D is the trap density. a is the trap cross sectional area. And, v is the mean thermal velocity of the electrons.

The average range of an electron in the crystal is given by

$$w = uET = Ew_0$$

where u is defined as the electron mobility with the units of velocity per unit applied electric field. w_0 is then the mean range per unit field. Using the relationship

$$t = x/uE$$

the number of electrons free after traveling a distance x in time t is

$$c = c_0 \exp(-x/w_0)$$

and the charge per electron is

$$q = ex/d.$$

With α being the absorption coefficient of the crystal and R being the reflectivity, the number of photons, N , at a depth x in the crystal is given by

$$N = N_0 (1-R) \exp(-\alpha x).$$

Differentiation of this gives the number of photons absorbed from x to $x+dx$ as

$$dN = -\alpha N (1-R) \exp(-\alpha x) dx.$$

The quantum efficiency of this process is the number of electrons released into the conduction band in the interval from x to $x+dx$ divided by the number of photons absorbed.

The number of electrons released over this interval is

$$dc = \alpha n N (1-R) \exp(-\alpha x) dx.$$

Integrating this over the thickness of the crystal gives the number of electrons released as

$$c = n N_0 (1-R) (1 - \exp(-\alpha d)).$$

The amount of charge detected can be written as

$$Q = ex \int_0^d \frac{dc}{d} = ex \psi ,$$

where ψ is defined as the saturation factor and x as the average displacement of the electron.

The saturation factor is calculated over the thickness of the crystal and it includes the electron displacement for both those trapped in the crystal and those stopped at the surface of the anode. With the light passing through the

cathode first and assuming that the average range of the electron is much smaller than the thickness of the crystal, the saturation factor is given by

$$\Psi = w/d.$$

Letting N become the number of photons per unit time incident upon the crystal allows the detected current in the crystal to be written as

$$I = e n N (1-R) (1-EXP(-\alpha d)) (w/d)$$

or as

$$I = e n' N (w/d)$$

with

$$n' = n(1-R)(1-EXP(-\alpha d)).$$

Using $w = w E = w V/d$ the above equation can be written in its familiar form as

$$n' w = \frac{I d^2}{N e V} \quad (2.8)$$

In this form all of the measureable quantities are on the right hand side. On the left hand side are n' the quantum efficiency per incident photon per given photon energy, and w the mean range of an electron per unit applied electric field.

Thermoluminescence

In the physical processes considered in this study, thermoluminescence is the phenomenon where electrons are

released thermally from a trap and are then trapped by an F^+ center thus forming an excited F center. The emitted light comes from F centers. The actual process is not usually simple because, for example, other traps may be involved, other means of the electron's reaching the ground state may exist, or retrapping may occur. Two equations can describe the TL seen in this study. The first shows the intensity of the light emitted from the F centers as a function of time and the second shows the intensity of the light as a function of temperature at the initial start of a peak. The second equation allows the calculation of the thermal depth of the trap.

The time rate of change of the number of electrons depends upon several temperature dependent parameters. These parameters are the concentration of electrons present, n , the concentration of F centers present, N , the average electron velocity, v , and the cross sectional area of the traps, a . This relationship can be written as

$$\frac{dn}{dt} = -nNva$$

or as

$$n = n_0 \exp(-Nvat),$$

where n_0 is the temperature dependent number of electrons present at the initial time t . The emission intensity, I , is proportional to the time dependent number of electrons. This relationship can be written as

$$I = K \frac{dn}{dt}$$

where K is a proportionality constant.

At the initial start of a TL peak, the following relationship for the intensity of light emitted can be written assuming the time rate of change of the temperature is held constant.

$$I = I_0 \exp(-E/kT) \quad (2.9)$$

where E is the thermal activation energy of the trap freeing the electrons.

Fluorescence

The fluorescence decay seen in the following experiments was composed of a first order part and a long lived second order part. The first order part can be written as

$$\frac{dI}{dt} = -k_1 I$$

which can be rewritten as

$$I = I_0 \exp(-k_1 t) \quad (2.10)$$

where $1/k_1$ is the characteristic lifetime and I_0 is the initial fluorescence intensity.

The second order part of the fluorescence decay can be written as

$$\frac{dI}{dt} = -k_2 I^2$$

This can be integrated to give

$$I^{-1/2} - I_0^{-1/2} = k \frac{t}{2} \quad (2.11)$$

where $1/k$ can be treated as the characteristic lifetime here also.

The fluorescence decay process described by the above equations is complex. Re-trapping of the electrons released from their traps is one possible explanation for the effect seen. A simple energy level diagram rate type calculation does not produce the desired equations either. The treatment of the kinetics of diffusion-limited reactions as set forth by Waite (11) was looked at also, but a different form of the equation was obtained.

MgO Theory

Following is an overview of the theoretical model for MgO presented by G.P. Summers et al. (15). Previous theoretical work (16) had been based on the work done on CaO where emission of the F center occurred from a T_{1u}^3 state which was loosely coupled to the lattice. In analogy to CaO , MgO was expected to show vibronic structure and have a lifetime on the order of milliseconds. Optically detected magnetic resonance experiments had shown that the emitting state was not a triplet (17, 23) and lifetime measurements showed the lifetime could vary from fractions of a second to many seconds over the whole temperature range below room temperature. Work contained in this dissertation shows this lifetime variation is directly linked to the concentration

of H^- ions located at oxygen vacancies in the crystal.

The electron detail is treated with a Hartree-Fock type approximation near the defect and by an effective mass approximation in the region away from the defect. The two-electron Hamiltonian also treats the effects of dielectric polarization and neglects lattice relaxation. One electron Slater-type orbitals that have been Schmidt orthogonalized to the one electron orbitals on the surrounding Mg^{2+} 1NN ions are used for the one electron orbitals in the two electron wave function.

The total system energy for the configuration coordinate diagram was calculated using the above for the electronic energy and classical ionic theory for the lattice relaxation energy. It was found that in the electronic structure calculations, the first order correction to the Toyozawa-Haken-Schottky expressions for the interaction between the electron and the hole via the electronic polarization field were needed.

The resulting radial charge density of the electron orbitals for the ground state and the predominant excited state are shown in Figure 6. An electron in the A_{1g} ground state is localized within the vacancy region while an electron in the T_{1u} excited state can average 40 NN from the vacancy. Figure 7 shows the configuration coordinate diagram for the F center. The relaxation parameter was calculated for the outward A_{1g} relaxation of the 1 NN Mg^{2+} ions. The model predicts a 2.2 eV luminescence band with a

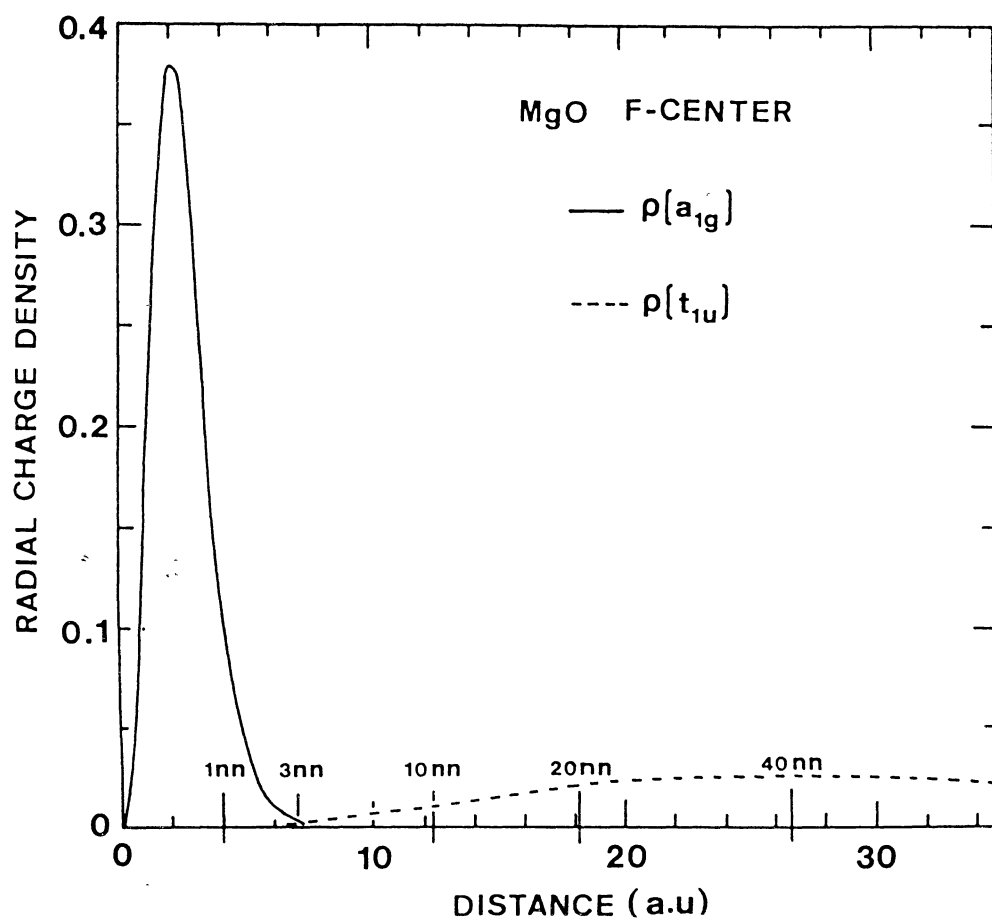


Figure 6. F Center Radial Charge Density

Source: Summers et al. (15)

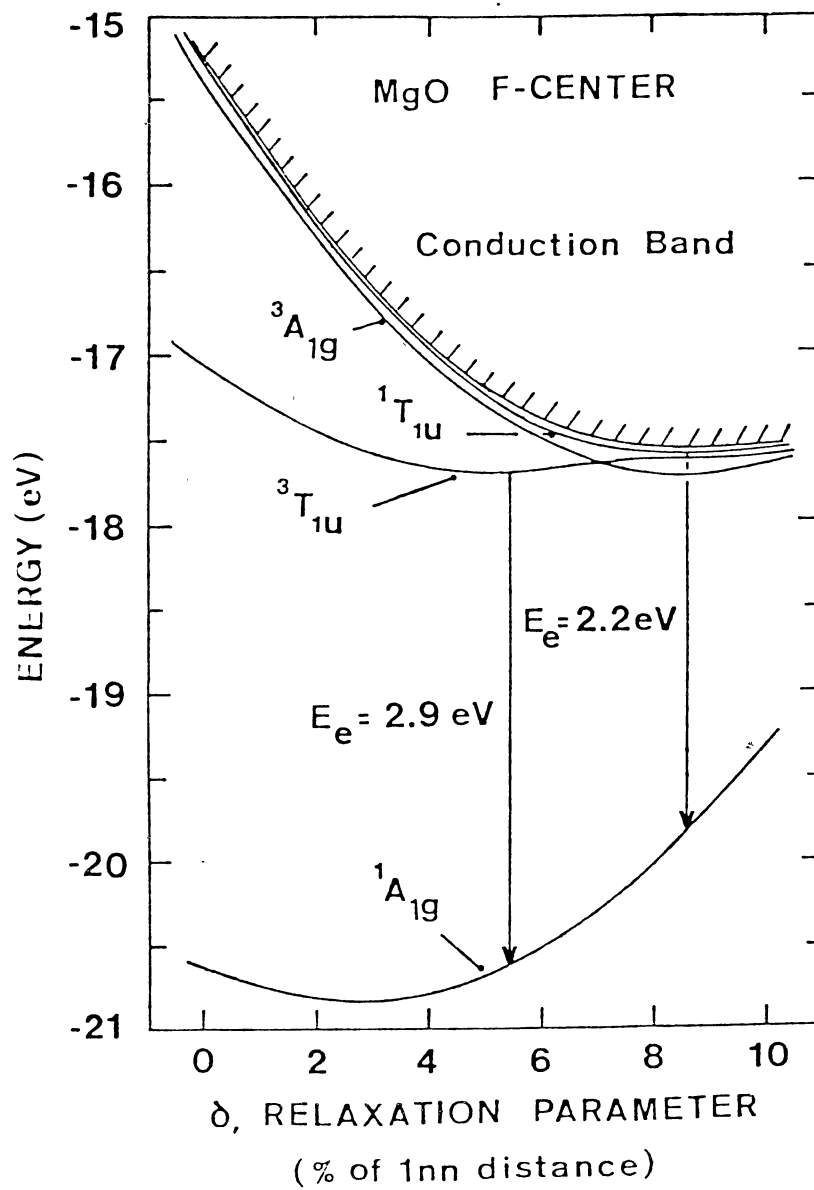


Figure 7. MgO F Center CCD

Source: Summers et al. (15)

0.60 eV half width from a T_{1u}^1 to a A_{1g}^1 state transition. This is an allowed transition and should have a relatively short lifetime.

Sapphire Theory

In a recent analysis of Al_2O_3 experimental results by Choi and Takeuchi (24) a semiempirical model of the electronic processes in F and F⁺ centers was formed.

Their conclusions are as follows. The ground state of the F center is approximately 6.5 eV below the conduction band because of the 6.1 eV absorption which can autoionize and the approximate 1.0 eV bandwidth. They also conclude that the thermal ionization of the F center is greater than 5.5 eV. They conclude that since no F⁺ center photoconductivity has been measured its optical ionization is greater than 6 eV. This is contrary to what should happen since the ionization of the F⁺ center should be reduced not increased.

They propose that removing an electron from the F⁺ center does not result in a bare vacancy. Their calculations show that the F⁺ center consists of a doubly charged deep trap which lies in the valence band in a resonance state. An energy level lies a few electron volts into the gap between the valence and conduction bands and a hole is trapped in the valence band. Excitation of an electron into the mentioned energy level results in two holes being trapped. The F center is reformed when a hole is removed from the center.

CHAPTER III

EXPERIMENTAL PROCEDURE

Introduction

The following information gives the experimental procedure followed in gathering data. Also included is information on the crystals used in these experiments.

Sample Preparation

The aluminum oxide, or sapphire, crystals used in these experiments were obtained from the following companies; INSACO, Crystal Systems, Adolph Meller, and Linde. They were all pure single crystals with very few impurities. They showed to a differing degree the 6.1 eV absorption band except for some of the samples from Linde. The lack of other absorption bands concurred with the analysis which showed that the concentration of most impurity ions were less than 10 ppm. The main impurities were Fe, Cr, V, and Mn ions. The CS samples were grown using the Schmidt-Viechnichi technique, the IN and AM crystals were grown using an adaptation of a Bridgman furnace, and the Linde samples were grown using the Czochralski technique. These techniques grow the crystals in a reducing atmosphere which produces high purity single crystals but also have a

tendency to grow defects into the crystal. The samples were all approximately one mm thick. The C axis of the crystals were all oriented parallel to the surface along the largest dimension except for one CS crystal which had its C axis perpendicular to the largest surface. Except for the crystals which had been irradiated, they were heated to approximately 770 K before each experiment to establish equilibrium and then quenched to room temperature by placing them on an aluminum slab. The neutron irradiated crystals which were used to study the concentration quenching of the F centers were received from Crawford at North Carolina State University.

The MgO crystals numbered one through six in the experiments in this dissertation were grown at Oak Ridge National Laboratories using the arc-fusion method. The high grade powder used was obtained from the Kanto Chemical Company, Tokyo, Japan. The samples were subsequently heated to 2100 to 2400 K at 4-7 atmospheres in the presence of Mg or Ca vapor in a tantalum bomb. This produced crystals with an absorption band at 5.0 eV and with H⁻ ions present. The neutron irradiated crystal number seven was also received from ORNL. Crystal number eight was approximately 0.5 mm thick and had a purple tint. Its thermoluminescence curve was very similar to crystal number seven's suggesting that it had been neutron irradiated also.

Optical Density

The optical density measurements were made with a Cary 14 Spectrophotometer. Measurements were made at room temperature and at 77K. The crystal's edges were masked by using either black plastic tape or a small sheet of indium. The measurements were made over a spectral range from 200 nm to 650 nm. Filters that allowed optical density measurements of up to 4.8 were used.

Thermoluminescence

The thermoluminescence measurements were made over a temperature range of from 5K to 300K. The apparatus was set up as shown in Figure 8. After the crystals were pretreated, preheated or electron irradiated for example, they were placed on the cold finger of the cryostat with their edges shielded on experiments where comparison of different crystal's thermoluminescence was necessary. Thus the exposed areas of the crystals could be kept the same. The cryostat was then cooled to the desired temperature of 5K or 77K. Upon some occasions the Oxford cryostat could be cooled to approximately 70K by vacuum pumping nitrogen through its cooling system.

After the cryostat was cooled, the system was allowed to thermally settle for several minutes. Next, the excitation light was shone upon the crystal's appropriate absorption band for five minutes. After the light was turned off the cold finger was then turned from facing the light source

THERMOLUMINESCENCE

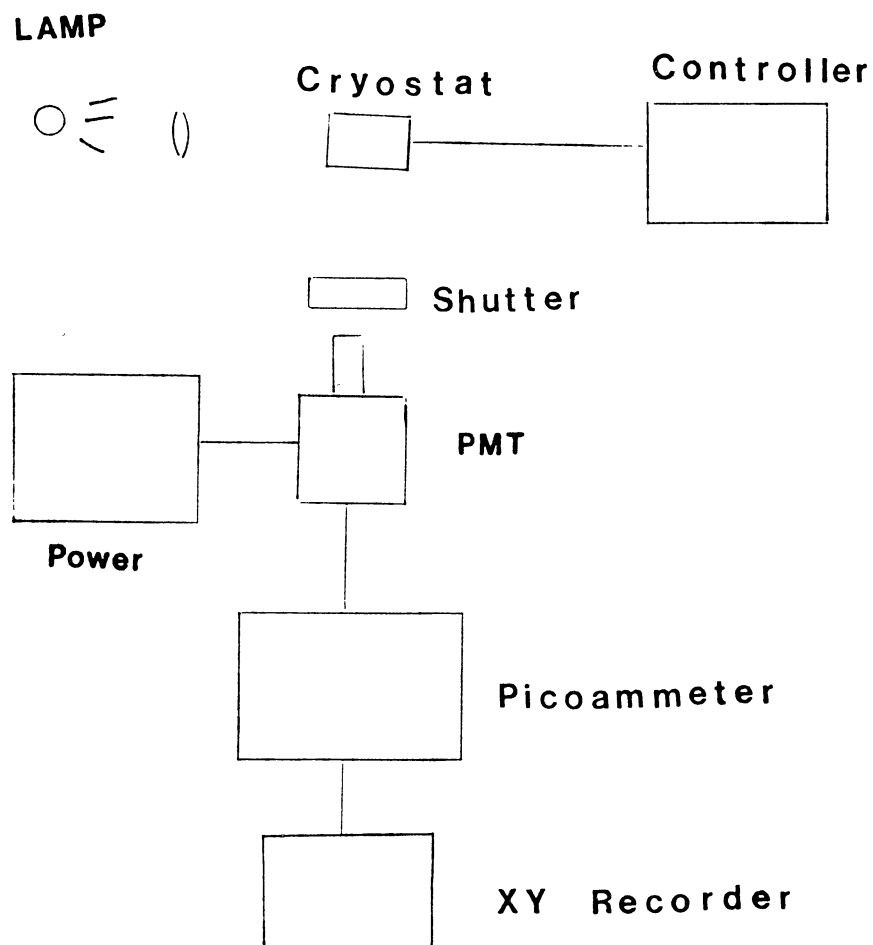


Figure 8. Thermoluminescence Apparatus

to facing the light detection system.

Next the Oxford cryostat's temperature controller's set point was set at 300K and then the controller was placed in AUTO. This automatic heating of the cold finger produced a constant heating rate of approximately 5 K/minute if the pressure of the thermal transfer gas in the cold finger chamber was kept at approximately 100 millitorr. A gold-chromel thermocouple attached to the cold finger was used to measure the crystal temperature. The thermocouple's voltage was read by a Keithley Instruments 155 Nulldetector micro-voltmeter, whose output was used to drive the x-axis of an Omnigraphic 2000 Recorder. Time was added to this axis by the use of tic marks at sixty second intervals. This data was then plotted on semilog paper.

Photoconductivity

Figure 9 shows a block diagram detailing the apparatus used for measuring the photoconductivity and Figure 10 shows the details of the sample holder used. The crystal was attached to the sample holder on the Oxford Instruments cryostat's cold finger which allowed measurements from 6 to 300 K. An excitation system composed of a 60 watt deuterium lamp and a GCA McPherson 218 0.3 m grating monochromator with a grating blazed at 3000 angstroms and having 12000 grooves/mm. Also it had a linear dispersion of 26.5 angstroms. The spectral output curve for this system is shown in Figure 11. After the crystal had been brought to the

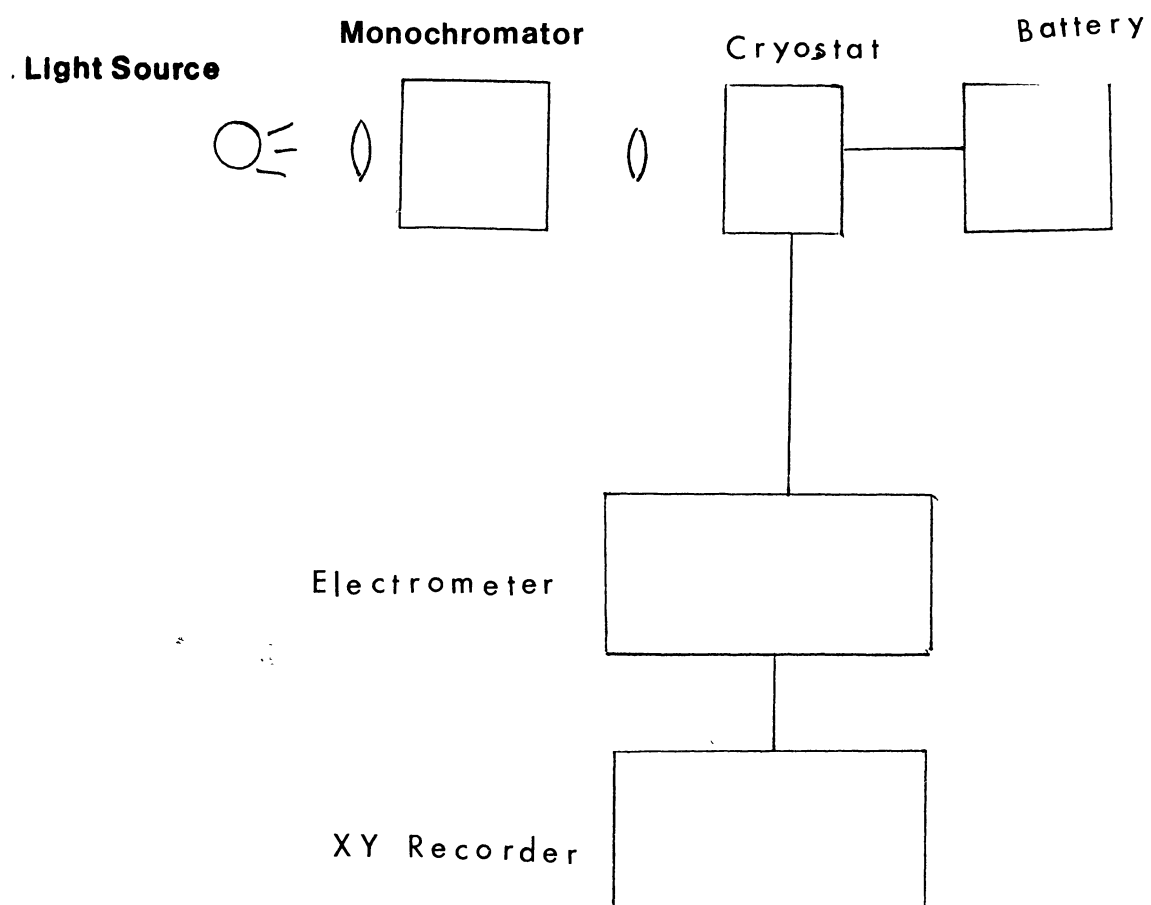


Figure 9. Photoconductivity Apparatus

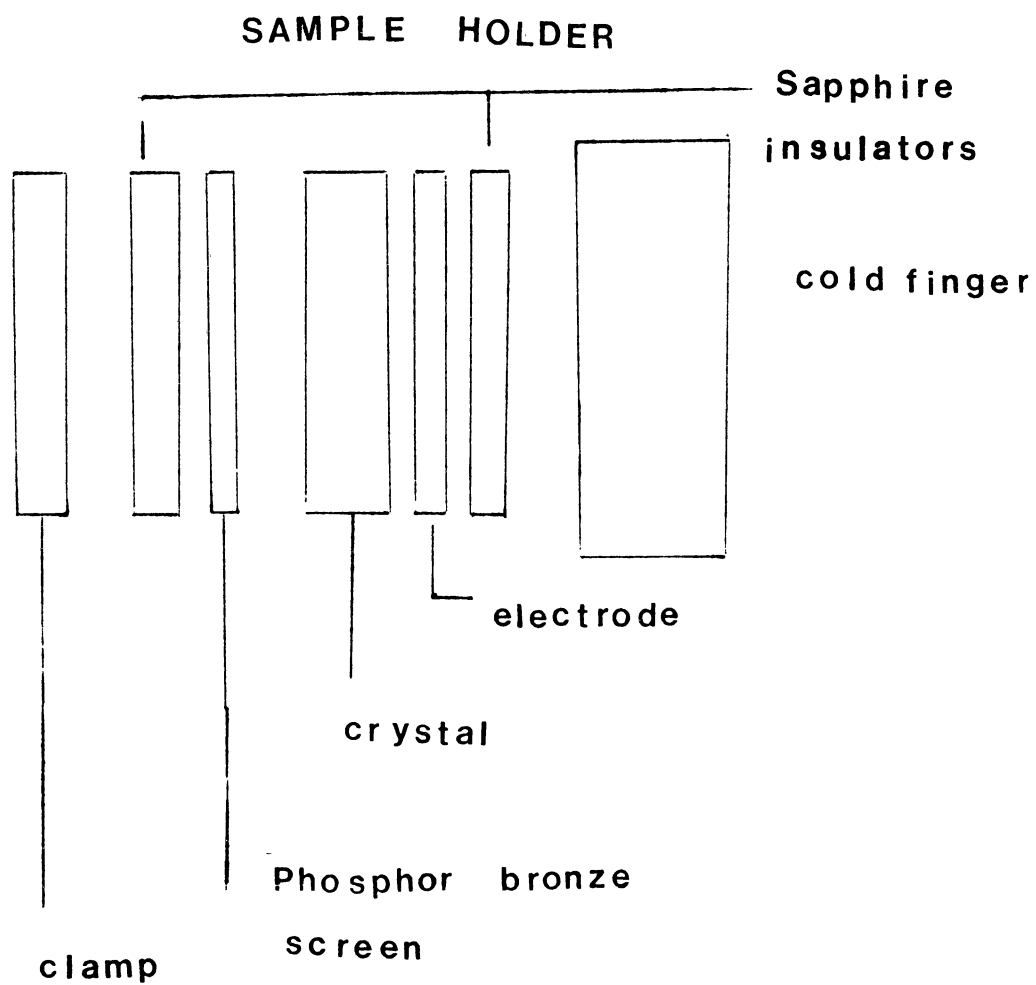


Figure 10. Sample Holder. Holder to minimize leakage currents

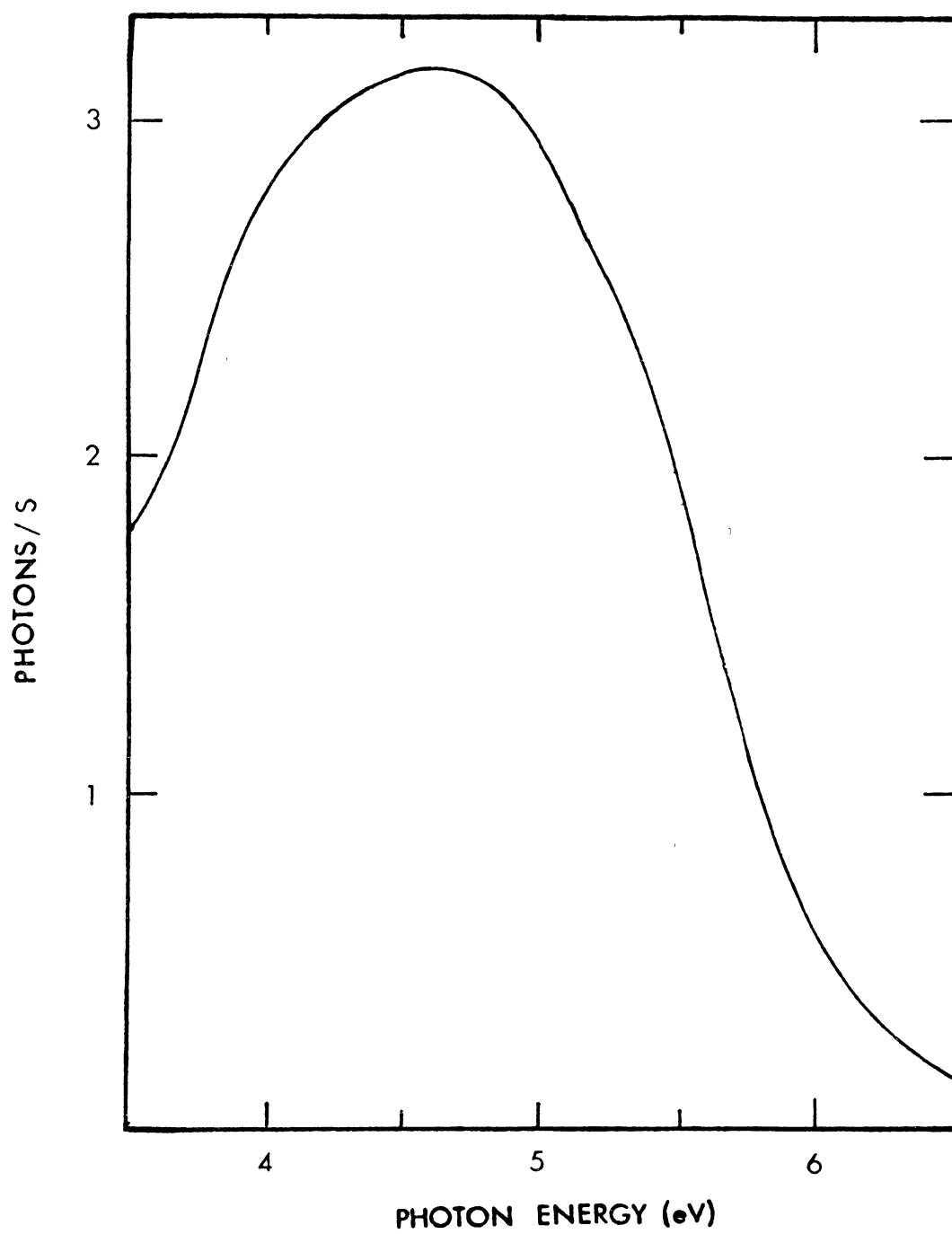


Figure 11. Excitation System Spectrum

desired temperature the battery was turned on and the system was allowed to stabilize. Next the shutter was opened with the monochromator set at its low energy setting and the system was again allowed to stabilize. The monochromator was then scanned from the low energy to high energy reading desired. The photocurrent produced in the crystal was recorded on an x-y recorder.

Photoluminescence

A block diagram of the photoluminescence apparatus is shown in Figure 12. A 60 watt deuterium or 150 Xenon lamp was used for the excitation light source. The lens used to focus the light onto the sample was made of S-1 UV grade quartz. Next the light passed through a shutter and then through an interference filter which restricted the excitation light to the required energy.

The next piece of apparatus in the optical path was an Oxford Instrument's continuous flow cryostat capable of using either liquid helium or nitrogen as the coolant. The cold finger was rotated to maximize the output of the detection system.

The light emitted by the crystal passed from the cryostat through a sharp cutoff filter used to prevent the light of the excitation system from reaching the detection system. The emitted light was then dispersed by a GCA McPherson 218 .3 m Monochrometer. It was detected by either an EMI 9658 or a thermoelectrically cooled RCA 31034 photo-

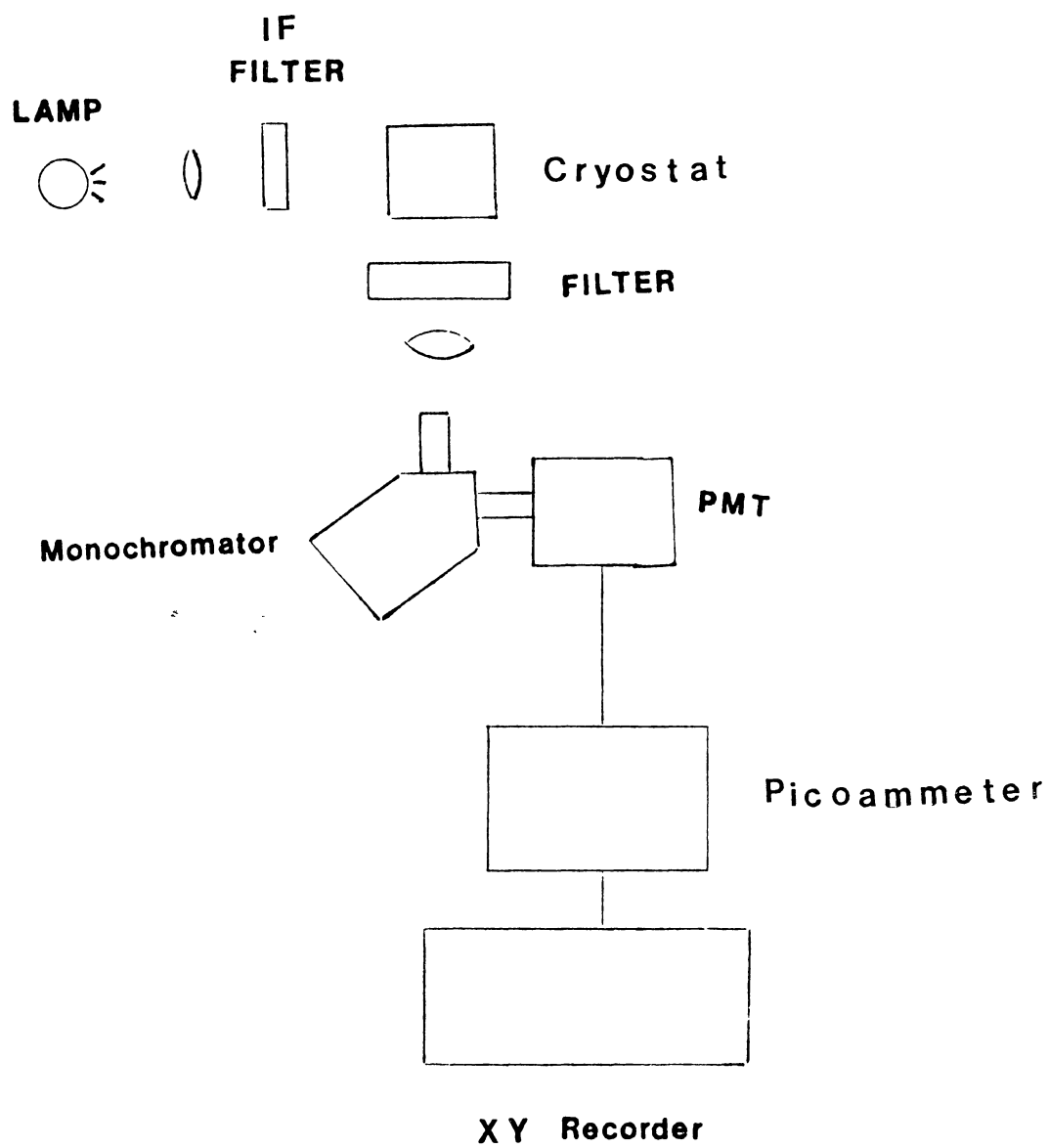
PHOTOLUMINESCENCE

Figure 12. Photoluminescence Apparatus

multiplier tube. The output of the PMT was connected to a Keithley 414s picoammeter which fed a signal to an Omnigraphic x-y recorder.

A Princeton Applied Research lock-in detector was used in the above system to look at lifetime effects in MgO and to measure the photoluminescence of Al_2O_3 . The only change required placing a light chopper in the excitation system and replacing the picoammeter with the lock-in detector.

Excitation

The block diagram for the excitation system is shown in Figure 13. A 60 watt deuterium lamp is used in conjunction with a GCA McPherson 0.3 monochromator as has been used above. This system is scanned over the energy range of the desired absorption band the emission band associated with that absorption is looked at with a photomultiplier tube. Either of the tubes used in the photoluminescence experiments was used. This PMT signal was fed to a Keithley 414S picoammeter which was connected to an Omnigraphic x-y recorder. A PAR lock-in detector or an Waveform Educator was used to look at only the short lifetime component of the emission.

EXCITATION

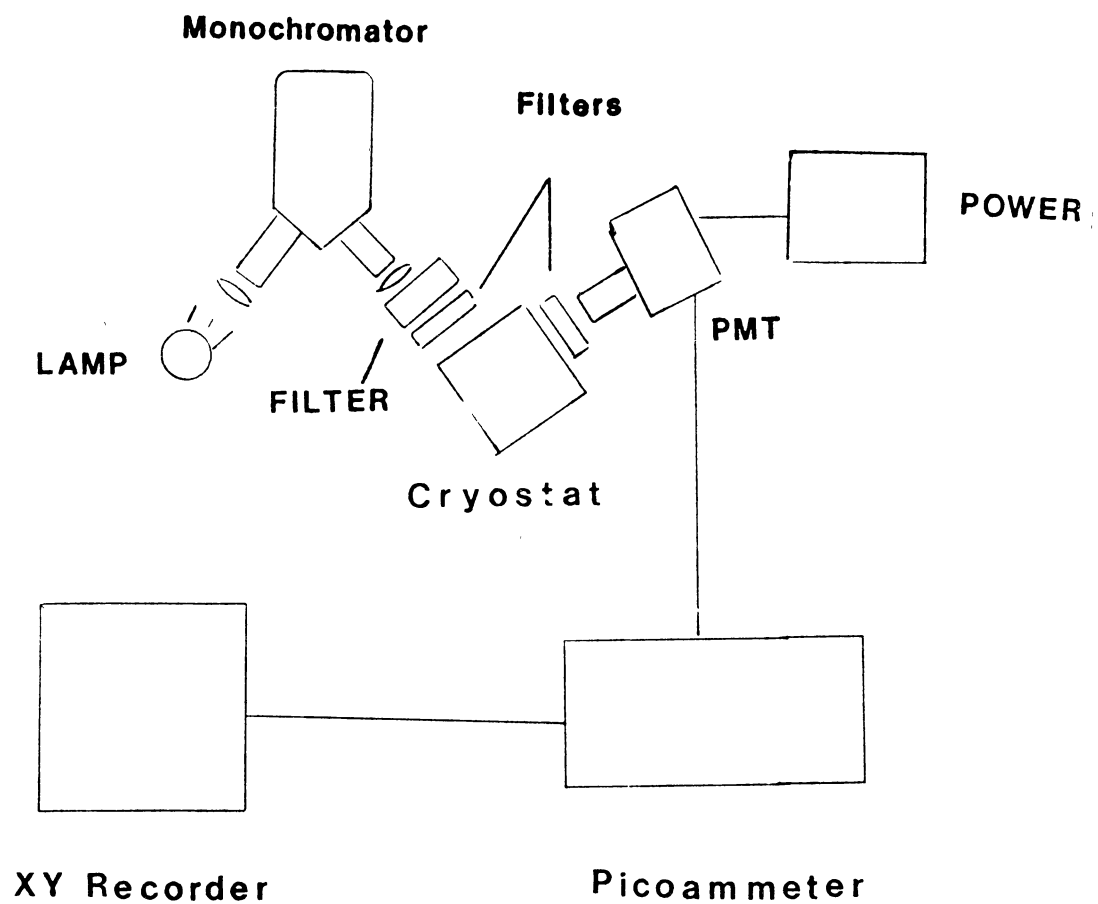


Figure 13. Excitation Apparatus

CHAPTER IV

SAPPHIRE EXPERIMENTAL RESULTS AND DISCUSSION

Introduction

The experiments on aluminum oxide in this chapter were used to look at the effects of trapping mechanisms on the optical properties of F centers. They were also used to determine the optical properties based upon a band shape analysis of the photoluminescence data.

Optical Density

Figure 14 shows the optical density of an as received crystal from Linde. This curve exhibits the background optical density of sapphire when it is relatively free from absorption by defects in the energy region of 3 to 6.2 eV.

The following set of optical densities of the as received single crystal sapphire samples from INSACO, Crystal Systems, and Adolph Meller were taken at 77 K on a Cary 14 spectrophotometer. Initially, each sample was heated to approximately 770 K for 15 minutes to bring it to a reproducible starting condition, before being quenched to room temperature. Optical densities were then taken over

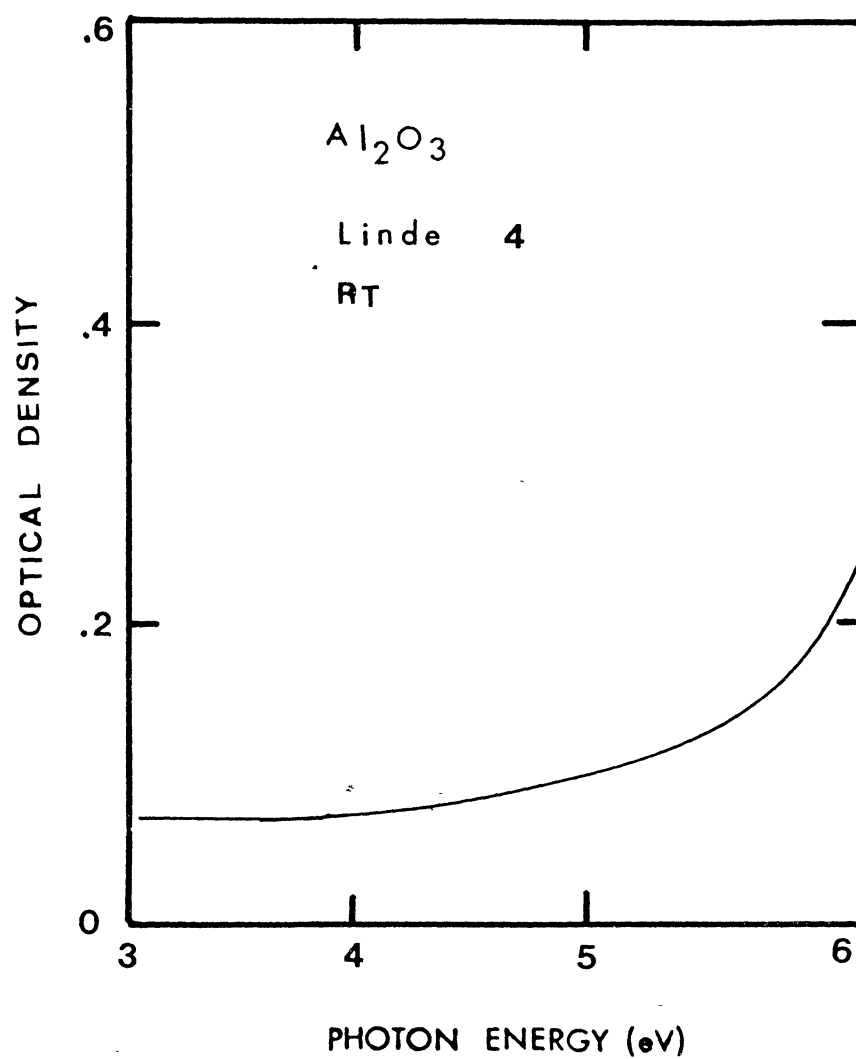


Figure 14. Linde Optical Density

the photon energy range from 4.5 to 6.2 eV. Each crystal was then bleached with 200 nm (6.2 eV) light from a deuterium lamp for 15 minutes and the optical density was remeasured. The crystals were subsequently bleached with 250 nm (4.96 eV) light for 15 minutes and the optical density of each was taken again. This sequence of measurements was performed on each crystal in turn.

The results for the INSACO sample are shown in Figure 15. Curve a shows the optical density after the initial heat treatment. Curve b shows the optical density after the crystal was bleached with 6.2 eV light and curve c after the subsequent bleaching with 4.96 eV light. After bleaching with 6.2 eV light, three bands are apparent, at 6.1, 5.5, and 4.9 eV respectively. A fourth band at approximately 4.0 eV was also apparent. The 6.1 eV band is due mainly to F centers and the 4.9 and 5.5 peaks correspond to F⁺ centers. Another F⁺ center absorption peak is believed to be hidden under the 6.1 eV absorption peak. The striking feature of this bleaching sequence is that bleaching with 200 nm light reduces the F center concentration while increasing the F⁺-center concentration. Whereas, bleaching with the 250 nm light produces the reverse effect. Subsequent measurements made by Kellan and Crawford indicate that the light with an energy of approximately 4.0 eV is most effective in producing the reverse effect (25).

The results of this process on the Crystal Systems and Adolph Meller crystals are shown in Figures 16 and 17. The

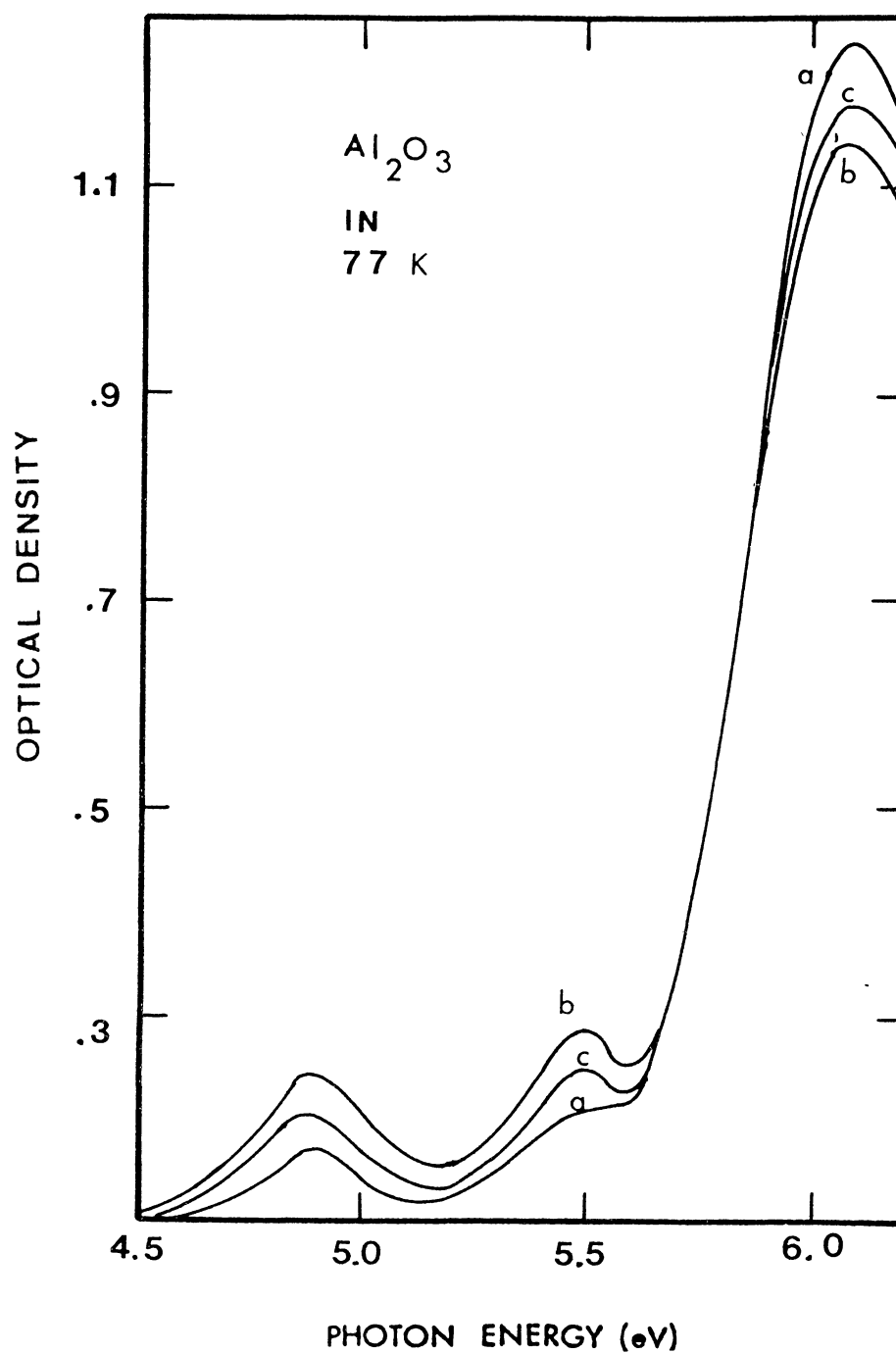


Figure 15. INSACO Optical Density
Curve a, initial curve;
Curve b, 6.2 eV bleach;
Curve c, 5.0 eV bleach

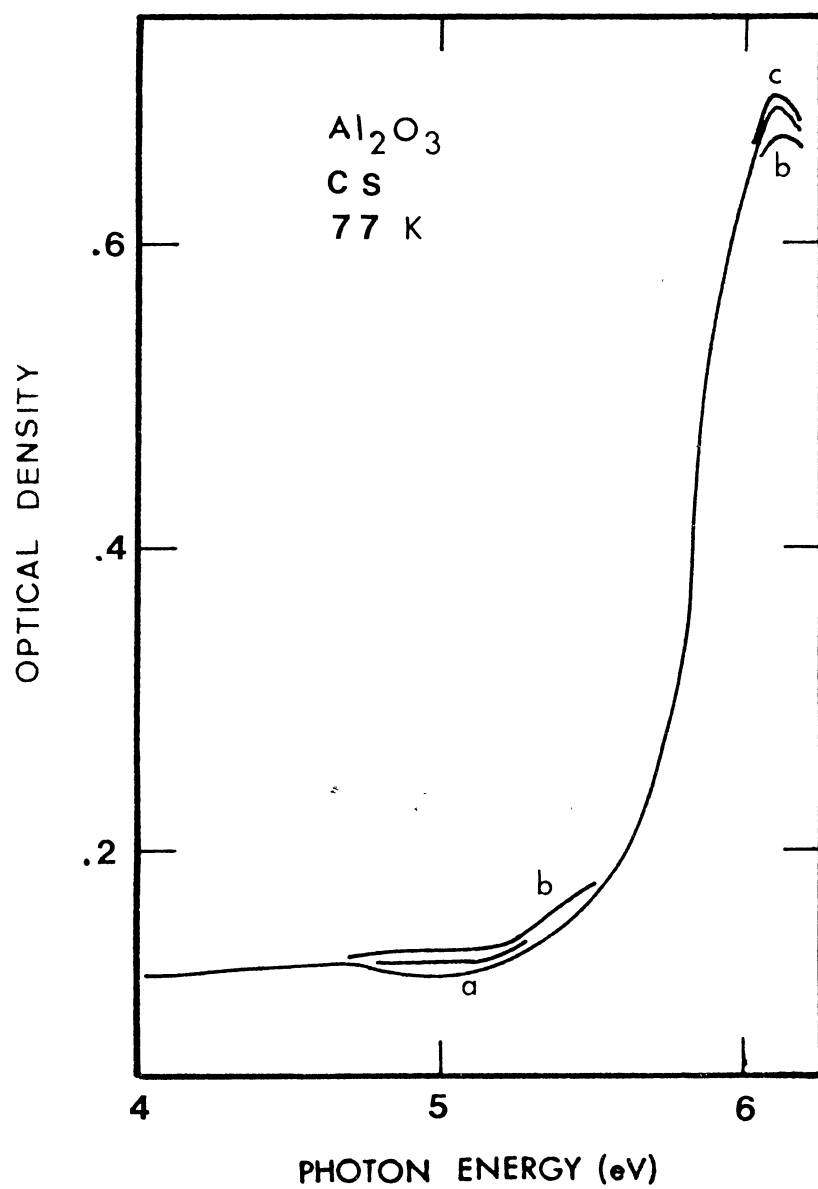


Figure 16. CS Optical Density
Very Little Bleaching
Effect

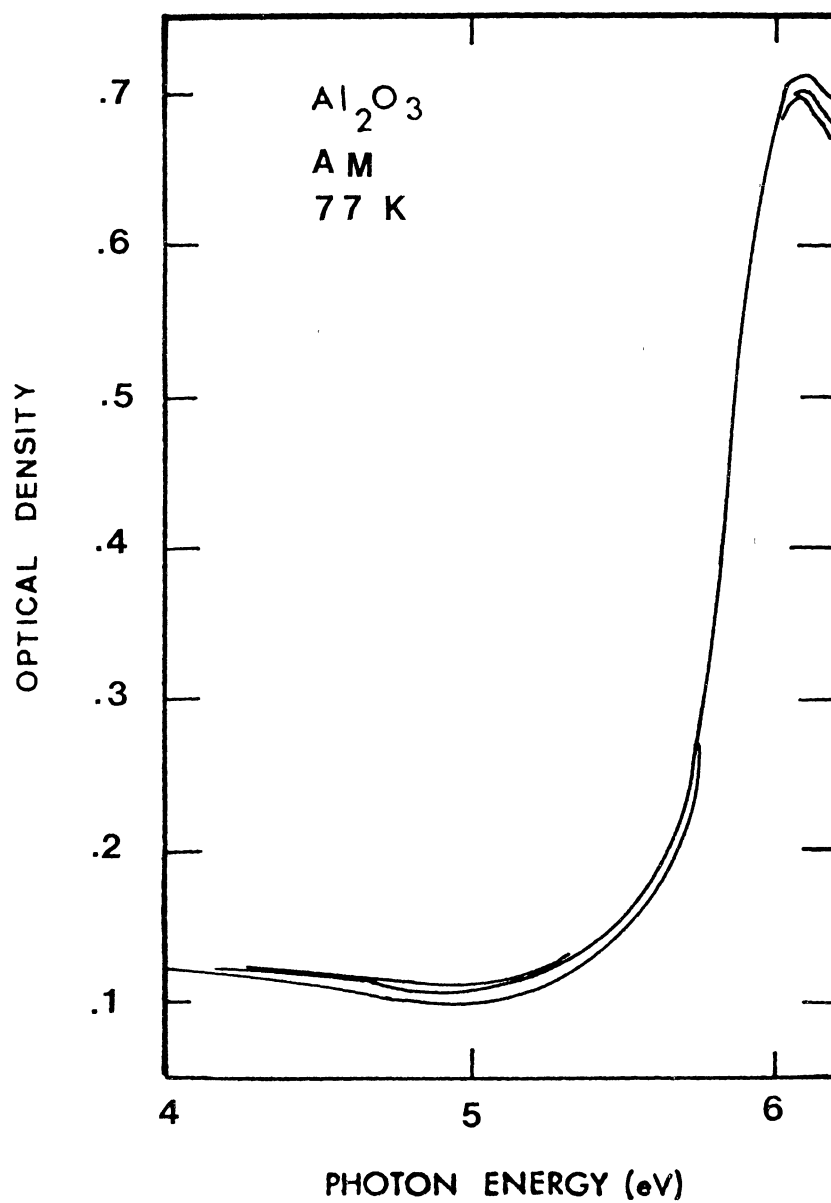


Figure 17. AM Optical Density.
Very Little Bleaching
Effect

interconversion process in these two crystals occurs on a much smaller scale.

The above behavior is caused by the availability of electron traps in the crystals. The sapphire crystals which exhibit the pronounced interconversion process will be identified as Type I crystals and the others will be identified as Type II crystals.

Figure 18 shows the 6.1 eV absorption band of an Adolph Meller crystal compared to a Gaussian curve.

Photoluminescence

The photoluminescence of the F center in aluminum oxide was studied over a temperature range from 4 K to 300 K. The crystals were excited with nonpolarized 6.1 eV light.

The emission associated with the excitation was observed at 3.0 eV. Because of the low symmetry of the F center site

(C) the emission was studied for its polarization depend-
2
ence relative to the crystalline C-axis. Figure 19 shows

the polarization dependent emission spectrum of a Crystal

Systems sample at a temperature of 20 K. The maximum

intensity occurs when the light is measured with its

electric field vector perpendicular to the crystal's C axis

and a minimum when parallel to the C axis. The ratio of the

peak heights of these emission spectra is approximately 1.7

from 4 to 55 K and ranges up to 2.0 at 300 K. Figure 20

shows the temperature dependence of the emission of a Type I

crystal with the electric field polarization perpendicular

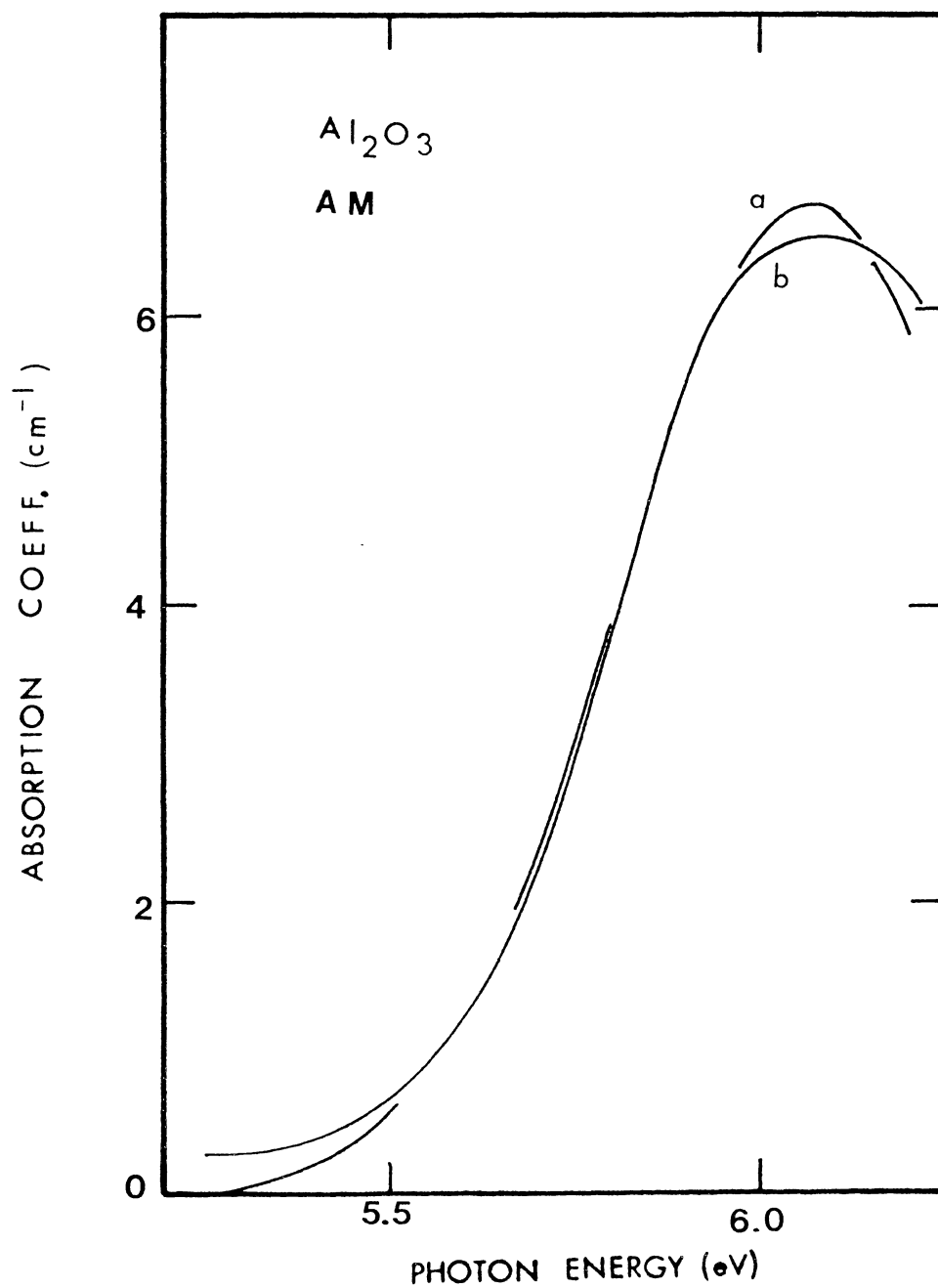


Figure 18. Absorption Gaussian Curve Comparison. Curve a, AM Absorption; Curve b, Gaussian Curve

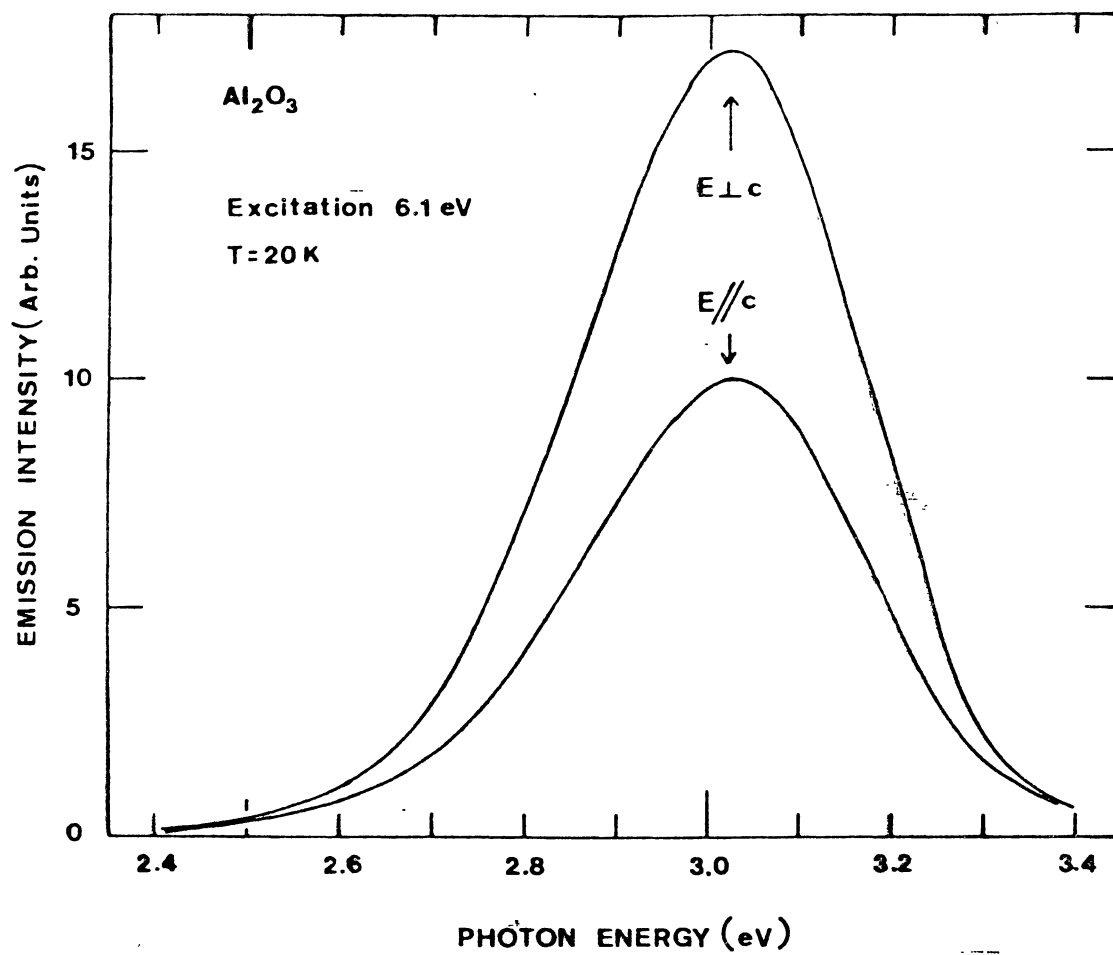


Figure 19. CS Emission. Polarization Dependent

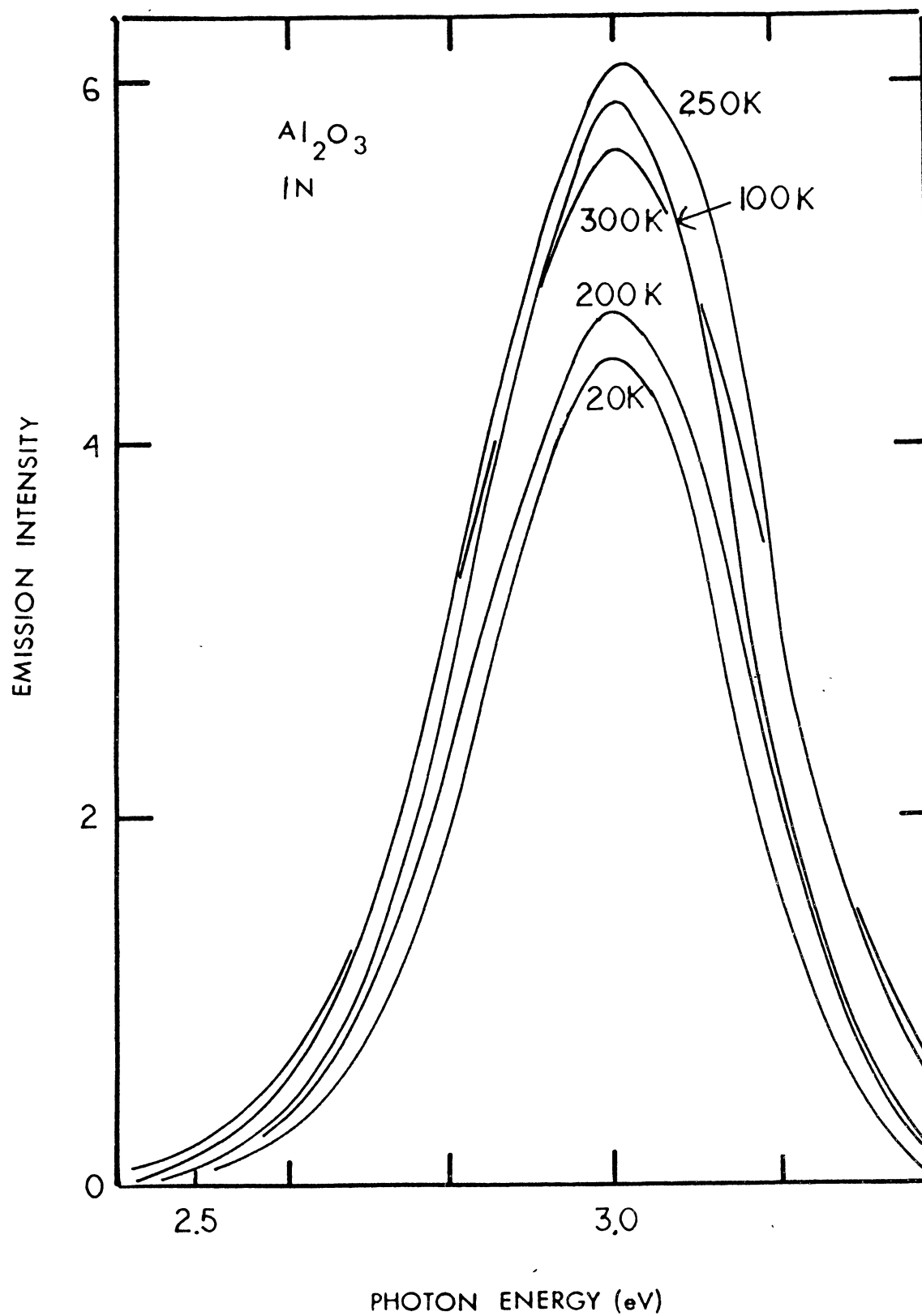


Figure 20. Type 1 Emission. Temperature Dependence

to the C axis. This dependence is quite different from that observed for F centers in other oxides such as SrO (26). It is obvious that some mechanism external to the F center is affecting the number of emitting F centers as a function of temperature.

Figure 21 shows that the emission spectrum at 20 K nearly approximates a Gaussian function except for a low energy tail. Based upon this curve shape, linear electron-lattice coupling theory can be used to perform the following detailed analysis of the photoluminescence data.

Figure 22 shows the temperature dependence of the bandwidth of the 3.0 eV F center emission. At temperatures up to approximately 100 K the full width at half maximum (FWHM) intensity is 0.36 eV. Between 100 and 300 K the FWHM increases to 0.44. The solid line is a computer fit of the equation

$$W^2(T) = W^2(0) \coth(h\nu/2kT) \quad (4.1)$$

to its experimental points. In fitting the data, $W(0)$ is the FWHM at low temperatures and w is the average frequency of the normal modes of vibration which are coupled to the emitting electronic state of the F center. From the fit a value of 0.361 eV is found for $W(0)$ and $h\nu$ is found to be 345 cm^{-1} . This value for $h\nu$ is close to the value of 340 cm^{-1} found by Draeger and Summers (6) for the F⁺ center 3.8 eV emission in sapphire.

Table I gives the results of a moment analysis of the emission curve at 20 K with the electric polarization

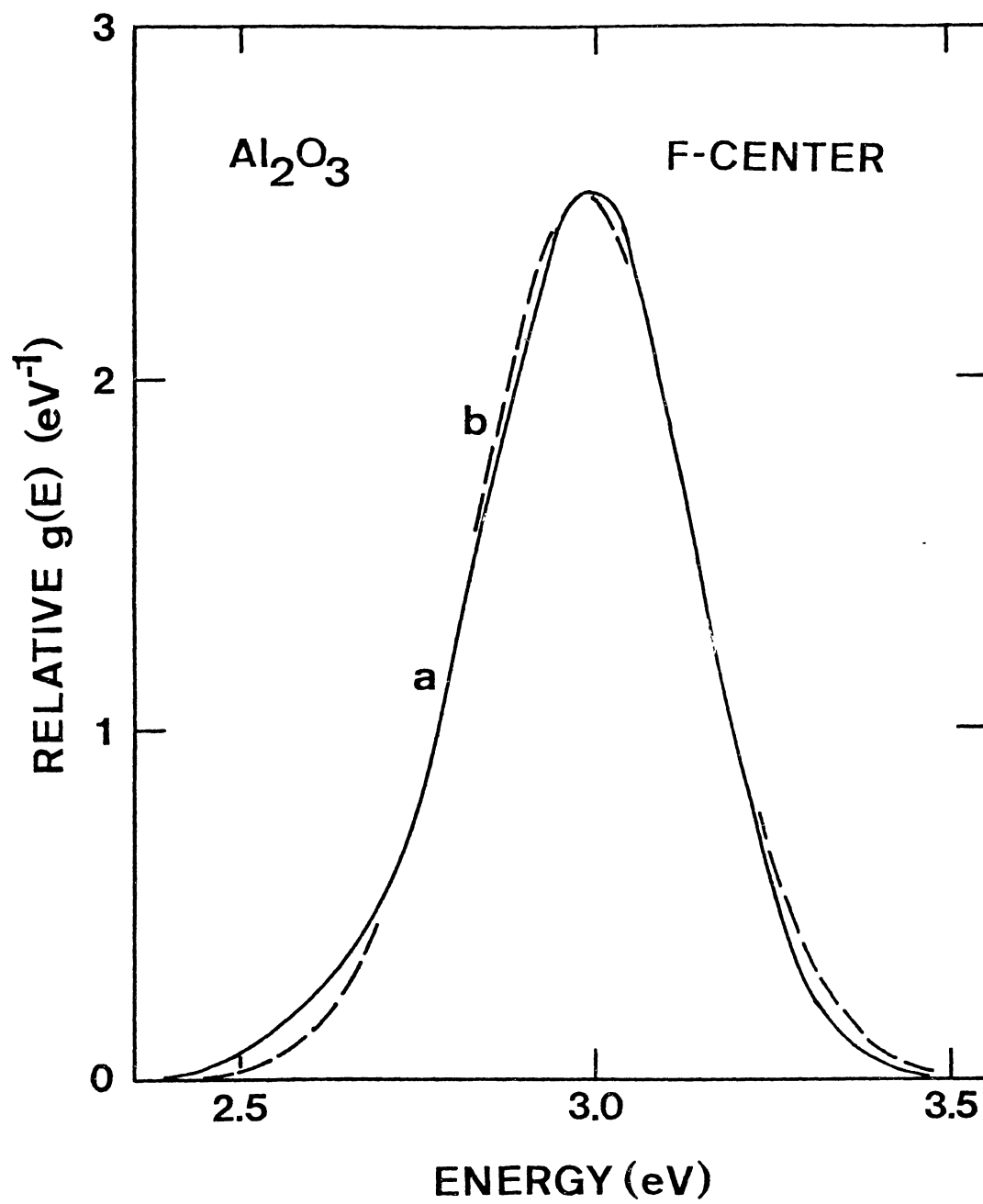


Figure 21., Emissionl Gaussian Comparison

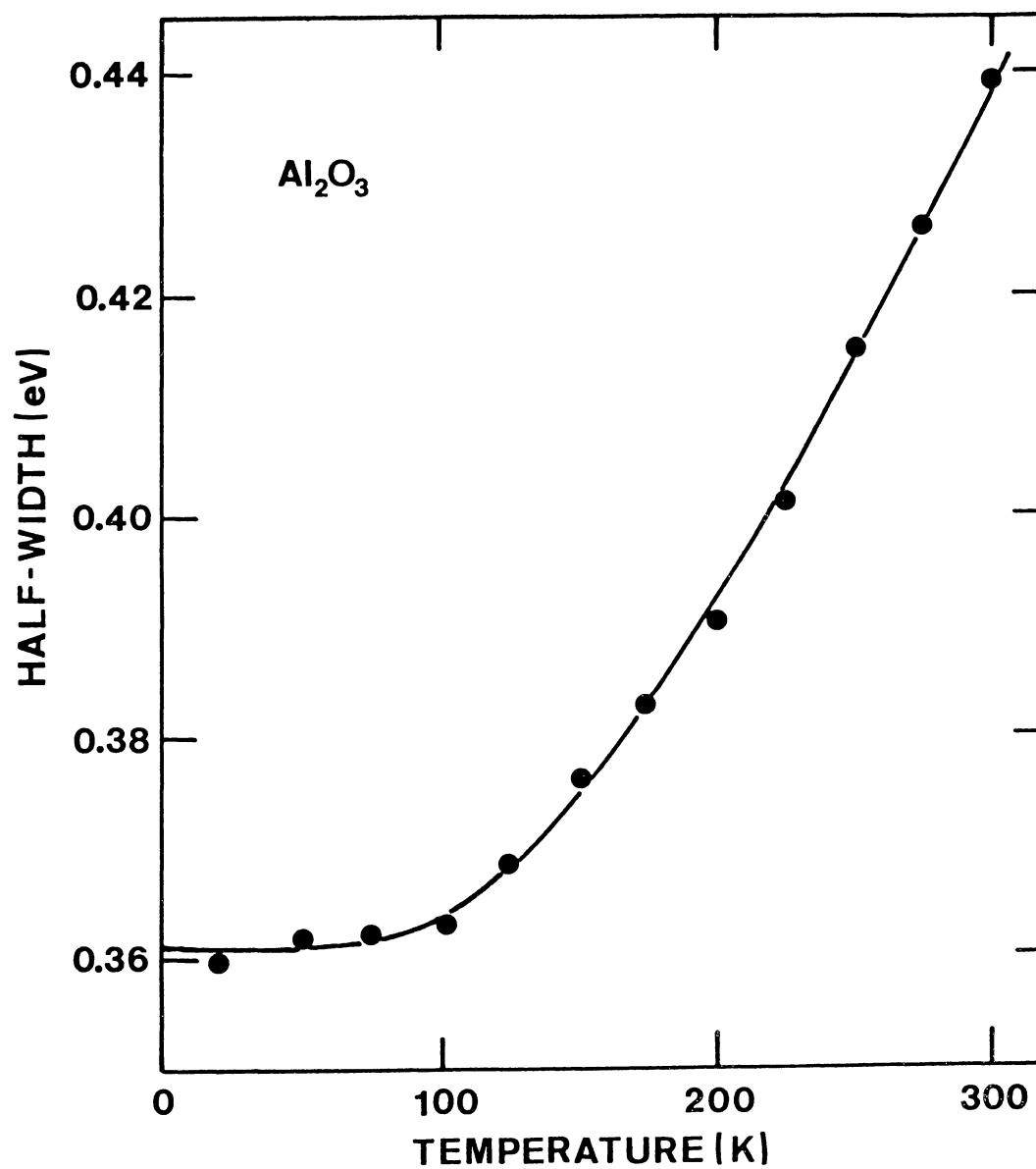


Figure 22. Bandwidth Temperature Dependence of the F Center

TABLE I
MOMENT ANALYSIS OF THE BAND SHAPE FUNCTION
FOR THE 3.0 EV EMISSION BAND

Moment	Formula	Value
Zeroth	$\sum_i g(E_i) E_i$	1 (Normalized)
First	$\bar{E} = \sum_i E_i g(E_i) E_i$	2.96 eV
First about \bar{E}	$\langle E \rangle = \sum_i (E_i - \bar{E}) g(E_i) E_i$	-0.430E-07 eV
Second about \bar{E}	$\langle E^2 \rangle = \sum_i (E_i - \bar{E})^2 g(E_i) E_i$	0.0273 eV ²

perpendicular to the C axis. The centroid or first moment is at 2.96 eV while the peak of the band is at 3.00 eV. The difference is caused by the presence of the low energy tail. The shape function is of the form

$$g(E) = I(E)/E^4 \quad (4.2)$$

Figure 23 is a plot of $g(E)$. The very small value, 4.32×10^{-6} eV, of the first moment about the centroid, \bar{E} , shows that the emission is nearly Gaussian which has already been discussed above. Table II shows that the centroid stays constant as the temperature increases from 20 to 300 K which might be expected because of sapphire's high melting point. The variation of the first moment shown in the table is reflected by the curve in Figure 24. The strength of the electron-lattice coupling can be estimated by calculating the Huang-Rhys factor, S . S can be obtained from the equation,

$$S = \langle E^2 \rangle / (\hbar \bar{\omega}), \quad (4.3)$$

where $\langle E^2 \rangle$ is the second moment about the centroid as listed in Table I. Here, $\hbar \bar{\omega}$ is the average phonon frequency as determined by the curve fitting of the temperature dependence of the FWHM. S is calculated to be 14.8. If the bandshape is gaussian, $\langle E^2 \rangle$ is calculated using the equation

$$\langle E^2 \rangle = W^2(0)/8 \ln 2. \quad (4.4)$$

The value calculated for S using this value is 12.8. These

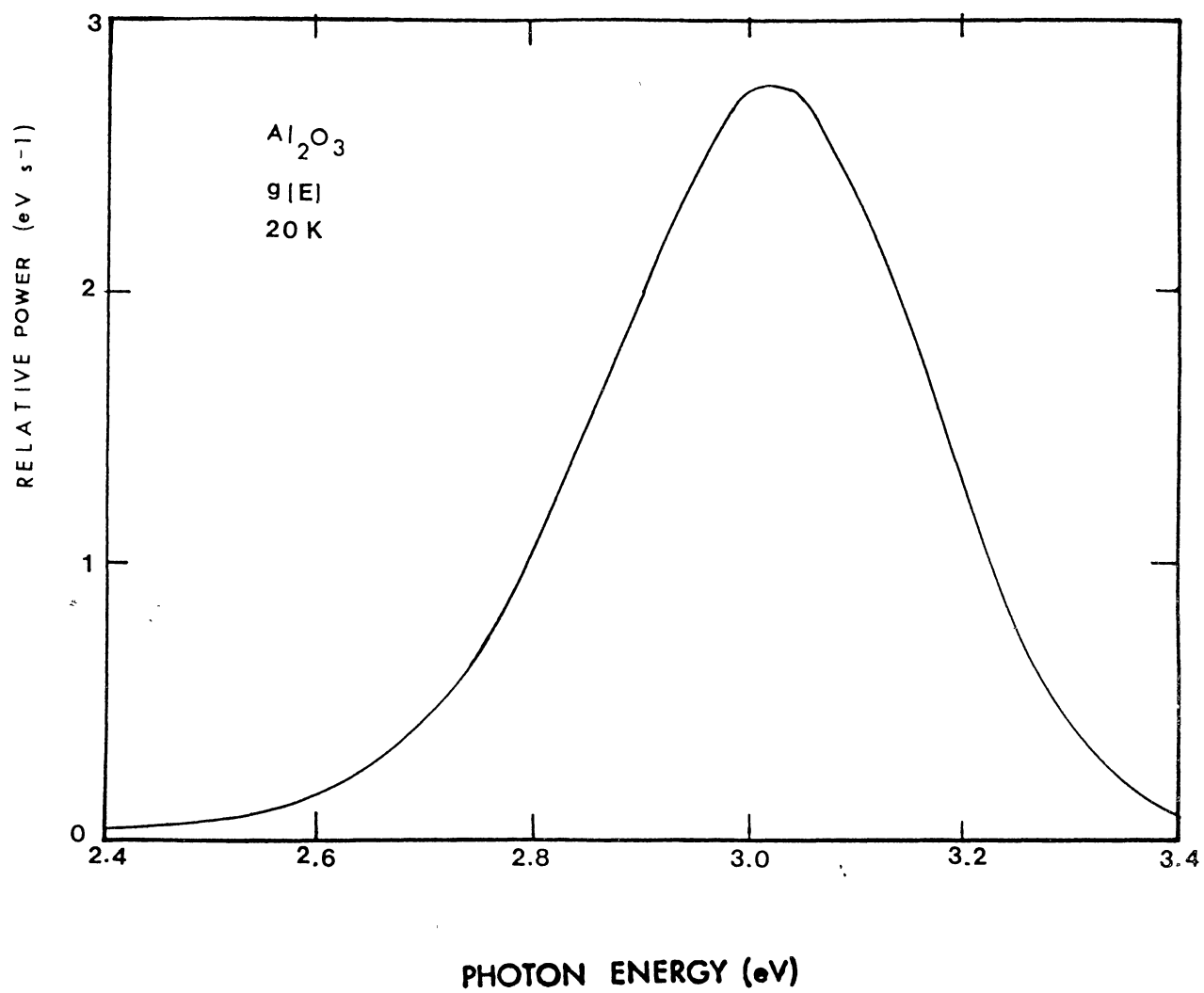


Figure 23. Emission Shape Funtion

TABLE II
TEMPERATURE DEPENDENT MOMENT ANALYSIS

Temperature (K)	Normalized Zeroth Moment	Centroid (eV)	$\langle E^2 \rangle$ (eV ²)
20	0.633	2.96	0.0273
50	0.802	2.96	0.0276
75	0.828	2.96	0.0268
100	0.838	2.96	0.0270
125	0.824	2.96	0.0272
150	0.795	2.96	0.0268
175	0.766	2.96	0.0279
200	0.722	2.96	0.0275
225	0.750	2.96	0.0291
250	1.000	2.97	0.0294
275	0.890	2.96	0.0312
300	0.969	2.96	0.0328

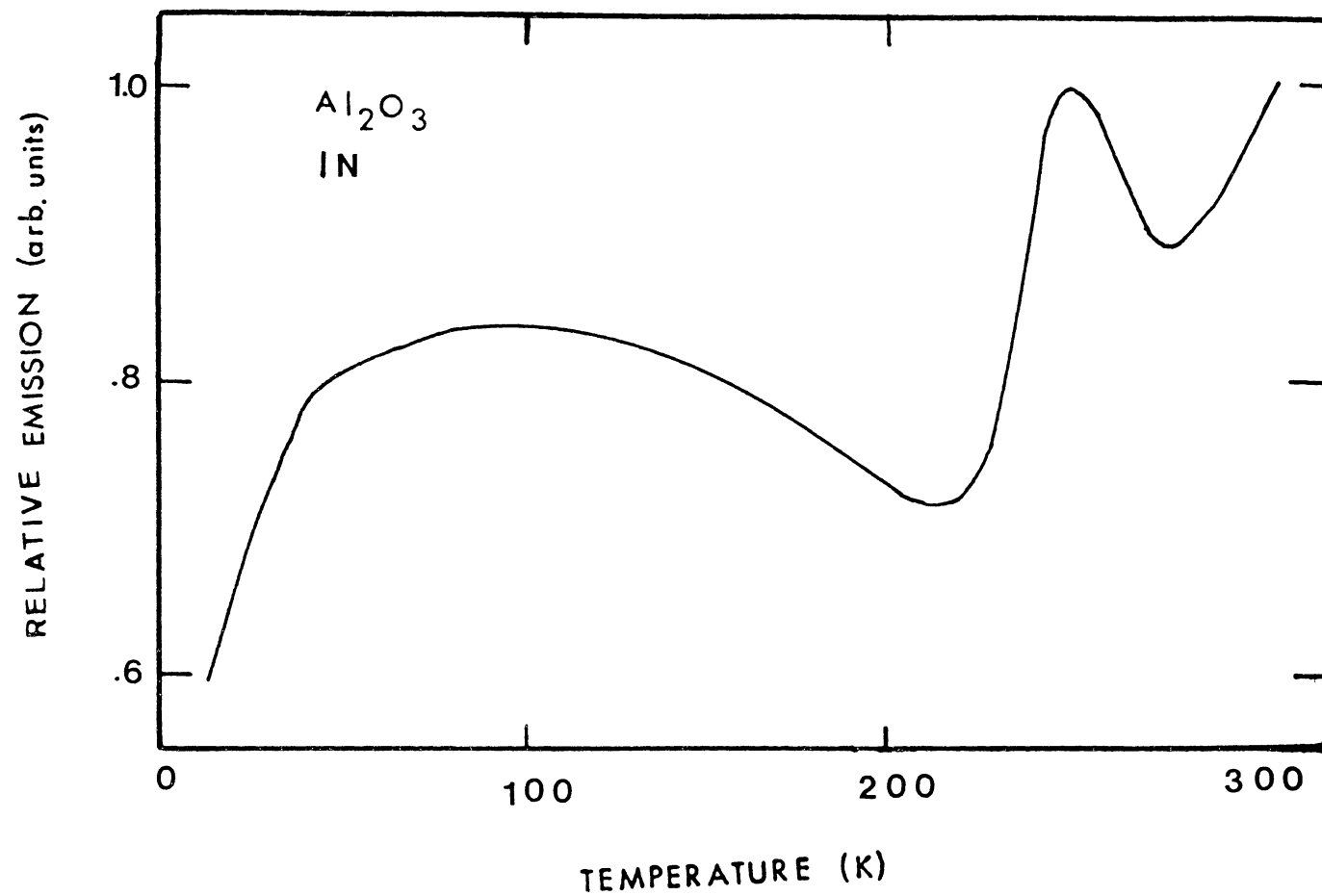


Figure 24. Type I First Moment Variation
as a Function of Temperature

These two estimates are close with the difference between the 12.8 value and the experimental value being 13 percent. The size of S says that the strength of the coupling is strong. Since the values are larger than 6 no zero phonon line or side band structure on the curve is expected and none was observed. The zero phonon line is seen when both absorption and emission occur from the lowest energy level of one state to the lowest energy level of the other. Thus both have a sharp line at the same wavelength. When the electron-lattice interaction is strong enough that S is larger than six this line is not seen.

The Stokes shift, E , is the difference between the absorption energy and the emission energy. If only a two level model is assumed for the model, the Stokes shift is experimentally determined from the equation,

$$E = h\nu(2S-1). \quad (4.5)$$

This gives a value of 1.30 eV for the Stokes shift. From this the emission energy should be expected to be approximately 4.8 eV instead of the 3.0 eV experimentally determined value. This difference in values suggests that the emission occurs from a different electronic state than the one into which it was excited. The lifetime analysis performed by Brewer et al. (10) confirms this also. They observed long fluorescence lifetimes which indicated that the emission transition was forbidden and probably originated from a triplett state split by the interaction with the crystal field.

Photoconductivity

The photoresponse per incident photon of several thermochemically reduced sapphire crystals and of a neutron irradiated crystal were measured. The crystal from INSACO has been called Type I and those from Adolph Meller and Crystal Systems called Type II. Figure 25 shows that the photocurrent is linear with the electric field varying up to approximately 3 kV/cm. Figure 26 shows that the photocurrent is linear up to the maximum amount of incident light the crystals were exposed to. The curves are for an as received crystal and for the crystal bleached with 6.1 eV light.

Figures 27 through 29 show the photoresponse of the INSACO crystal at three temperatures ranging from 6 K to room temperature. Figures 30 and 31 show the photoresponse for an Adolph Meller crystal at 77 K and room temperature, and Figures 32 and 33 show the same for a Crystal Systems crystal. These measurements were made with the local electric field vector perpendicular to the crystal's C axis. On all seven figures, curve a was obtained after the crystals had been heated for fifteen minutes to 770 K and subsequently quenched to room temperature. Curve b was obtained on the sixth repetitive scan. Curve c was then obtained after bleaching the crystal for five minutes with 6.2 eV light, and curve d after bleaching for five minutes with 4.96 eV light.

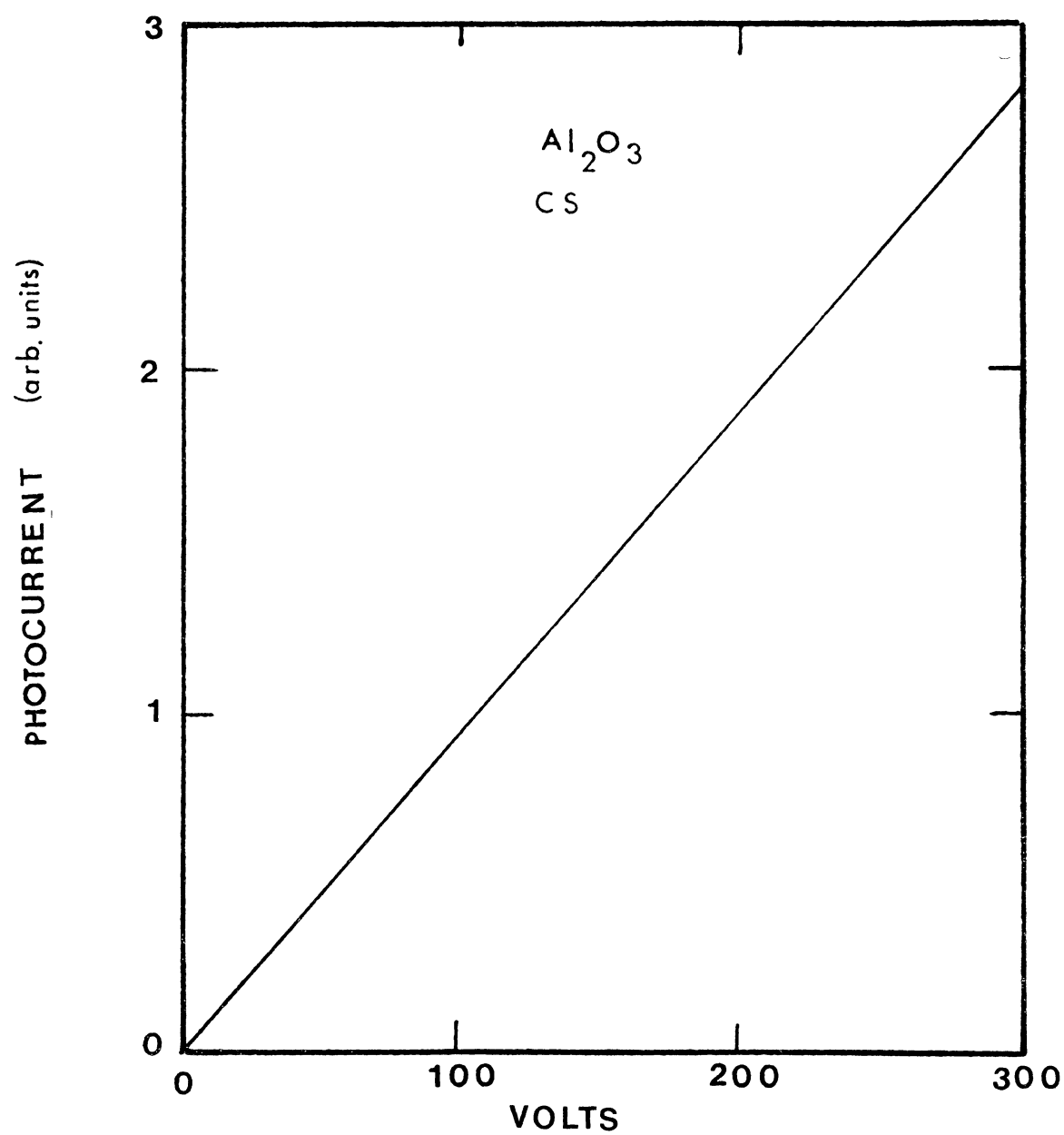


Figure 25. Photocurrent vs Electric Field

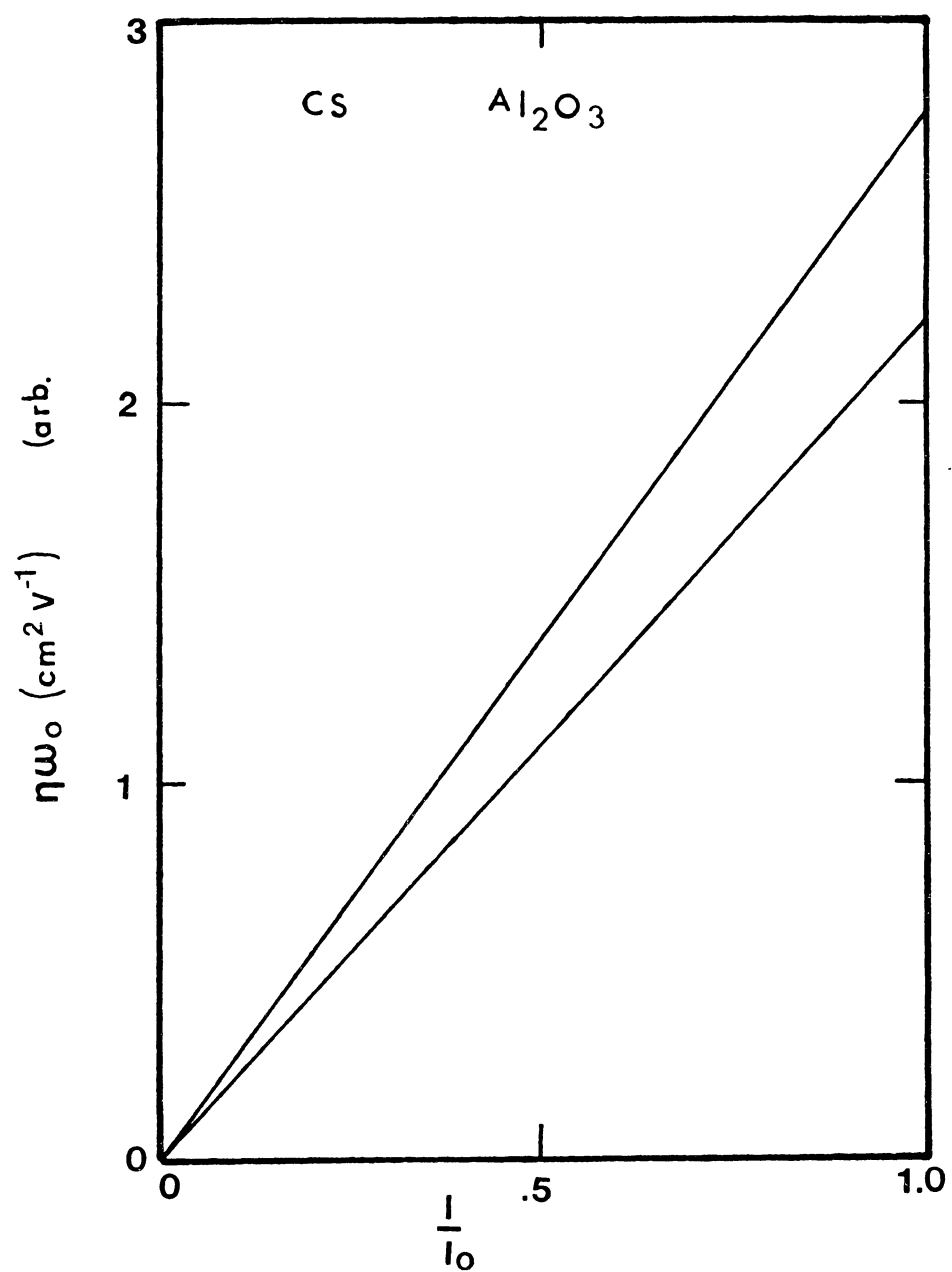


Figure 26. Photocurrent vs Light Intensity

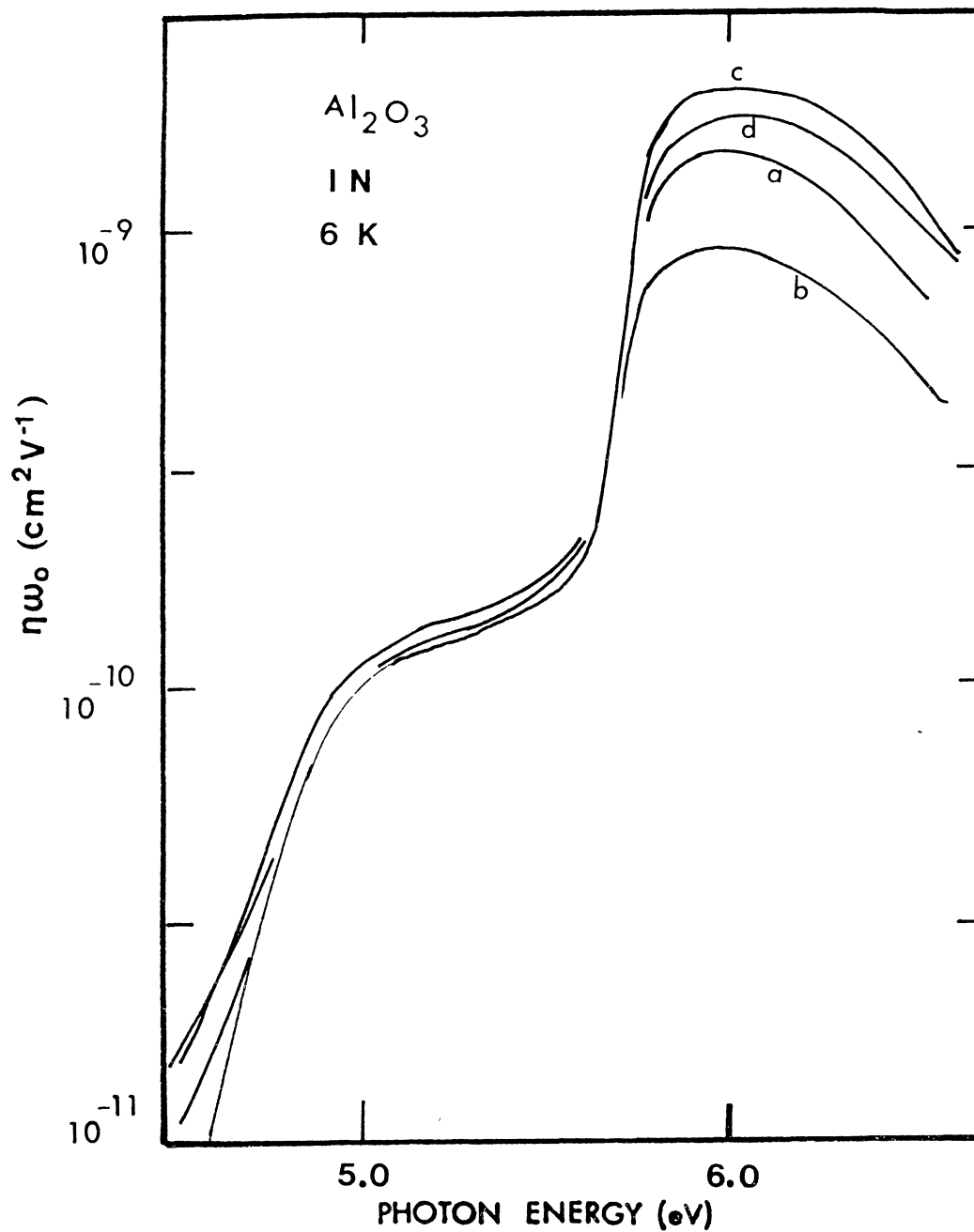


Figure 27. INSACO PC at 6 K; Curve a, Initial scan; Curve b, 6th scan; Curve c, 200 nm bleach; Curve d, 250 nm Bleach

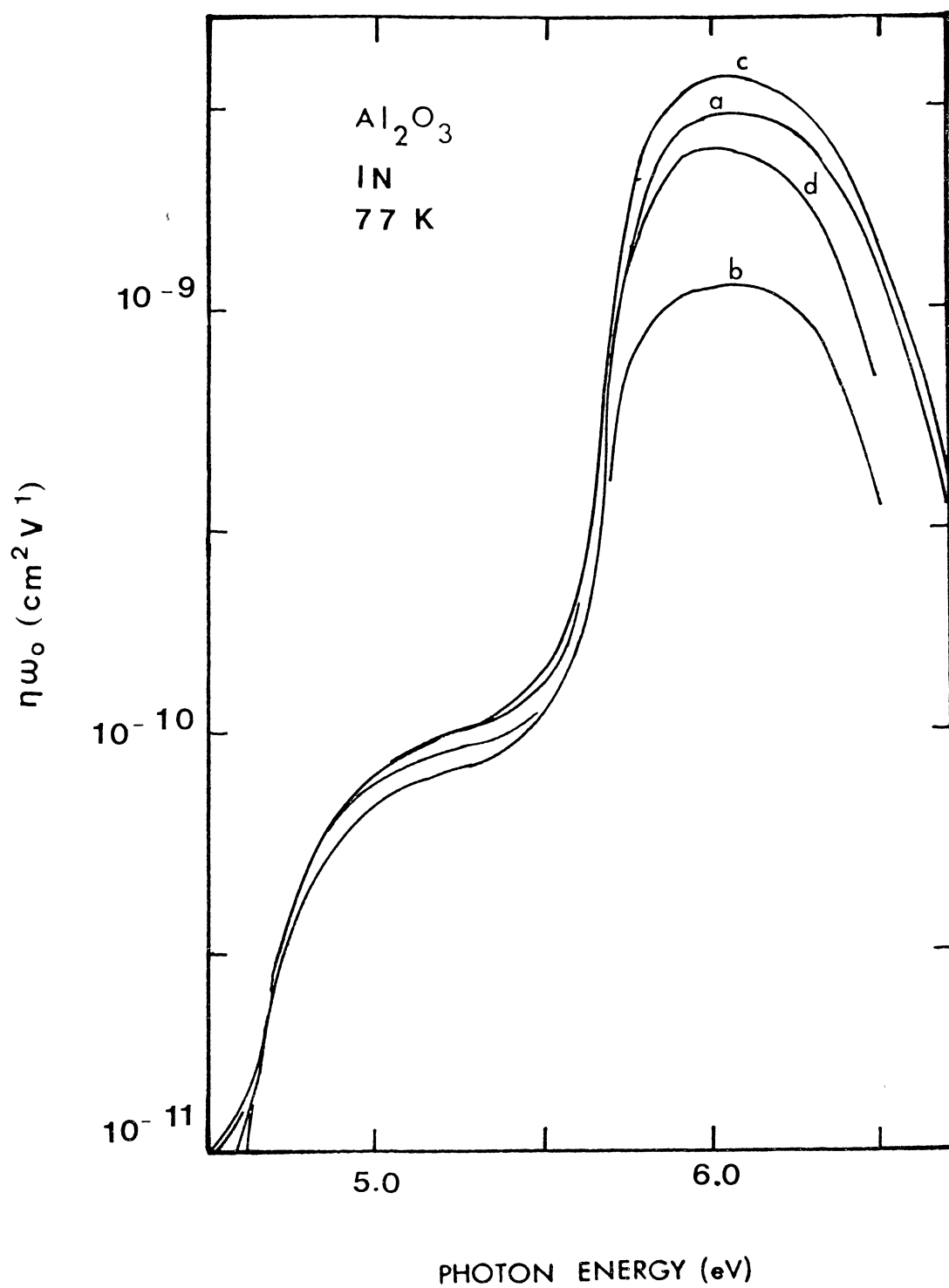


Figure 28. INSACO PC at 77 K; Curve a, Initial scan; Curve b, 6th scan; Curve c, 200 nm bleach; Curve d, 250 nm Bleach

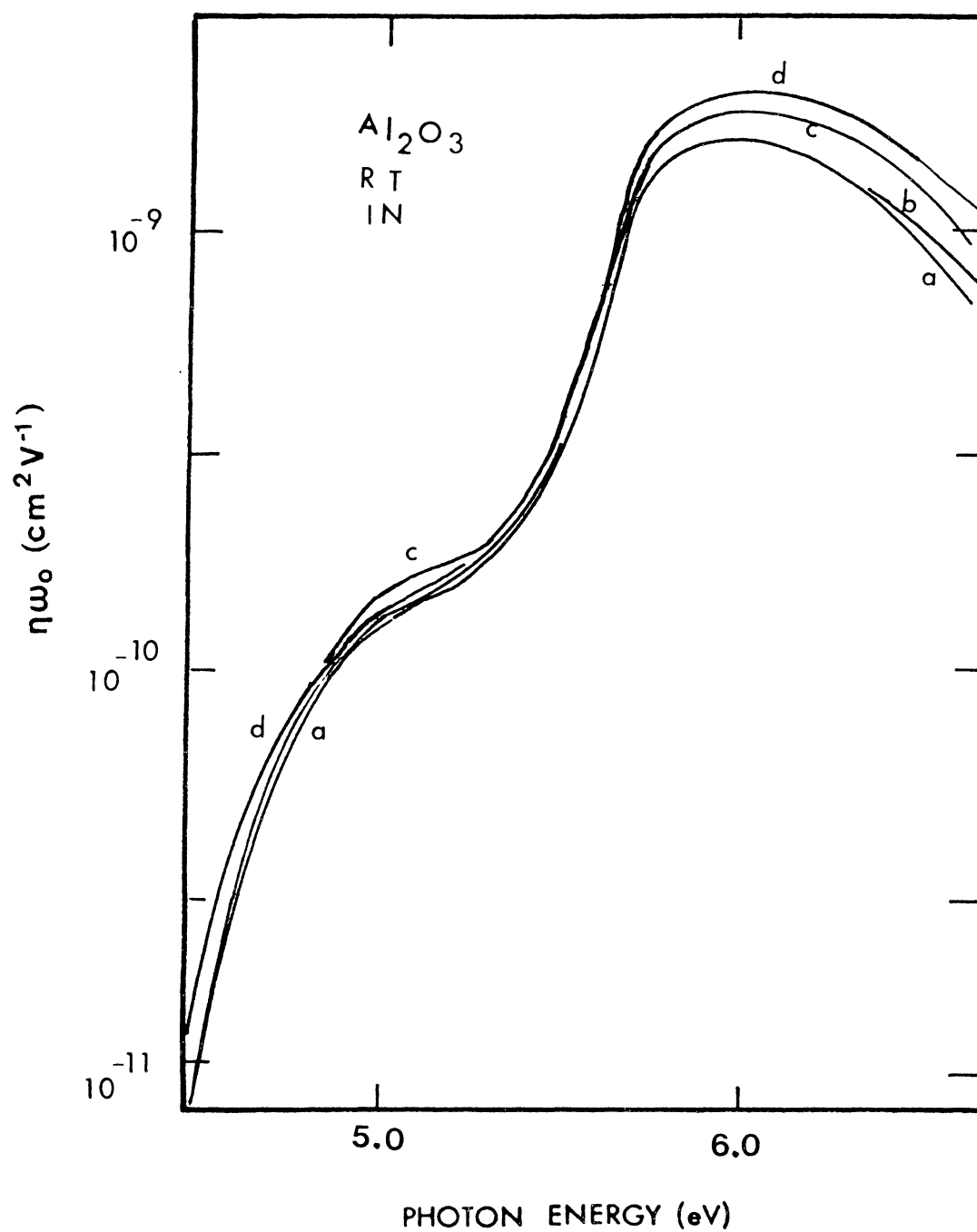


Figure 29. INSACO PC at RT; Curve a, Initial scan; Curve b, 6th scan; Curve c, 200 nm Bleach; Curve d, 250 nm Bleach

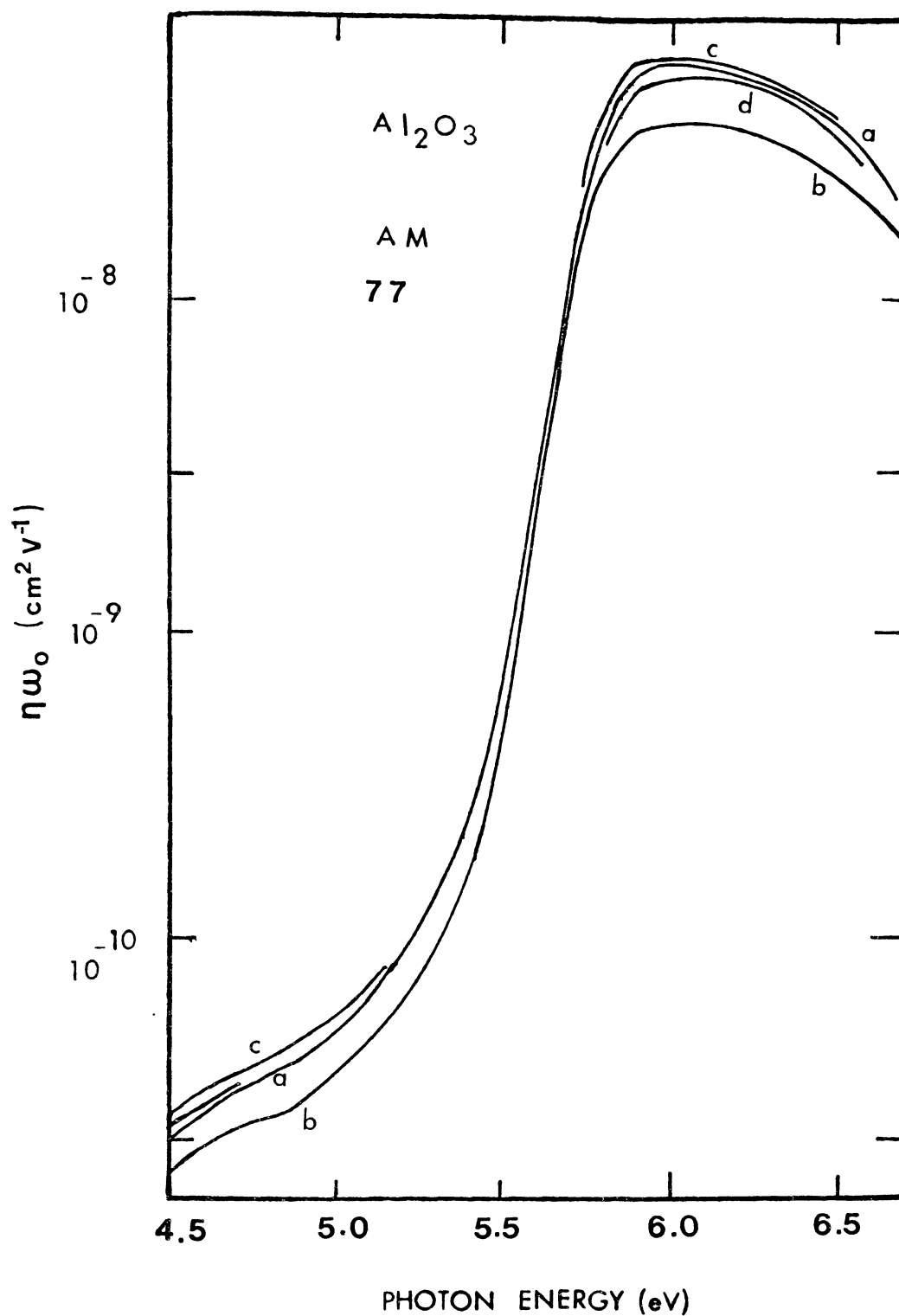


Figure 30. CS PC at 77 K; Curve a, Initial scan; Curve b, 6th scan; Curve c, 200 nm Bleach; Curve d, 250 nm Bleach

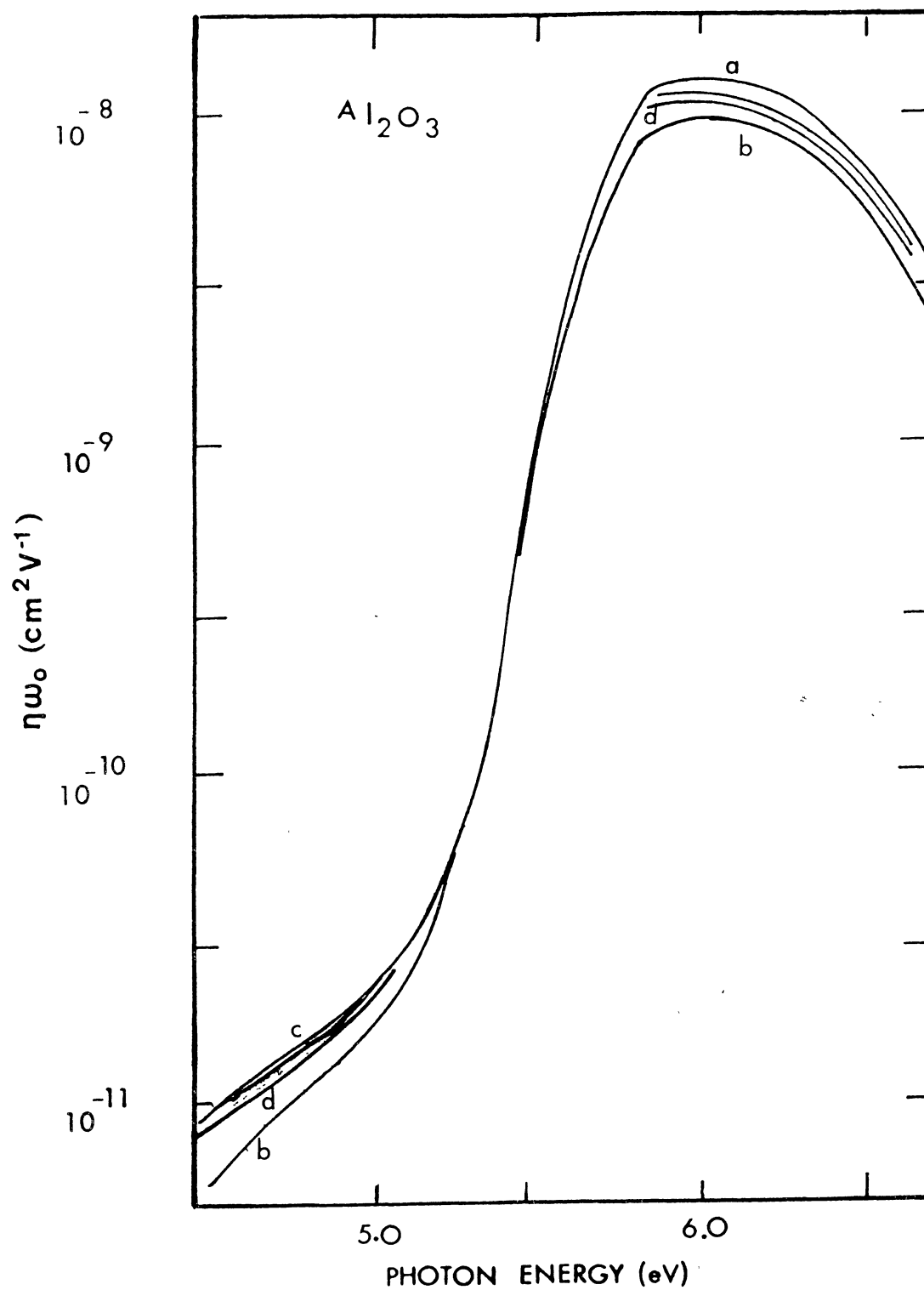


Figure 31. CS PC at RT; Curve a, Initial scan; Curve b, 6th scan; Curve c, 200 nm Bleach; Curve d, 250 nm Bleach

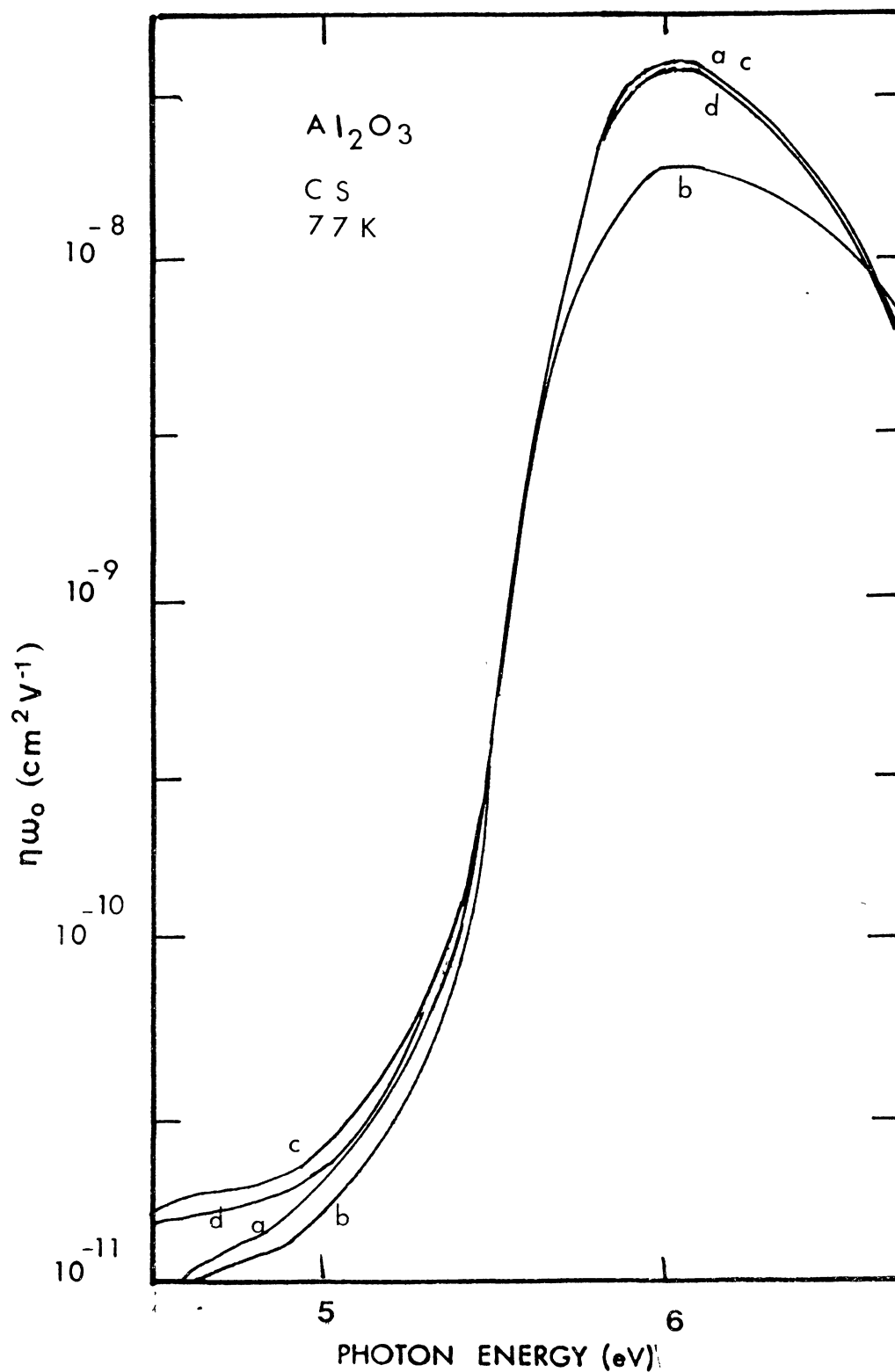


Figure 32. AM PC at 77 K; Curve a, Initial scan; Curve b, 6th scan; Curve c, 200 nm Bleach; Curve d, 250 nm

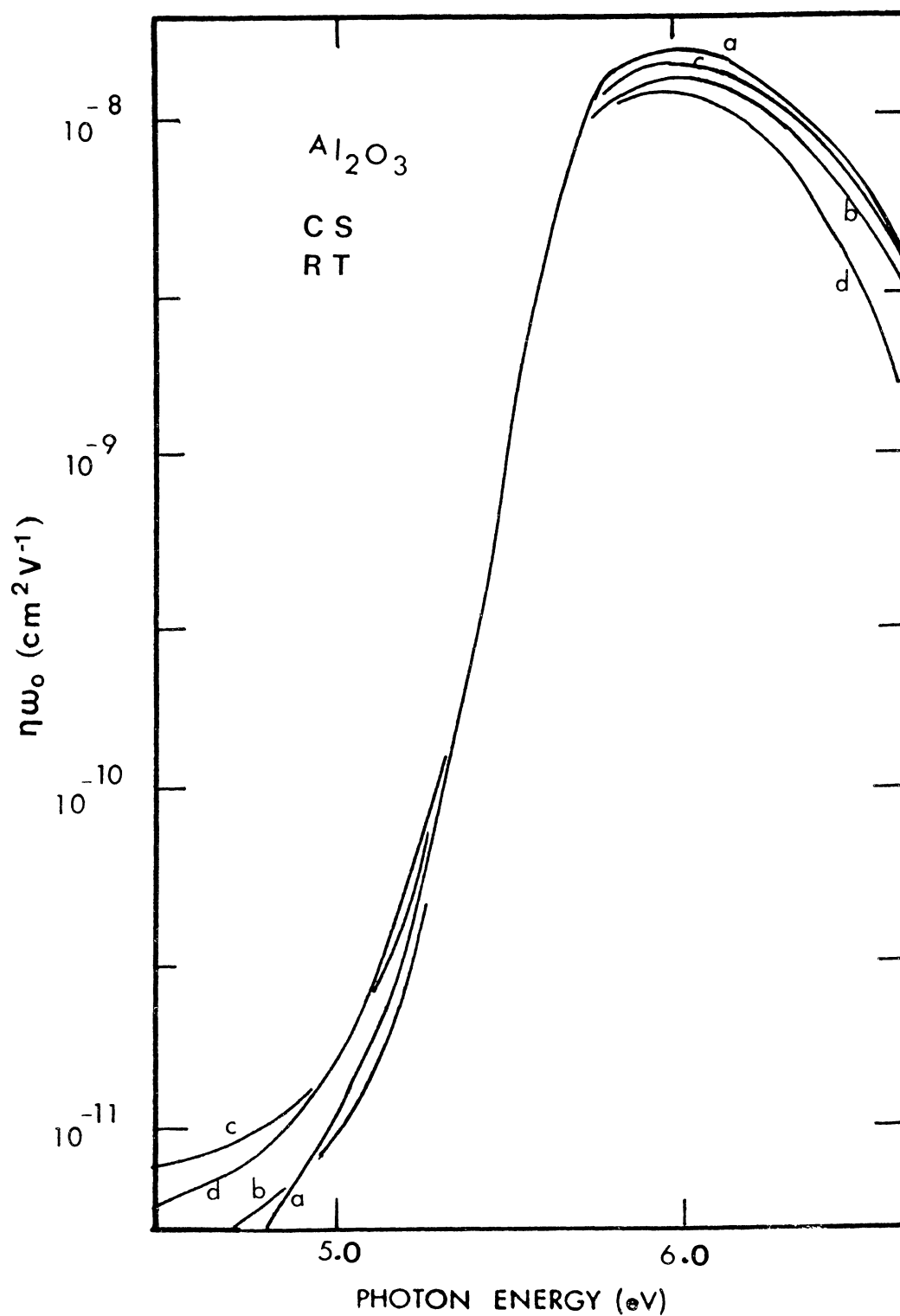


Figure 33. AM PC at RT; Curve a, Initial scan; Curve b, 6th scan; Curve c, 200 nm Bleach; Curve d, 250 nm

For the INSACO crystal, repeated scanning from 4 to 6 eV caused the photoresponse to decrease both at 6 K and 77 K. After optically bleaching the crystal at 6.1 eV the photoresponse increased an average factor of 2.5. Bleaching with 5.0 eV light the photoresponse decreased not quite by a factor of two. During the above optical bleaching process the 5 eV shoulder exhibited the same behavior. At room temperature repeated scanning had little effect on the 6 eV peak but slightly increased the 5 eV shoulder's photoresponse. 6.1 eV bleaching increased the photoresponse over the measured energy spectrum and 5 eV bleaching increased the 6 eV peak while decreasing the 5 eV shoulder.

The Crystal Systems and Adolph Meller crystals both exhibited a decrease in the photoresponse for repeated scannings of the crystals. At 77 K, 6.1 eV optical bleaching increased the photoresponse back to the original value but the 5 eV bleaching had very little effect. However, at room temperature, the 5 eV bleaching effect was much more noticeable. It was similar to the effect shown in the INSACO crystal at 77 K. It was noticeable that the neither the CS or AM samples showed the 5.0 eV shoulder.

Figures 34 and 35 are the photoresponse for a Crystal Systems crystal with the local electric field vector parallel to the crystal's C axis. The photoresponse curves are essentially the same as the curves with the exciting light perpendicular to the C axis.

In Figure 36, curve a is the photoresponse of a Crystal

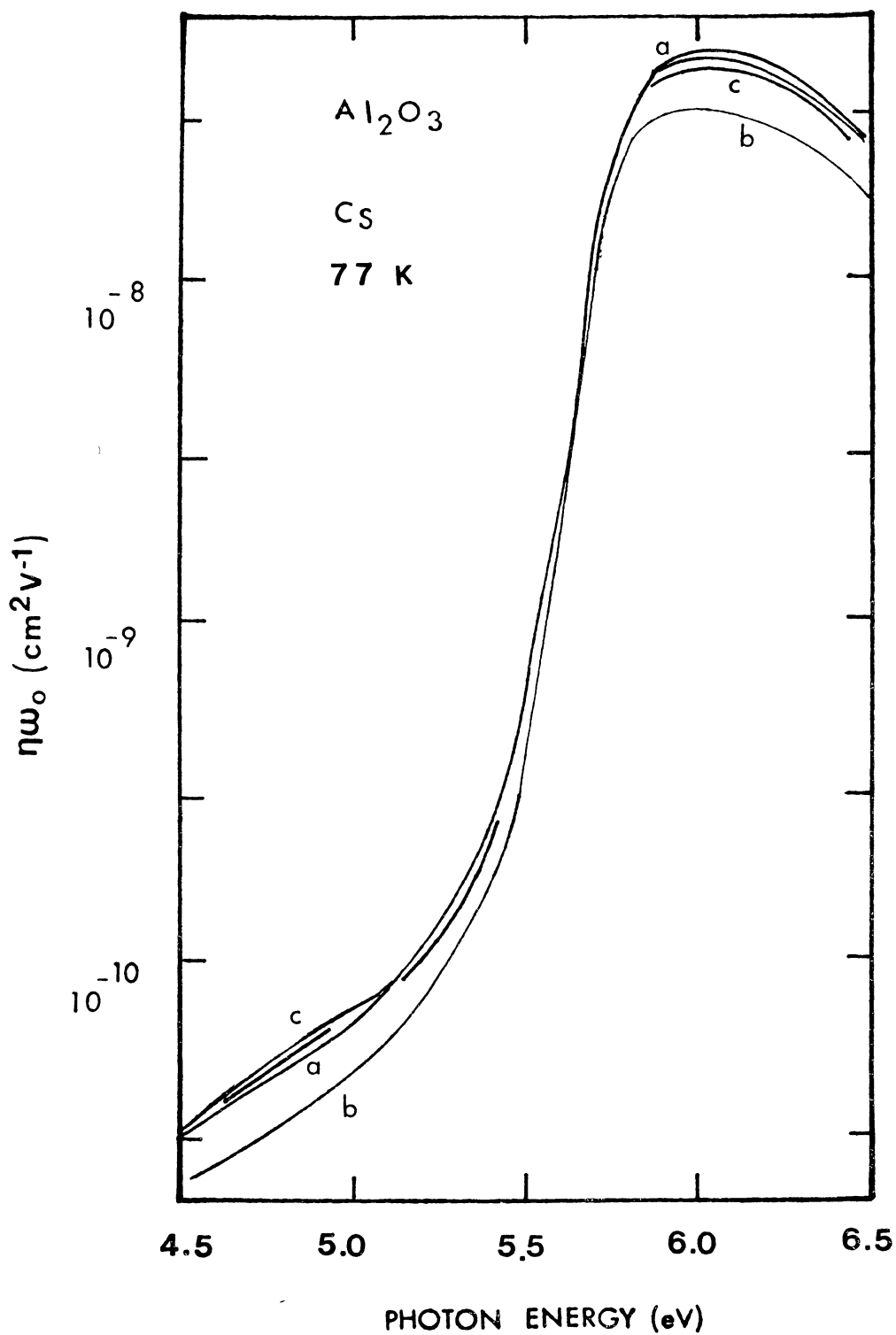


Figure 34. CS PC at 77 K; Curve a, Initial scan; Curve b, 6th scan; Curve c, 200 nm Bleach; Curve d, 250 nm

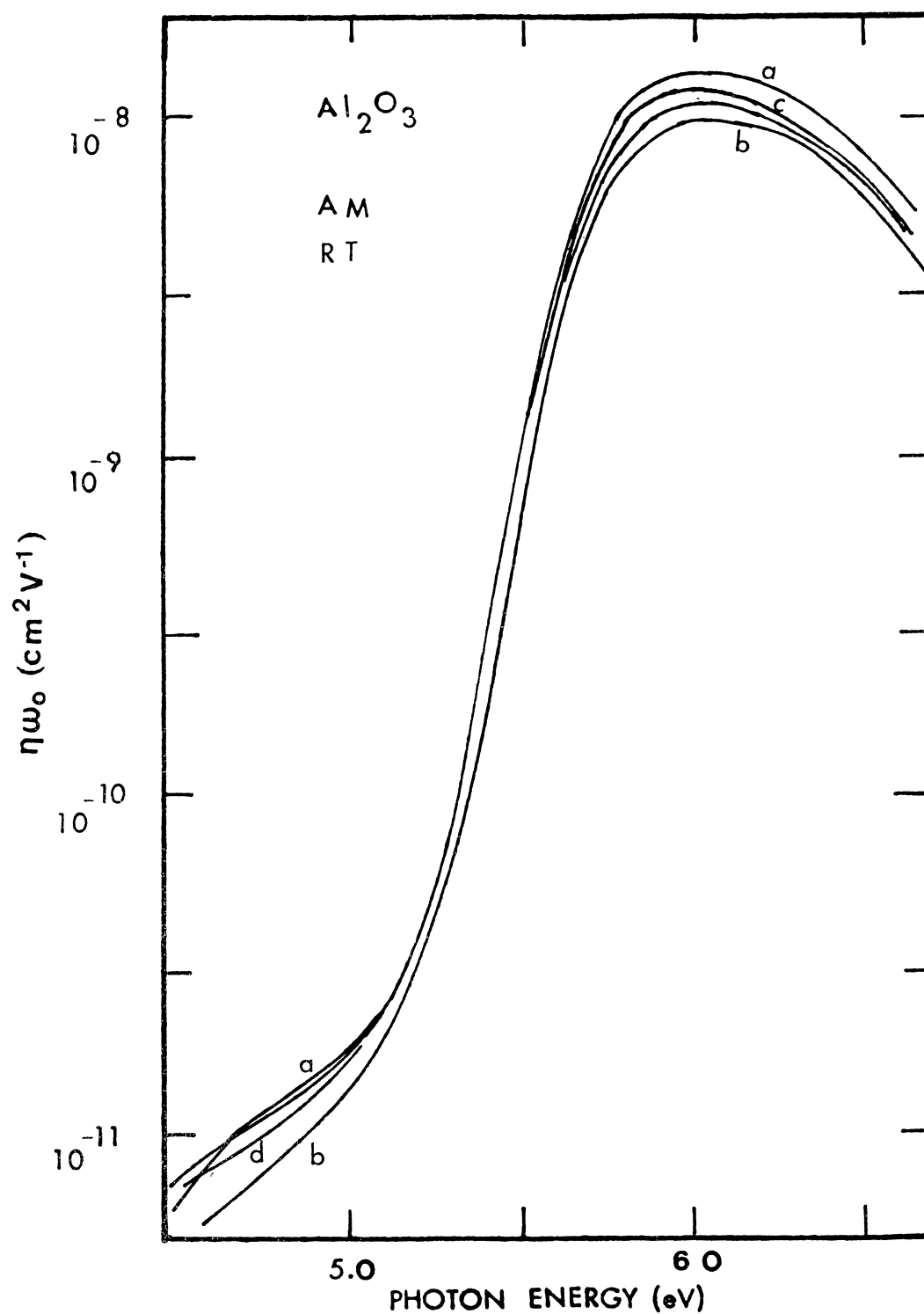


Figure 35. CS PC at ; Curve a, Initial scan; Curve b, 6th scan; Curve c, 200 nm Bleach; Curve d, 250 nm Bleach

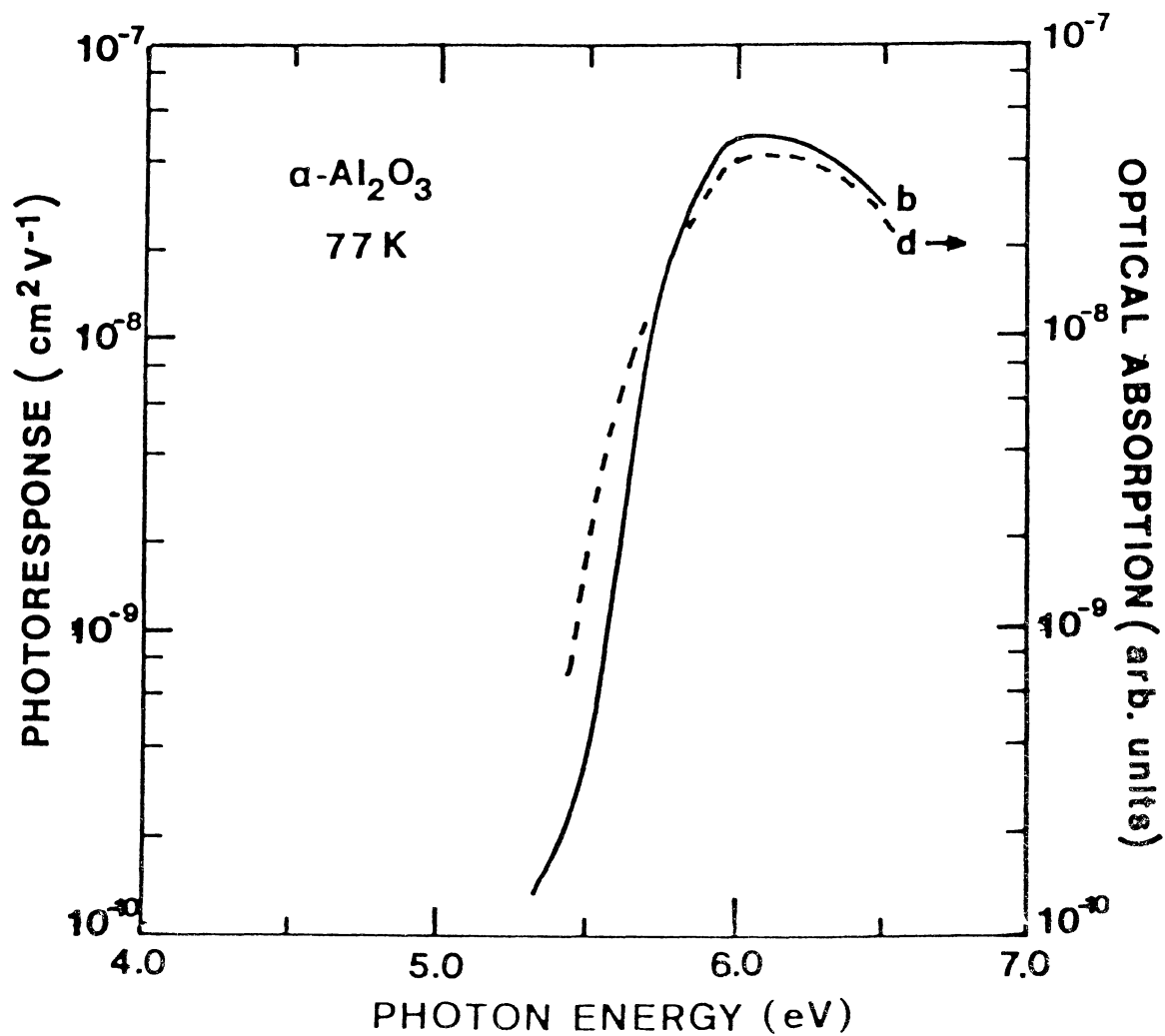


Figure 36. Photoconductivity vs Optical Density.
b, photoresponse; c, Optical density

Systems crystal at 77 K and curve b is a plot of the optical density of that crystal. The similarity of the two curves shows that the 6 eV photoresponse is due to the excitation of the F center electrons into the conduction band of the crystal.

The photoresponse per absorbed photon can be calculated by dividing the photoresponse by the fraction of photons absorbed by the crystal. At 6.1 eV for the INSACO and the Crystal Systems crystals, the photoresponse per absorbed photon is 3.74×10^{-9} and 6.38×10^{-8} respectively. This means that the mean range of the charge carriers (electrons) is approximately six times longer in the Type II CS crystal than in the INSACO sample.

Figure 37 shows the relative photoresponse of an INSACO compared to an Adolph Meller crystal as a function of temperature. The exciting light fell on the crystals for as short a time as possible and the measurement was repeated three times at each temperature. The photocurrent of each crystal was normalized at a temperature of 200 K. The two curves were similar until the temperature reached approximately 200 K. Above 200 K the relative photoresponse of the Type I, INSACO, crystal increased significantly until approximately 240 K. This increased photoresponse is due to an increase in the mean range of the carriers caused by the thermal emptying of the electron trap.

Figure 38 shows the same experiment for a crystal irradiated with a dose of approximately 5×10^{16} neutrons/cm².

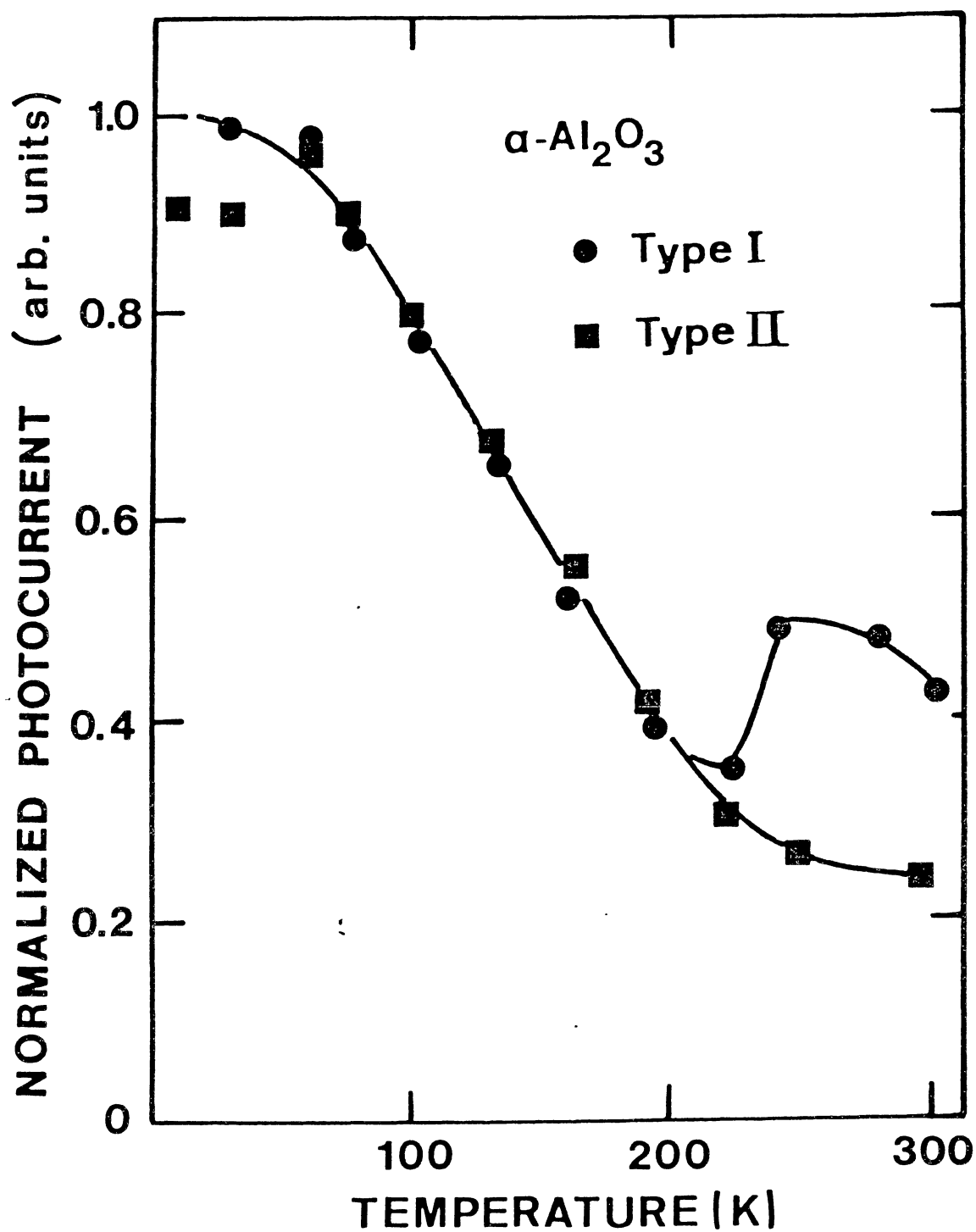


Figure 37. Relative Temperature Dependent PC

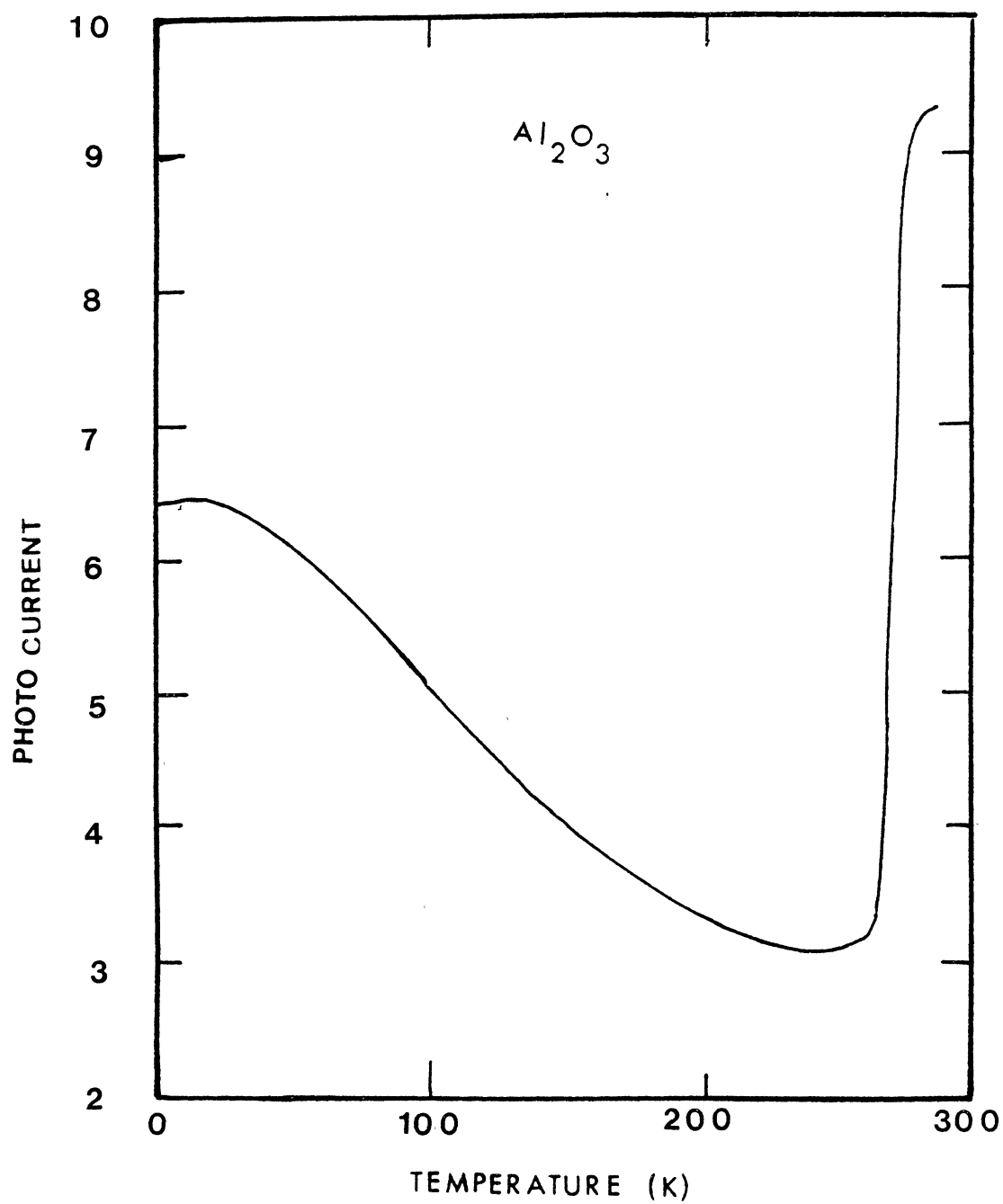


Figure 38. Temperature Dependent PC,
Neutron Irradiated

The difference exhibited by this crystal is the increase in the mean free path occurs at approximately 270K. This electron trap is most likely due to the presence of H^- ions present in oxygen vacancies as is determined by the experiments on MgO shown in the next chapter.

Thermoluminescence

The following section describes the thermoluminescence of growth colored crystals of Al_2O_3 which have been classified as Type I or Type II previously. Also included are studies on crystals obtained from Linde which are relatively free of defects. These crystals were irradiated using several different means to study electron traps.

Figure 39 shows the thermoluminescence (TL) for three growth colored crystals. Curve a is for a Type I crystal while curves b and c are for Type II crystals. The optical density of the Type I crystal is approximately twice that of the Type II crystals. This difference in the optical densities does not account for the difference in the magnitude of the TL curves.

Figure 40 is a plot of the leading edge of the Type I crystal. This curve shows that the trap responsible for the 260 TL peak has an energy depth of 0.728 eV which agrees very well with other experiments (10,26). Figure 41 shows the plot of curve c. This curve shows that the trap associated with the 230 TL peak has an energy depth of 0.578 eV.

Figures 42 and 43 show the results of studying the

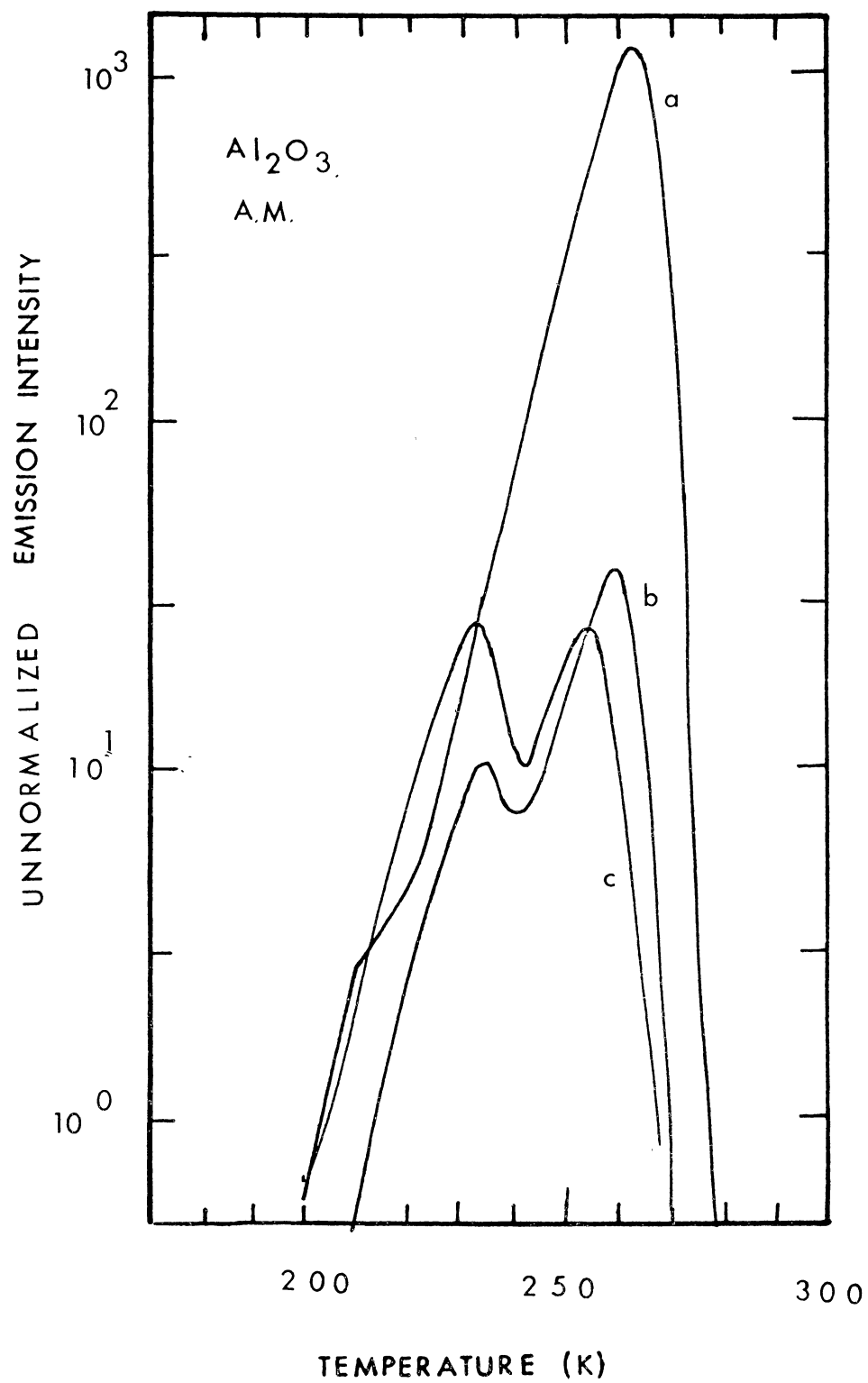


Figure 39. Thermoluminescence

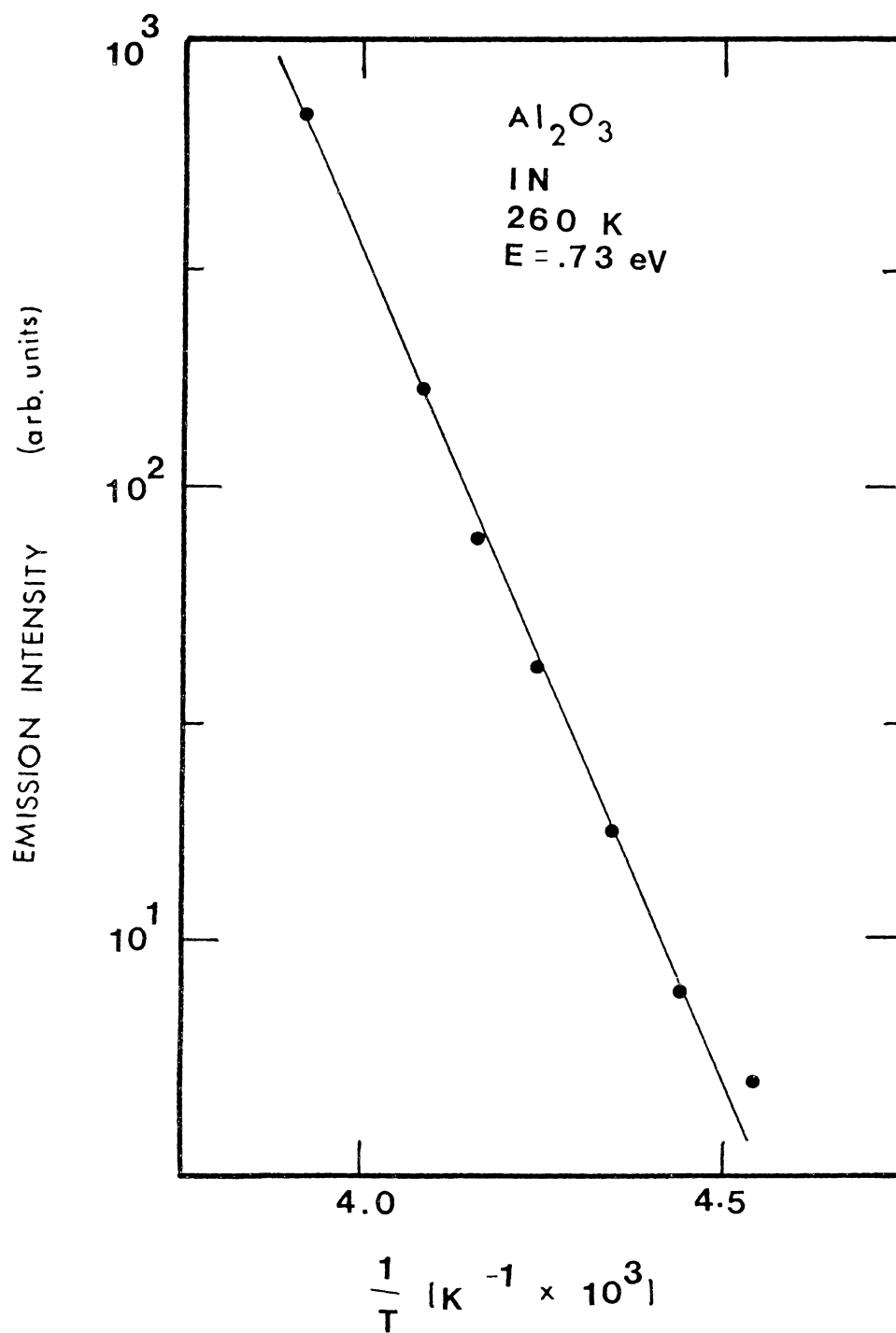


Figure 40. Leading Edge Plot

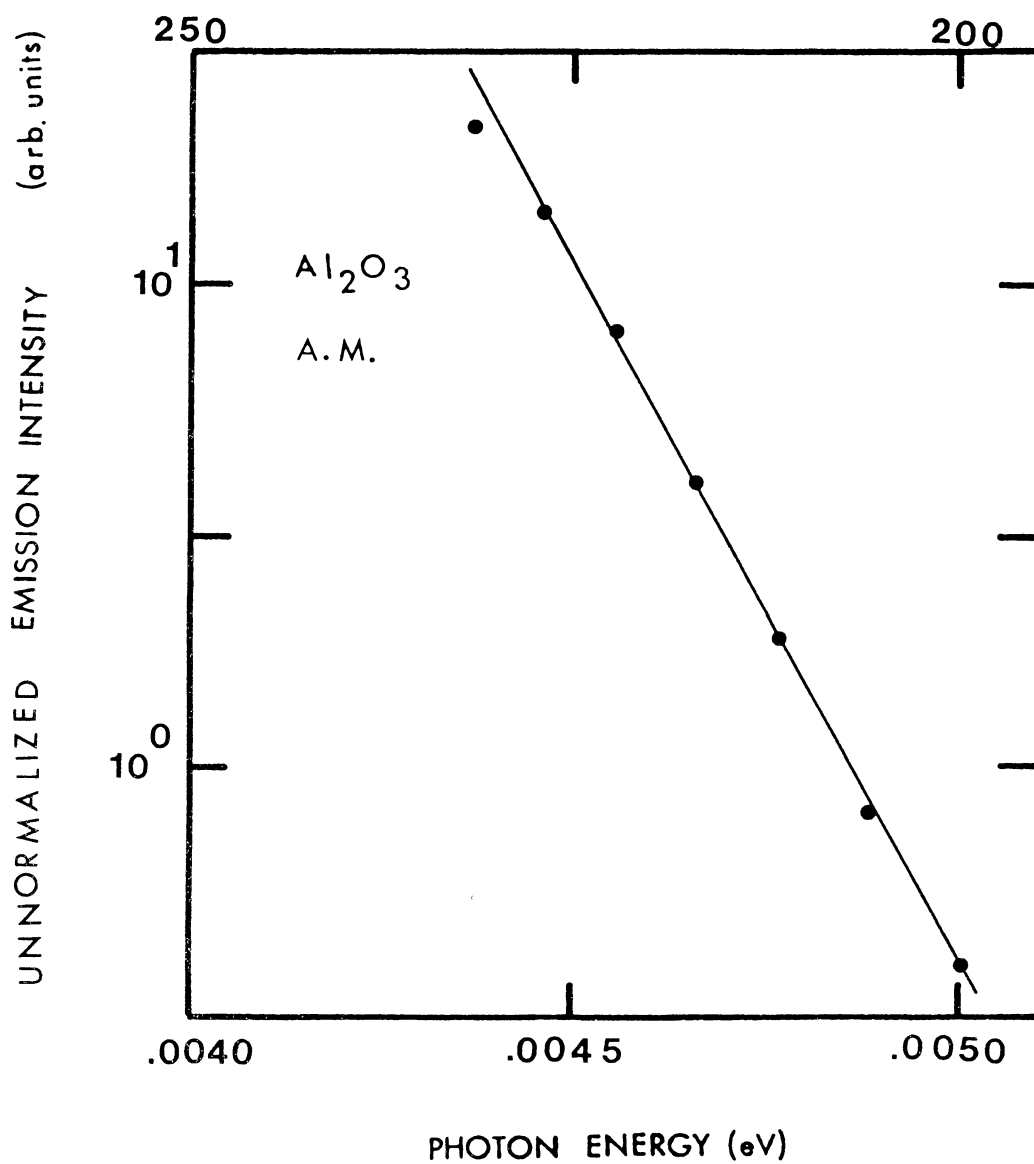


Figure 41. Leading Edge Plot

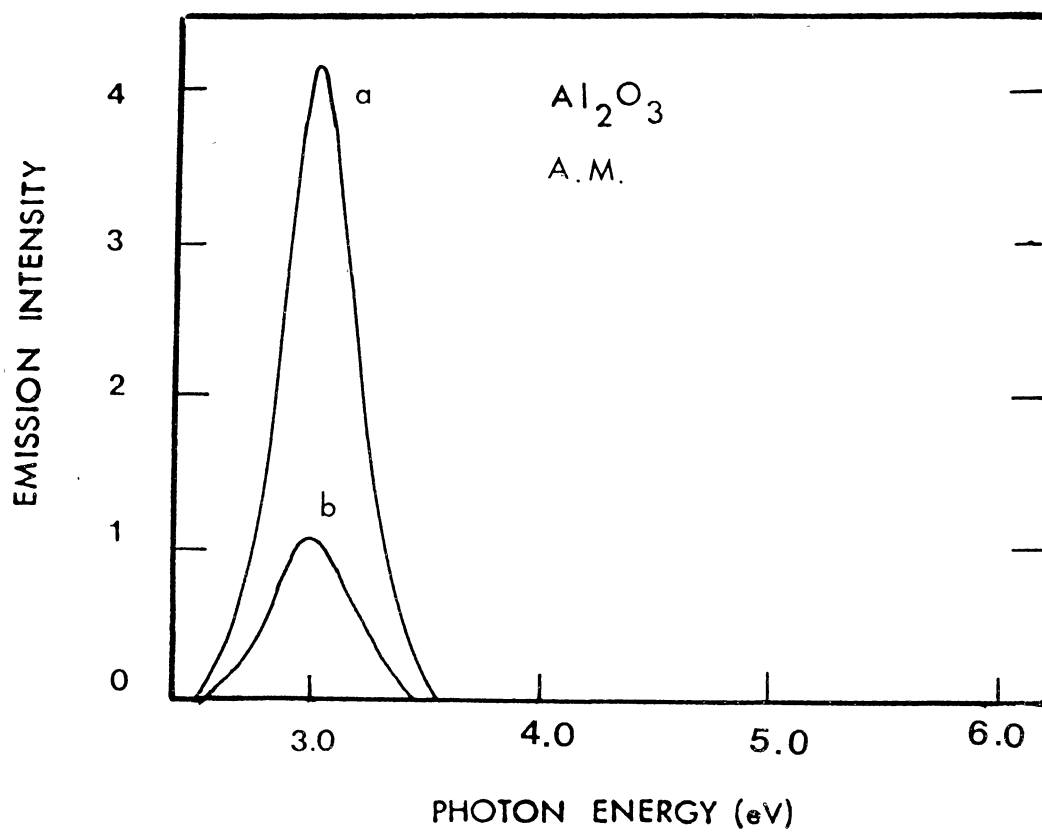


Figure 42. Type 11 TL Emission Spectrum

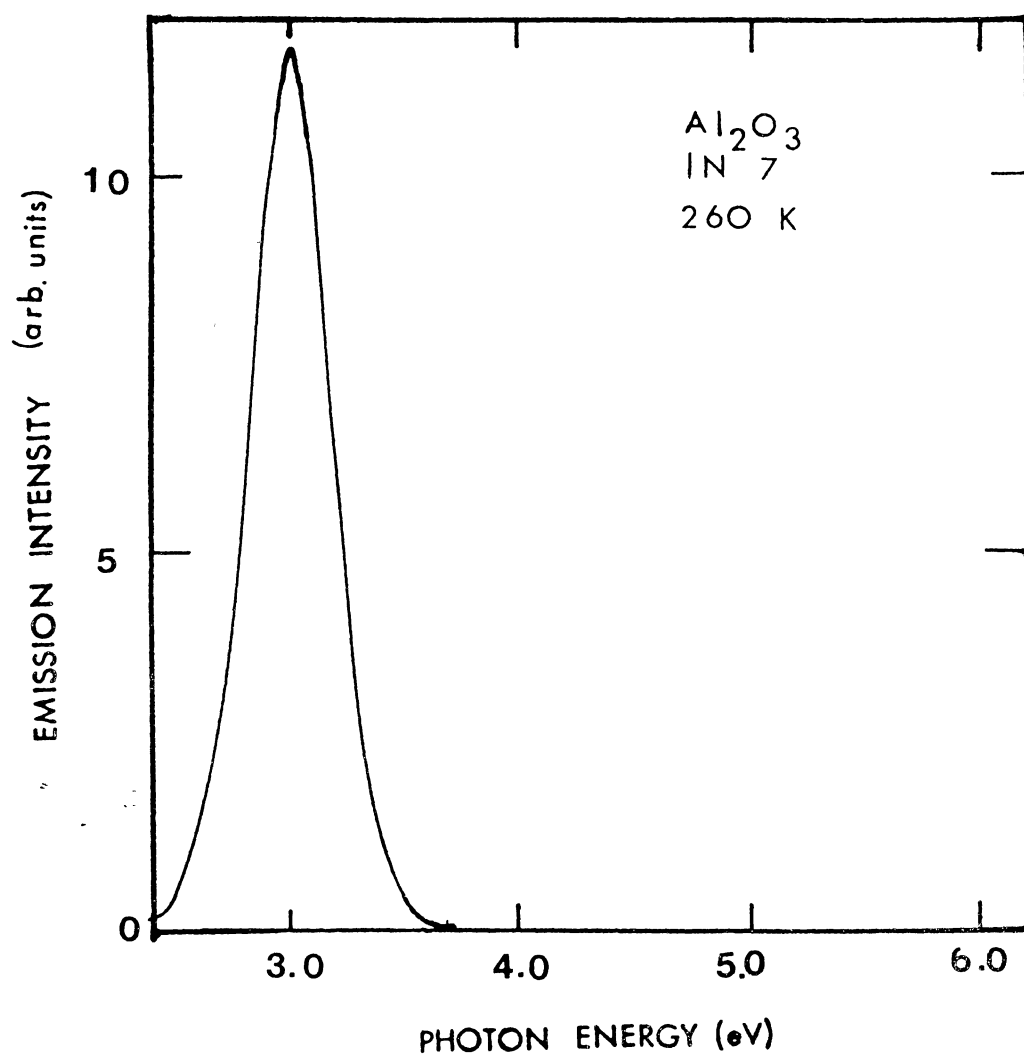


Figure 43. Type I TL Emission Spectrum

spectral dependence of the emission spectrum of the additively colored crystals. The first figure shows that for the type II crystals only F center emission was observed for both of the peaks. The second figure gives the same results for the large peak exhibited by the Type I crystal. Figure 44 shows another TL peak of another Type I.

Figure 45 shows the results on an as received Linde crystal of bleaching at different excitation energies. For curves a and c the bleaching was done at 4.9 eV and for curve b the bleaching was done at 6.2 eV. The curves show that the bleaching significantly effected the 260-270 peak with a much smaller effect upon the 230 peak. Figure 46 shows a study done on the same crystal approximately one year later. Curve a shows the TL before the study was started. Curve b shows the TL approximately one hour after the crystal was irradiated with gamma radiation obtained from using one MeV electrons. Curve c is the TL obtained approximately three weeks after curve b. The TL had decayed significantly over that period. Gamma radiation does not produce F centers in Al_2O_3 so another mechanism was responsible for the large increase and then fairly rapid decrease of the TL. F centers do not anneal out in this manner.

Figures 47, 48, and 49 show a study done on another Linde crystal. Curve a in Figure 47 shows the TL after the crystal was irradiated with approximately 10^{16} electrons. This crystal was then annealed for 15 minute spans at

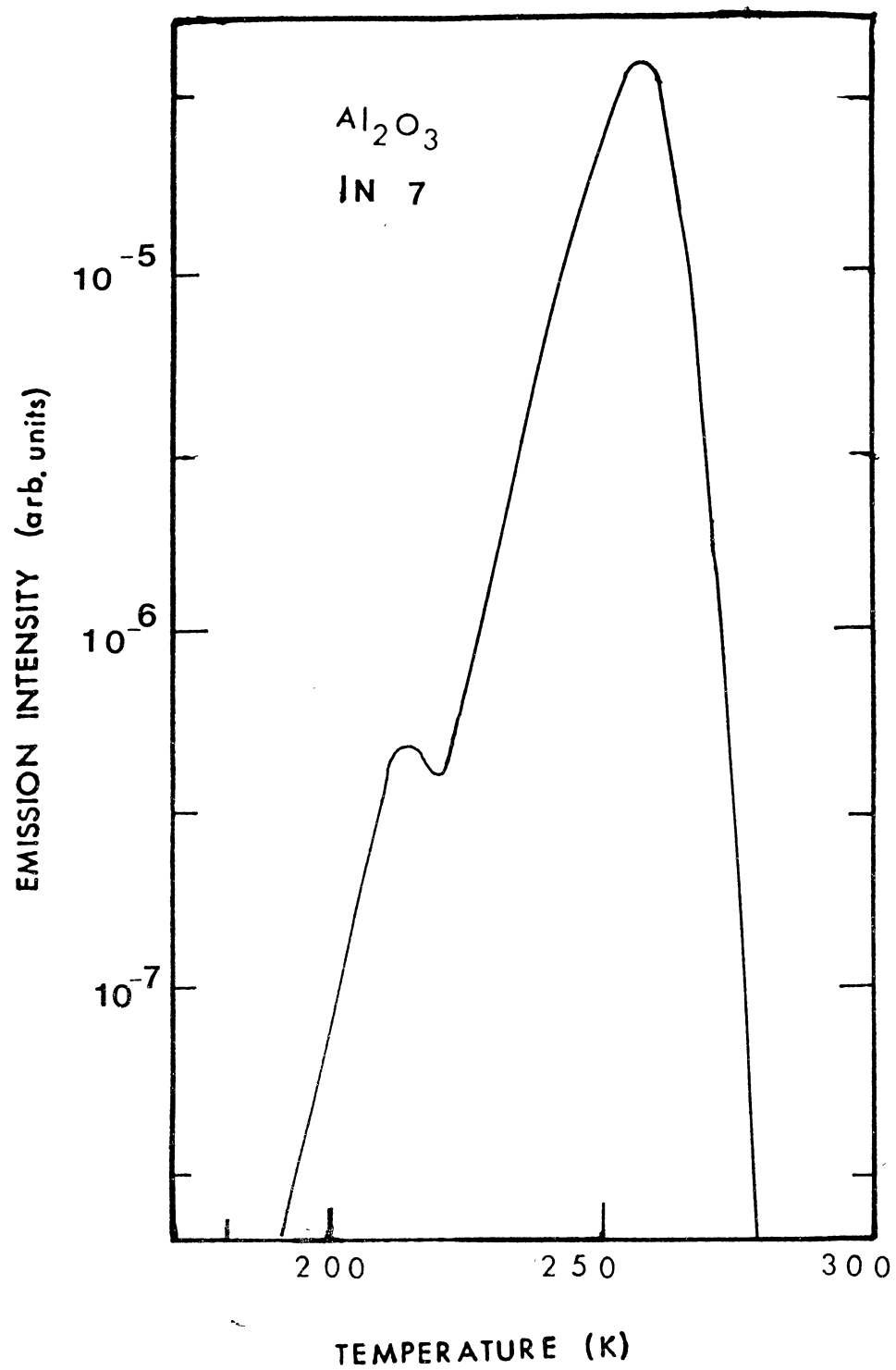


Figure 44. Type I TL Peak

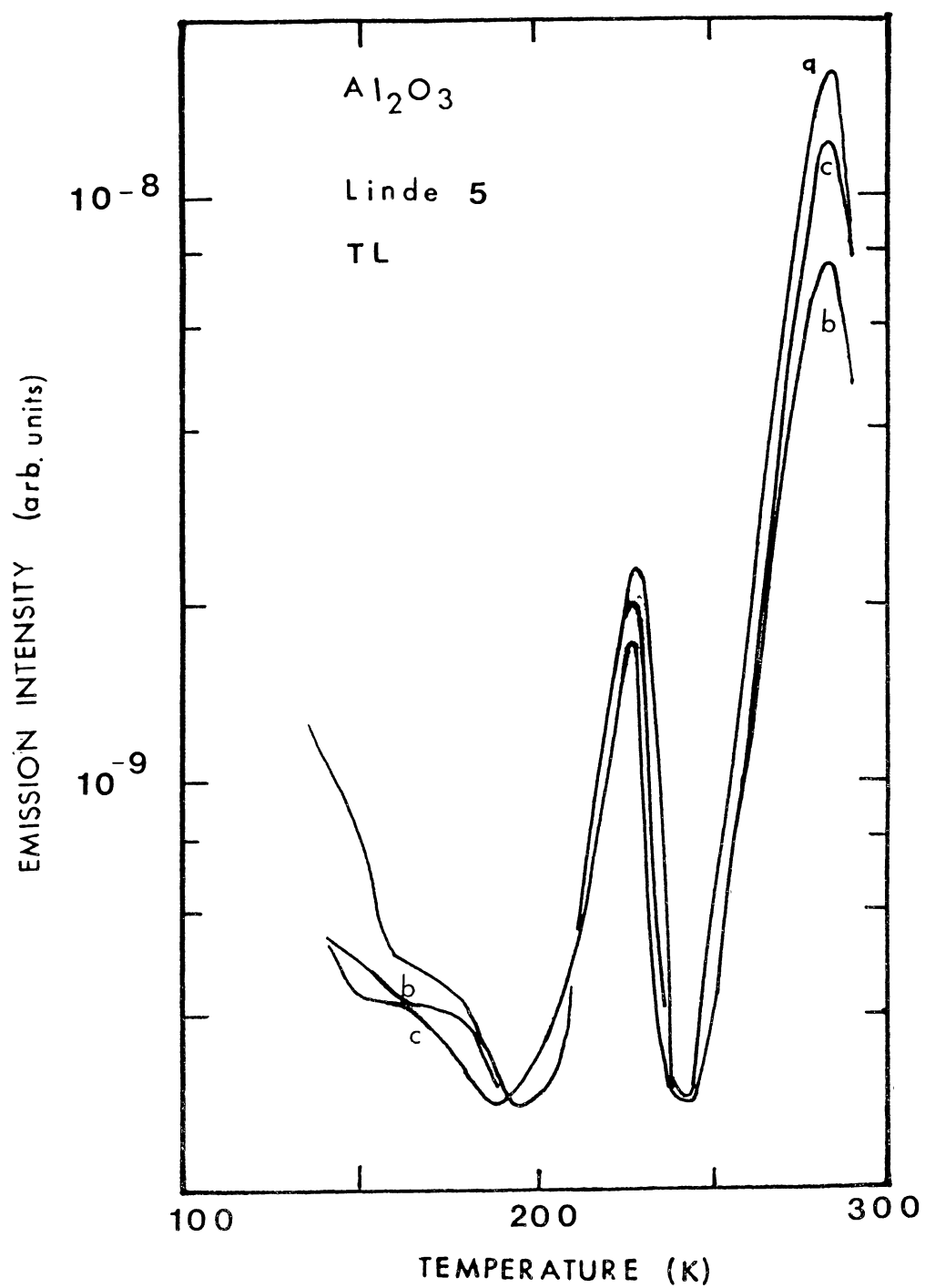


Figure 45. Linde TL Peaks vs Bleaching

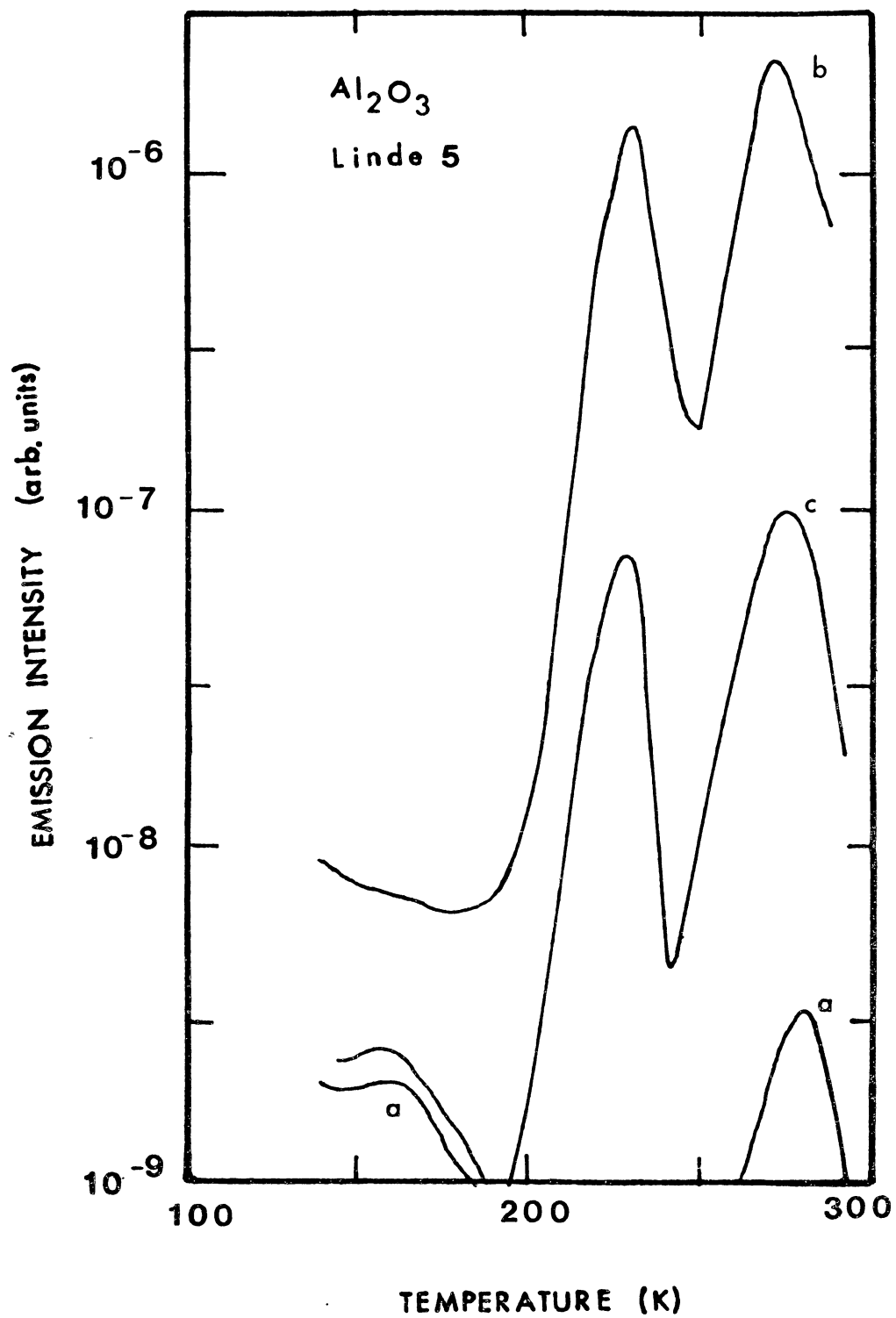


Figure 46. Linde TL Peaks vs Gamma Irradiation

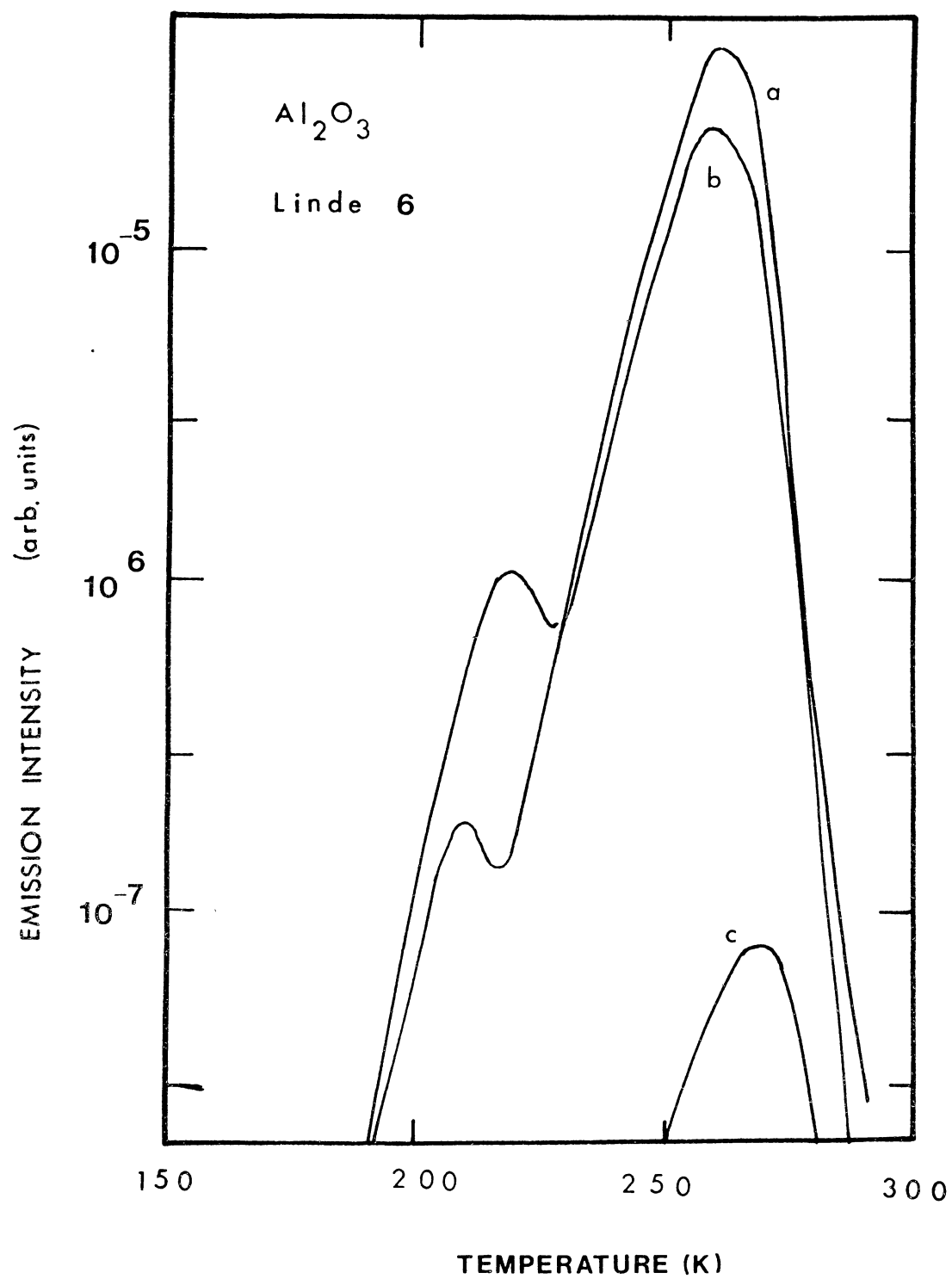


Figure 47. Linde TL vs Anneal

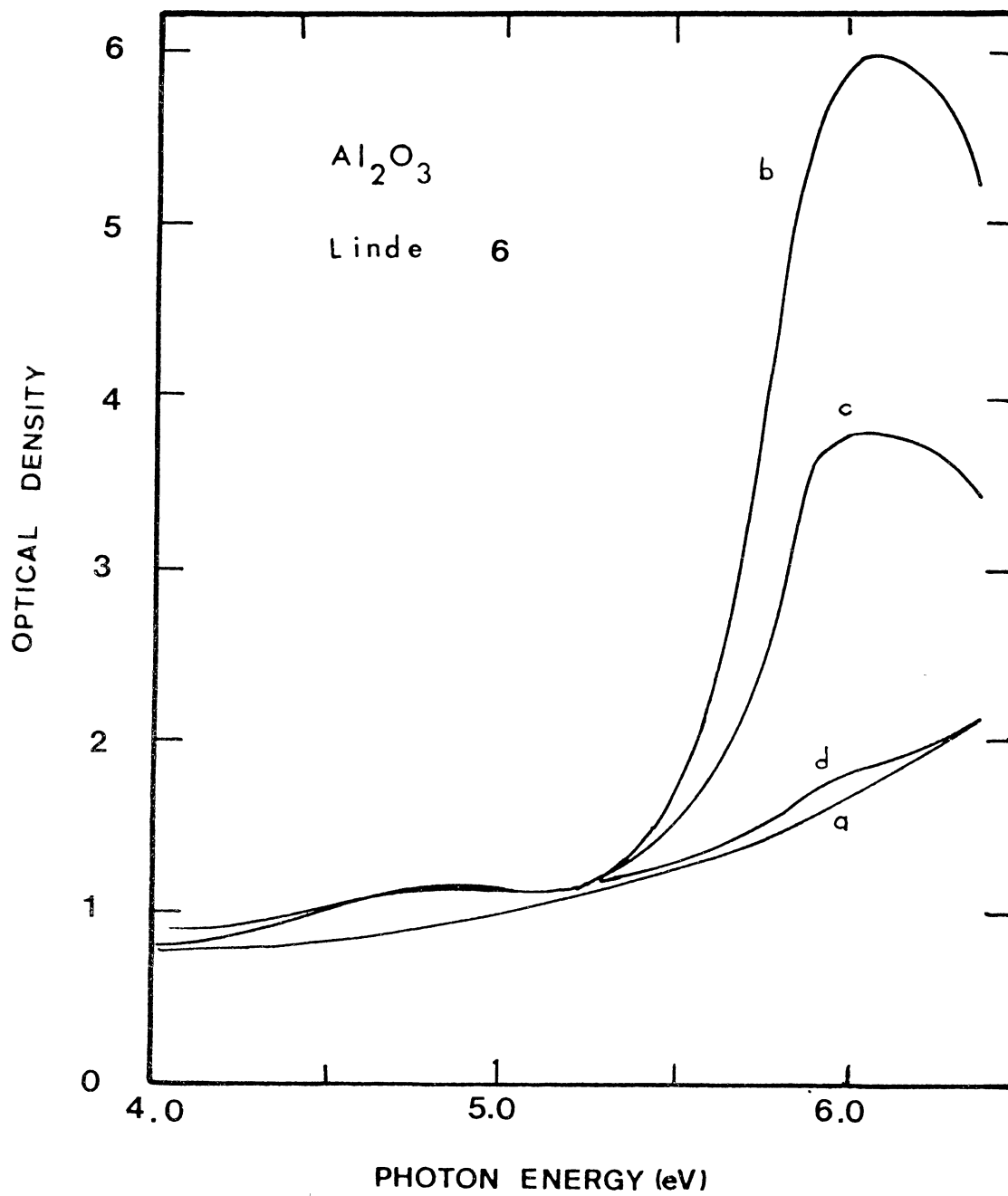


Figure 48. Linde Optical Density vs Anneal

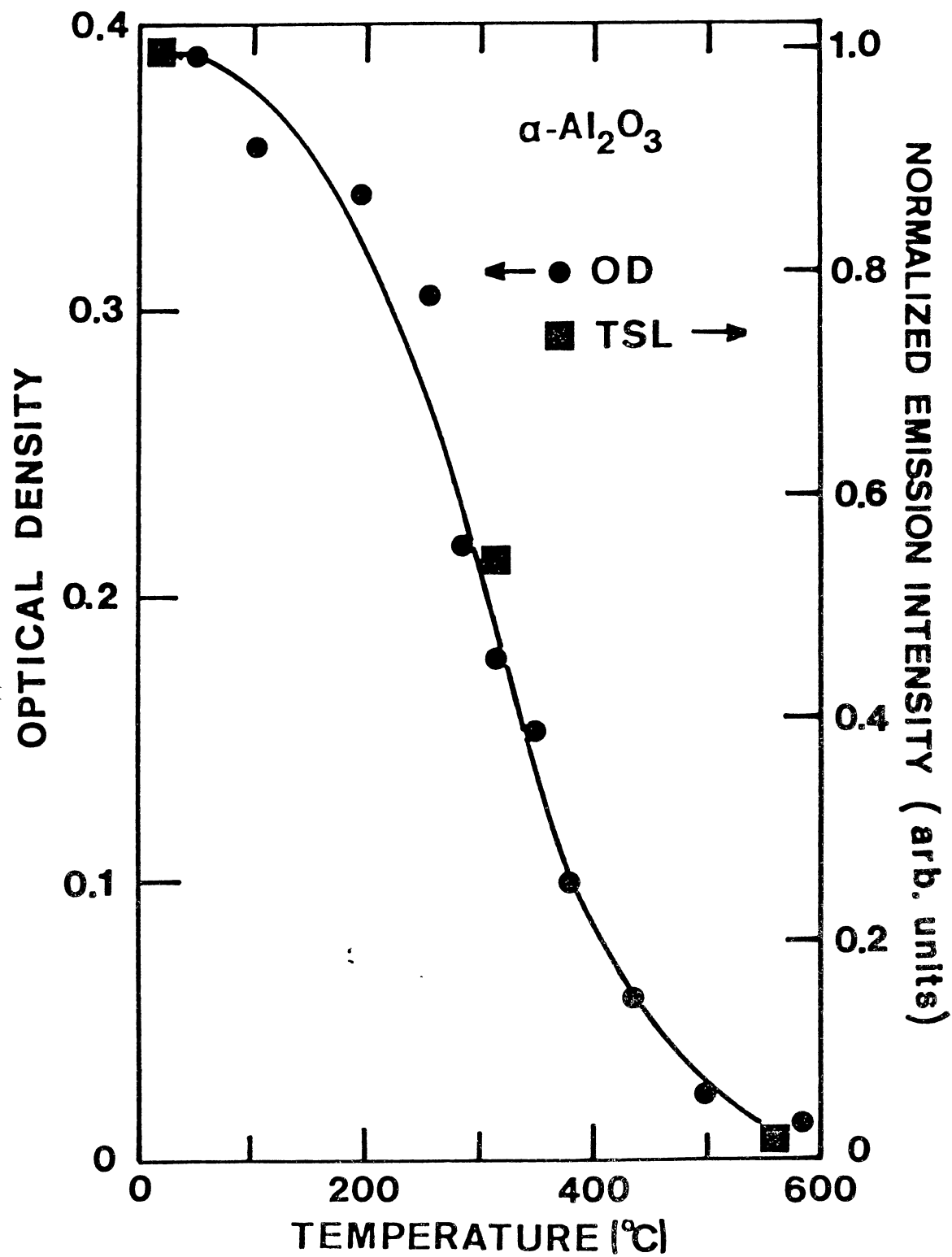


Figure 49. Linde Anneal Comparison

successivly higher temperatures. The temperature change was approximately 50 K but did vary. Curve b was obtained after the anneal at 586 K and curve c was obtained after the final anneal at 861 K. Figure 48 shows the corresponding optical density curves. Curve a was taken before the electron irradiation and curve b was taken ater. Curve c was taken after the 586 K anneal and curve d after the 861 K anneal. Figure 49 shows a plot of the optical densities and the TL as a function of the anneal temperature. The decrease in the TL intensity of the 260 K peak is shown to be related directly to the relative number of F centers present. Figure 47 shows that the 230 K peak anneals out much faster.

Figure 50 shows the effect of neutron irradiation upon the TL of three Linde samples. The crystals were irradiated with neutrons at the rate of 10^{16} neutrons per cm^{-2} per minute. Curve a shows the TL for a crystal irradiated for 17 minutes, curve b for 83 minutes, and curve c for 500 minutes. The TL increases up to curve b but has decreased by the time curve c was taken. This is due to the increasing closeness of the produced F centers. This closeness accomidates non-radiative recombination of the electrons with the F centers. This is more clearly shown in the next section. Notice that the 230 K TL appears later but follows the same trend.

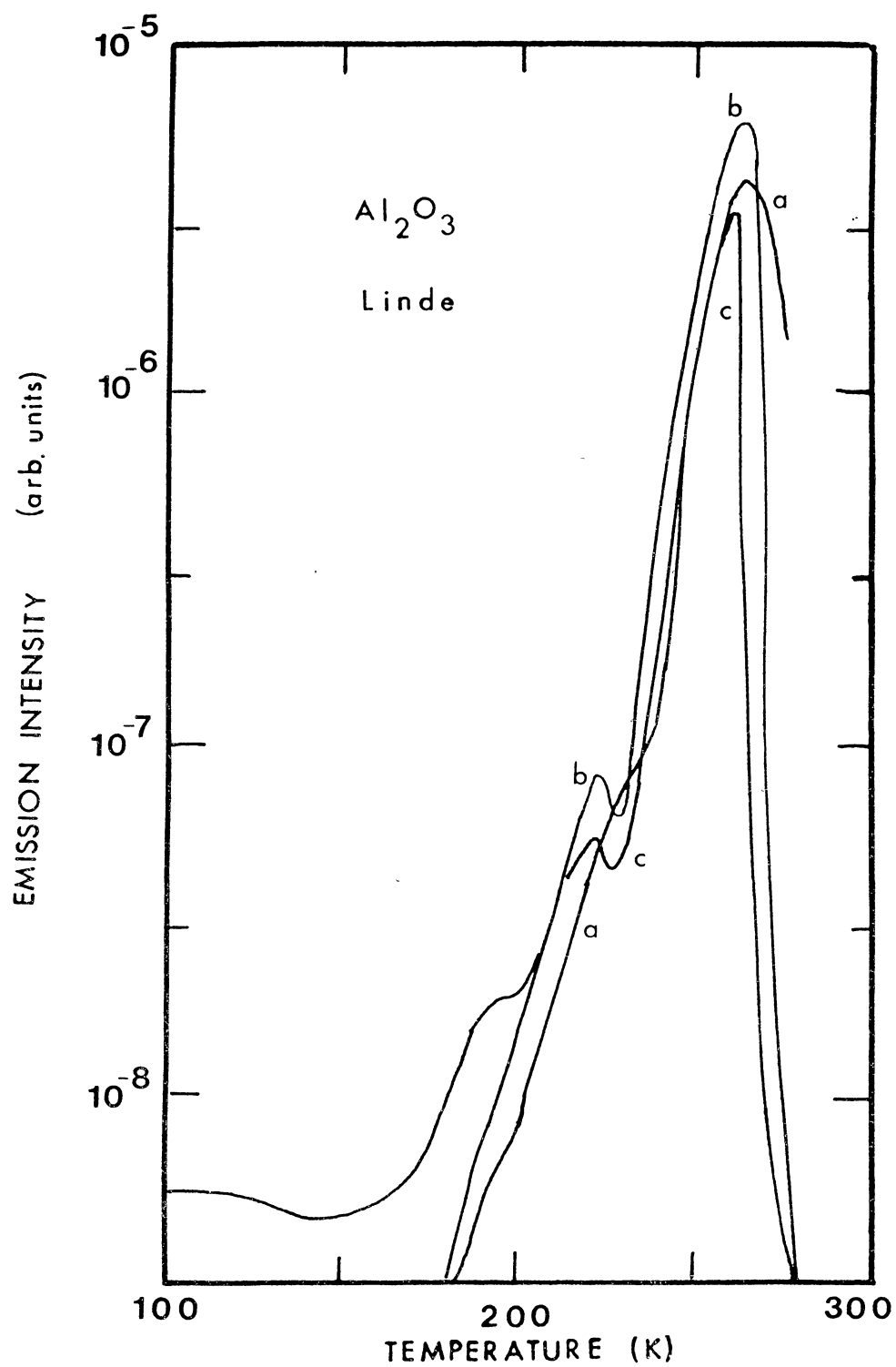


Figure 50. Linde TL vs Neutron Irradiation

Fluorescence

The following study was done on a crystal obtained from Union Carbide and irradiated with 10^{17} neutrons. The crystal was annealed for 15 minutes at successively higher temperatures. After each anneal the fluorescence peak intensity at 3.0 eV was measured at room temperature using 6.1 eV excitation. Also the optical density was measured. The fluorescence peak intensity was divided by the optical density to obtain the relative intensity per F center. Figure 51 shows this plotted as a function of the anneal temperature. Also plotted is the absorption coefficient as a function of the temperature. From the figure it is seen that neither the number of F centers nor the relative intensity per F center does not change until the anneal temperature reaches approximately 473 K. Above this temperature the relative intensity per F center increases rapidly and the number of F centers decreases. This effect is caused by concentration quenching of the F center optical emission. As a check, a Crystal Systems, Type II, emission was used as a comparison because its absorption coefficient of 10 was comparable to that of the neutron irradiated crystal. It displayed an emission intensity per F center of approximately 30 for an exposed surface the same as that of the neutron irradiated crystal. This made it quite obvious that concentration quenching was present.

Also plotted in the figure are the points for the F+ centers. The effects show only a small increase in the

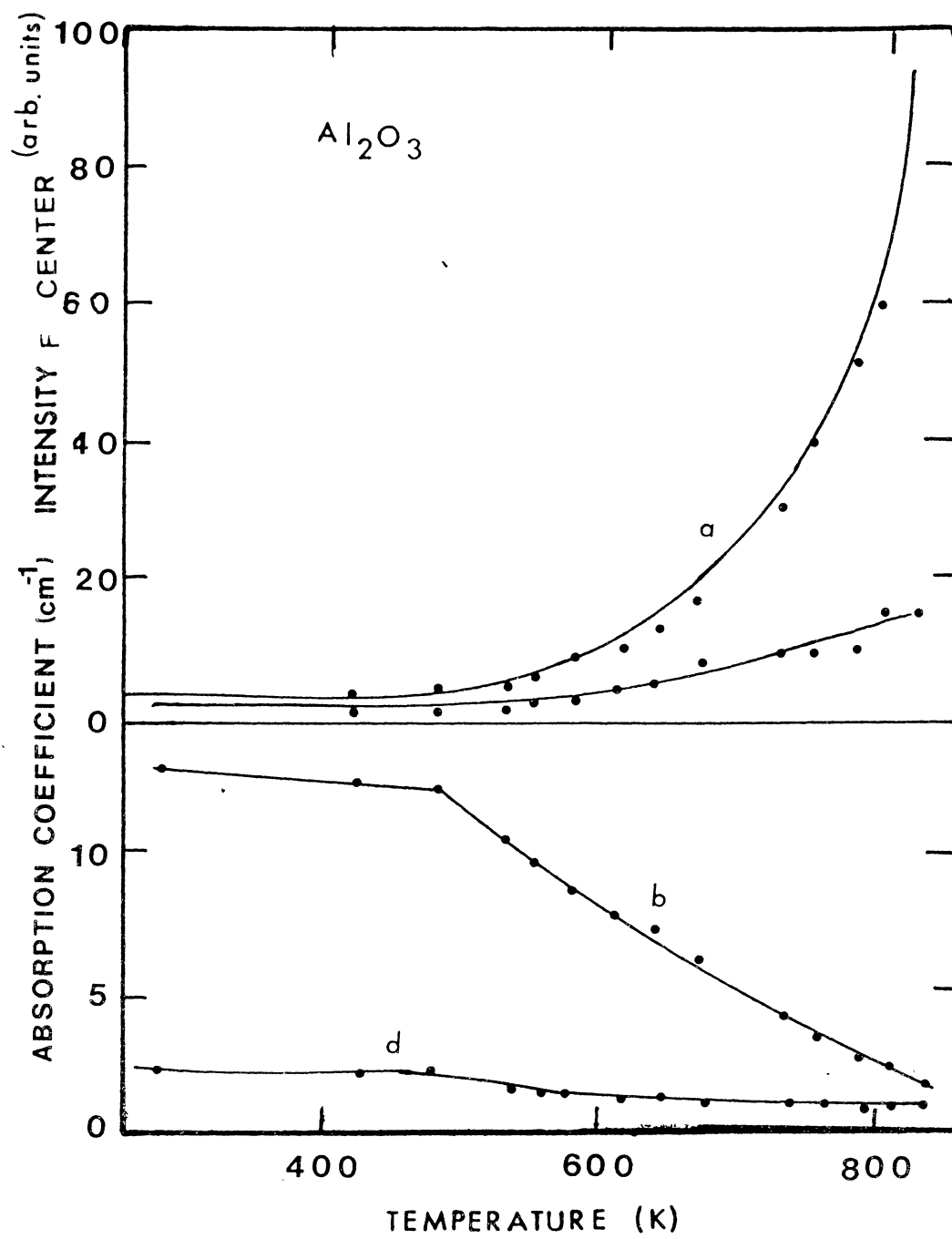


Figure 51. Concentration Quenched Anneal Study

intensity per F+ center with a decrease of 50 percent in the absorption coefficient. This is much less than for the F center. Another sapphire crystal that had been irradiated with 10^{16} neutrons/cm² was examined. The F center concentration was an order of magnitude less and the 3.0 eV band and could barely be seen. After it was annealed for 15 minutes at 770 K, its intensity per F center was at approximately 10 on the figure's scale.

Analysis and Discussion

The experimental results are discussed in relation to the electron traps present and to the physical properties of the F center. Some of the results obtained by Brewer et al. (22) are compared to these results.

The optical density measurements show that the conversion between F and F+ centers is more pronounced in the type I INSACO crystal than in the type II Crystal Systems and Adolph Meller crystals. This is shown by the relative changes in the 6.1, 5.4, and 4.8 eV band intensities at 77 K. 6.2 and 4.96 eV were used as the two bleaching light energies. This interconversion is also shown in the photoconductivity results for the INSACO crystal and it is quite small for the type II crystals. The photoresponse shows that the electron is effectively released from the excited F center into the conduction band at temperatures as low as 6 K.

The trap responsible for the effects at temperatures

below 77 K is not as effective at room temperature. This is shown by the room temperature photoconductivity of the INSACO crystal where the interconversion was relatively smaller. The bleaching effect was especially small on the 6.1 eV band where at lower temperatures the photoresponse dropped much more after the crystal had been illuminated for some time showing the effect of the presence of an electron trap.

The efficiency of an absorbed photon in exciting an electron into the conduction band appears to be very high even at 6 K. This is shown above by the fact that the photoresponse is bleached at 6 K and also by the curves in Figure 37. These curves, which show the temperature dependent normalized photocurrent for the 6.1 eV peak, start at a maximum at low temperatures. The small initial intensity variation is not the same for all crystals and the cause is not known. The decrease in the photocurrent for both type I and II crystals is caused by a decrease in the mean range per unit electric field (w_0) of the photoconducting electrons if the quantum efficiency can be assumed to be equal to one over the entire temperature range. w_0 depends upon the effective mobility and the trapping time. The effective mobility is expected to decrease as the temperature increases because of scattering by phonons. The observed temperature dependence of w_0 also depends upon other factors also such as the ratio of the trapping time to the reemission time.

In the type I crystal there is the large TL peak at 260 K with a small shoulder at 220 K. The increase in w_0 in type I crystals is caused by the effect of this electron trap which decreases the reemission time. This trap is also responsible for the photoresponse at 6.1 eV being an order of magnitude smaller in Type I samples and for the interconversion of F and F⁺ centers below this temperature.

The nature of the two TL peaks is implied by several of the experiments performed. The experimental results showed that the 220 K peak could be produced by gamma radiation and that its intensity decreased to one twentieth of its maximum value if the sample were stored at room temperature over a period of four weeks. This is in contrast to the 260 K peak the intensity of which is affected by either electron or neutron irradiation.

As demonstrated, the 260 K peak is annealed by heating the crystal. Thus, the 220 K peak is most likely caused by a trap, most likely a hole released from an O⁻ ion located near a Mg impurity (27). The 260 peak is likely caused by electrons released from H⁻² ions. We have no definite proof of this identity but the similarity with the behavior in MgO is striking. The optical density of a thermochemically reduced type I crystal was studied as a function of annealing up to a temperature of 1500 degrees C (28). As the crystal was heated first at 1250 degrees C for 12 hours and then at 1500 degrees C for 12 hours, an absorption peak at 5 eV was formed. This energy coincides with the 5 eV

photoresponse peak evident in type I crystals. This peak introduced during the annealing may be due to an aggregation of defects such as vacancies. Although these two peaks cannot definitely be related it is possible that structural defects could act as electron traps.

The anneal study comparing the optical density of the electron irradiation induced F center with the peak height of the 260 K TL peak showed that both the TL peak and the F center annealed out together. This did not show if any traps were produced by the irradiation or if only F centers were produced.

Neutron irradiation produced the 260 K TL peak with a relatively very small 220 K peak. The luminescence in these crystals is much weaker than in electron or thermochemically colored crystals because of concentration quenching. The TL exhibited the same effect. The 83 minute irradiation TL peak was larger than that of the 500 minute irradiation.

The above discussed gamma irradiated crystal most likely exhibited only charge redistribution, and the electron and neutron irradiated crystals did not show definite creation of the 260 K TL peak but had results which were not inconsistent with it occurring. The strongest evidence for it originating from a structural defect were from the appearance of the 5.0 eV absorption peak in the annealed crystal.

A trap prevalent in oxides is caused by hydrogen being present in the crystal. Engstrom et al. (29) looked at the

3280 OH stretching mode in a crystal with a thickness of 12.7 mm and observed an absorbance of 0.025 which corresponded to a concentration of $2.6 \times 10^{16} \text{ cm}^{-3}$. The type I crystals had a thickness of one tenth of the above. The noise inherent in the spectrophotometer corresponded to a 0.001 absorbance and the absorption band at 3280 cm^{-1} was not observed. This showed that if the OH were present it had to be of a smaller concentration than $1.0 \times 10^{16} \text{ cm}^{-3}$. Thus we were not able to show the presence of hydrogen in sufficient concentrations. However, recent results in MgO suggest that H ions are likely electron traps in reduced oxides includingt sapphire.

The only other noticeable trap encountered was when the crystals were heated to 770 K. The light emitted was blue suggesting F center emission. Only the thermochemically colored crystals were heated to this temperature because particle irradiation produced F centers would anneal out at this temperature.

The anneal study on the neutron irradiated crystal showed the effect of concentration quenching on the F center emission. For crystals with the same absorption, the F center emission intensity is much smaller for neutron irradiated crystals than for thermochemically colored crystals. The F center concentration in the damaged areas of the neutron irradiated crystals was calculated to be approximately $2 \times 10^{19} \text{ cm}^{-3}$. The extent of the excited state wave function is expected to be on the order for those for other

oxides. The excited electron can easily escape into the conduction band and is expected to lie outside of the vacancy. This state is expected to be weakly bound and have a wide orbit. This coupled with the large concentration would imply that overlapping of the excited state wave functions would be very likely and allow non-radiative transitions to the ground state. The results shown in Figure 51 confirm this. The F center concentration starts to bleach out 475 K but the intensity per F center does not really start to increase until approximately 650 K. It is well defined where the oxygen ions start to migrate back to the vacancies. As expected because of their compact excited state orbitals and their relatively fewer numbers, the F⁺ centers show very little change in their intensity per F⁺ center.

The analysis of the temperature dependent photoluminescence showed a Stokes shift of 1.30 eV which gave an expected peak emission band energy of 4.8 eV. This does not agree with the experimental value of 3.0 eV. The following model is used to explain this discrepancy.

The local C_{2v} symmetry of the F center is shown in Figure 2. The ground state is expected to be a $1A_1$ state with an optical transition to a p -like excited state. This excited state will lie very near to the conduction band. The F⁺ center shows three bands in absorption, whereas the F center band shows only one absorption band. This is due to the excited state of the F center being very near the bottom

of the conduction band and the wave function being quite extended. This fact was brought out in the above discussed concentration quenching of the excited state in neutron irradiated crystals.

Brewer, et.al. (10), observed that there were two lifetime components evident below 55 K with lifetimes of 23 and 157 milliseconds at 4.4 K which are much larger than those expected for an allowed electric dipole transition. The presence of these two relatively long lifetimes suggests that the emitting state is a spin triplet such as is present in other oxides like CaO for instance (16). The suggested state is a 3P -like state split into three components of 3A , 3B , and 3B character with the bottom two having mainly B character. Figure 52 shows the schematic diagram of the energy levels. This model was used to explain their fluorescence lifetime measurements and the discrepancy between the results of the experimental and the calculated Stokes shift.

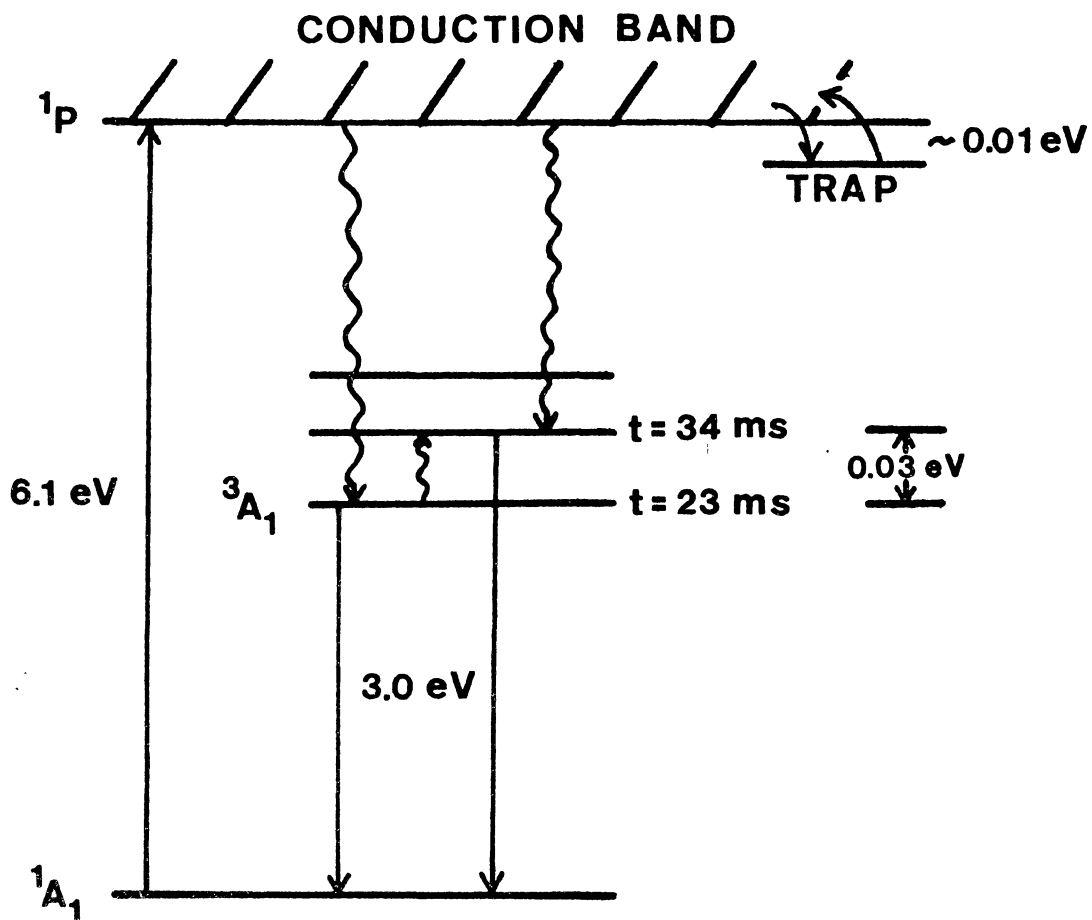
$\alpha\text{-Al}_2\text{O}_3$ F-CENTER

Figure 52. F center Model

CHAPTER V

MgO EXPERIMENTAL RESULTS AND DISCUSSION

Introduction

The experiments on magnesium oxide detailed in this chapter look at eight different crystals using a variety of techniques. The first six crystals were grown at Oak Ridge National Laboratory with varying amounts of hydrogen ions and varying amounts of anion defects present in the final crystals. The seventh crystal was obtained from ORNL and had been irradiated with approximately 10^{17} neutrons/cm⁻². The last crystal was noticeably different from the others because of its purple tint, probably due to a combination of gamma and neutron irradiation.

The number of anion vacancies and H⁻ ions present in crystals number one, three, and six are shown in Table III. The second column is the absorption coefficient for the F center taken at 4.95 eV and the third column is the concentration of F centers. The fourth and fifth columns are the absorption coefficient and concentration for H⁻ centers respectively. This absorption coefficient was measured at 1053 nm.

TABLE III
 CHARACTERISTICS OF THERMOCHEMICALLY
 COLORED MgO SAMPLES

Sample	α_F (cm ⁻¹)	η_F (cm ⁻³)	α_H (cm ⁻¹)	η_H (cm ⁻³)
MgO 1	110	5.5E17	0.2	6E16
MgO 3	820	4.1E18	0.5	1.5E17
MgO 6	330	1.6E18	11	3.3E18

Reference (15)

Thermoluminescence

The experimental set up described in Chapter III was used to conduct these experiments. The crystals were first cooled in an Oxford Instruments continuous flow helium cryostat to a temperature of approximately 10 K and then irradiated with a 60 watt deuterium lamp for five minutes. When the exciting light was first turned off all of the crystals exhibited a decaying fluorescence. After this fluorescence had nearly died out, the set point of the cryostat temperature controller was set to 298 K and turned on. The heating rate produced by this apparatus was approximately 5 K/min except at the very start where it was faster and above 260 K where it started to decrease. The light emitted by the crystals was detected using photomultiplier tube and an picoammeter and recorded on an x-t recorder.

Figure 53 shows the thermoluminescence curves for crystals one, three, and six, and Figure 54 shows the curves for crystals two, four, and five. The intensities have been normalized so they can easily be compared. Except for crystal number six which was cooled to liquid nitrogen temperature, all of the crystals exhibited a peak at approximately 40 K. Peaks also occurred in the vicinity of 100 K and 200 K in most of the crystals. A fourth peak occurred which starts to rise at approximately 220 K and depending upon the intensity of the thermoluminescence may peak between 260 and 270 K. It is this fourth peak which becomes

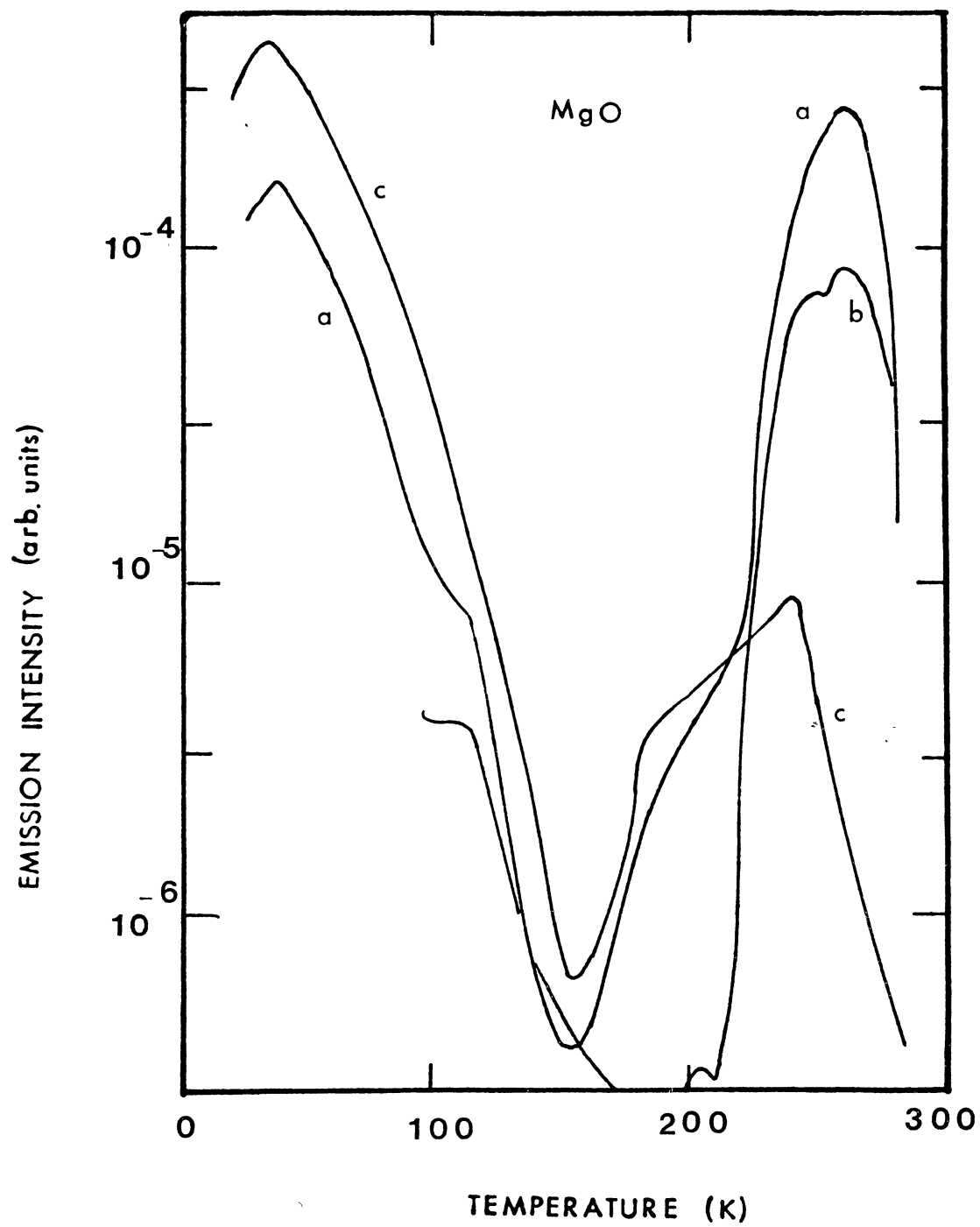


Figure 53. Thermoluminescence Peaks

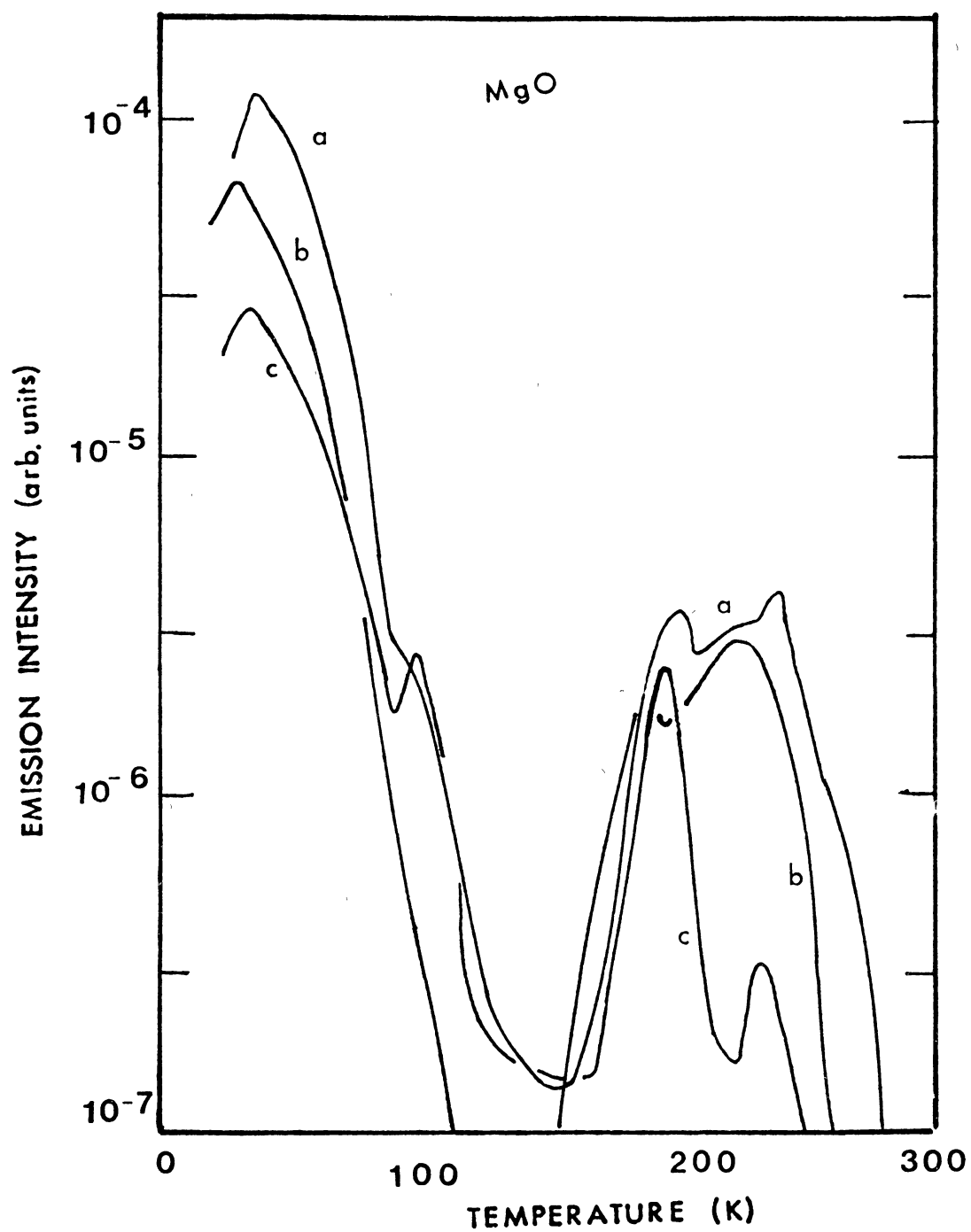


Figure 54. Thermoluminescence Peaks.

the most noticeable when compared with the other experiments.

Figure 55 shows the thermoluminescence curves for crystals seven and eight. They both exhibited the low temperature behavior seen above and the peaks at approximately 100 and 200 K. Crystal seven, which had been neutron irradiated, also exhibited a peak at 50 K. The most noticeable effects are the relatively small overall intensity of their thermoluminescence curves and the almost total lack of the 260 K peak.

Comparing the maximum intensity of the 260 K peaks with Table III shows that the concentration of F centers is the most important factor in determining the magnitude of the peak as long as there are sufficient traps available.

Luminescence Decay

The luminescence decay of crystals one, two, three, and six was measured at 260 K, which is the location of the thermoluminescence peak. A 60 watt deuterium lamp, used with a 2275 nm interference filter and an electronic shutter, was shone on the crystal until the luminescence of the crystal had reached a maximum and then the shutter was closed. This luminescence was directed through a Corning CS0-71 cut off filter into a EMI 9813B photomultiplier tube set at from 900 V to 1180 V. The output of the photomultiplier tube was displayed on a x-t recorder.

Figure 56 shows the decay of these four crystals norm-

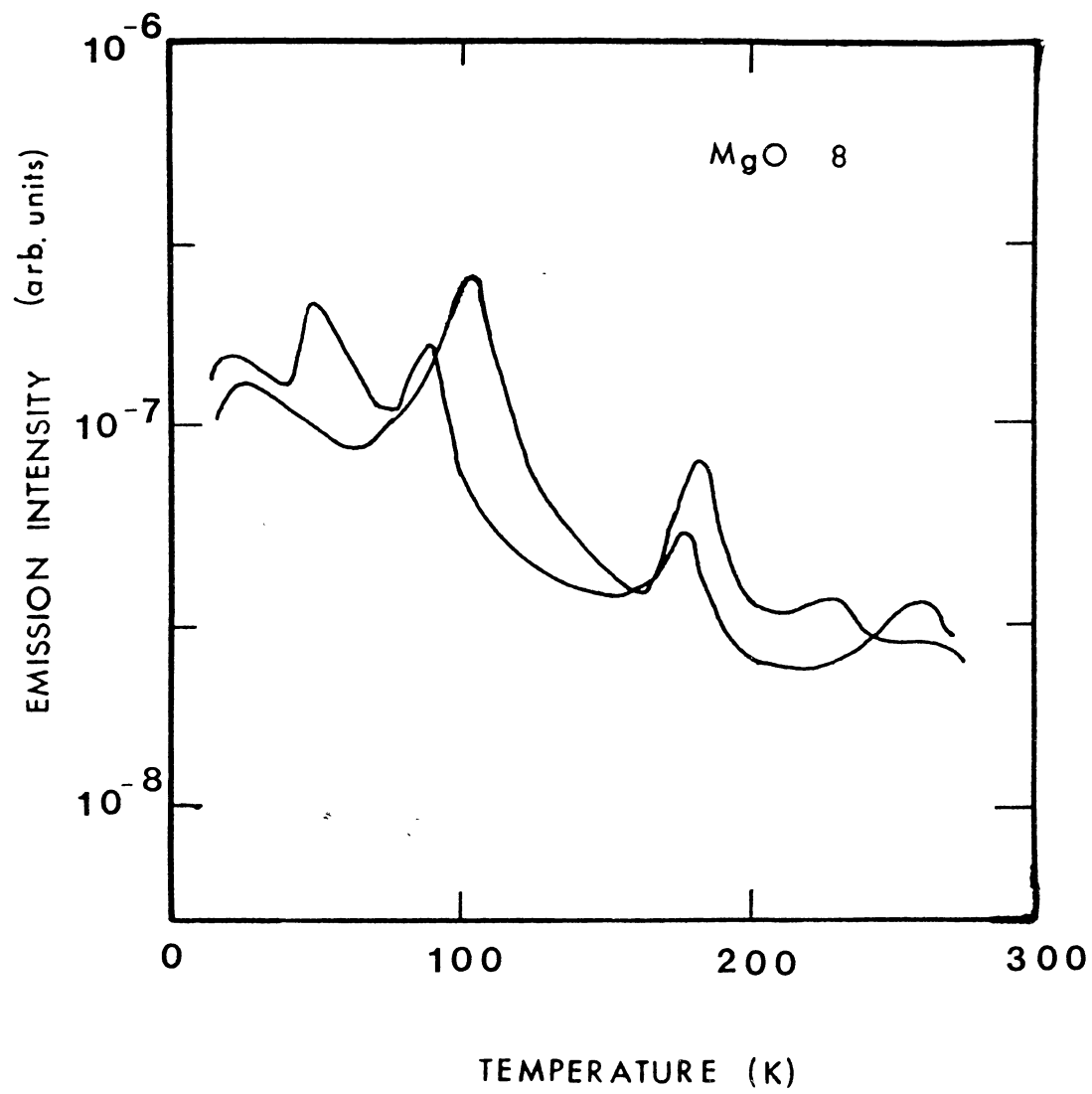


Figure 55. Thermoluminescence Peaks.

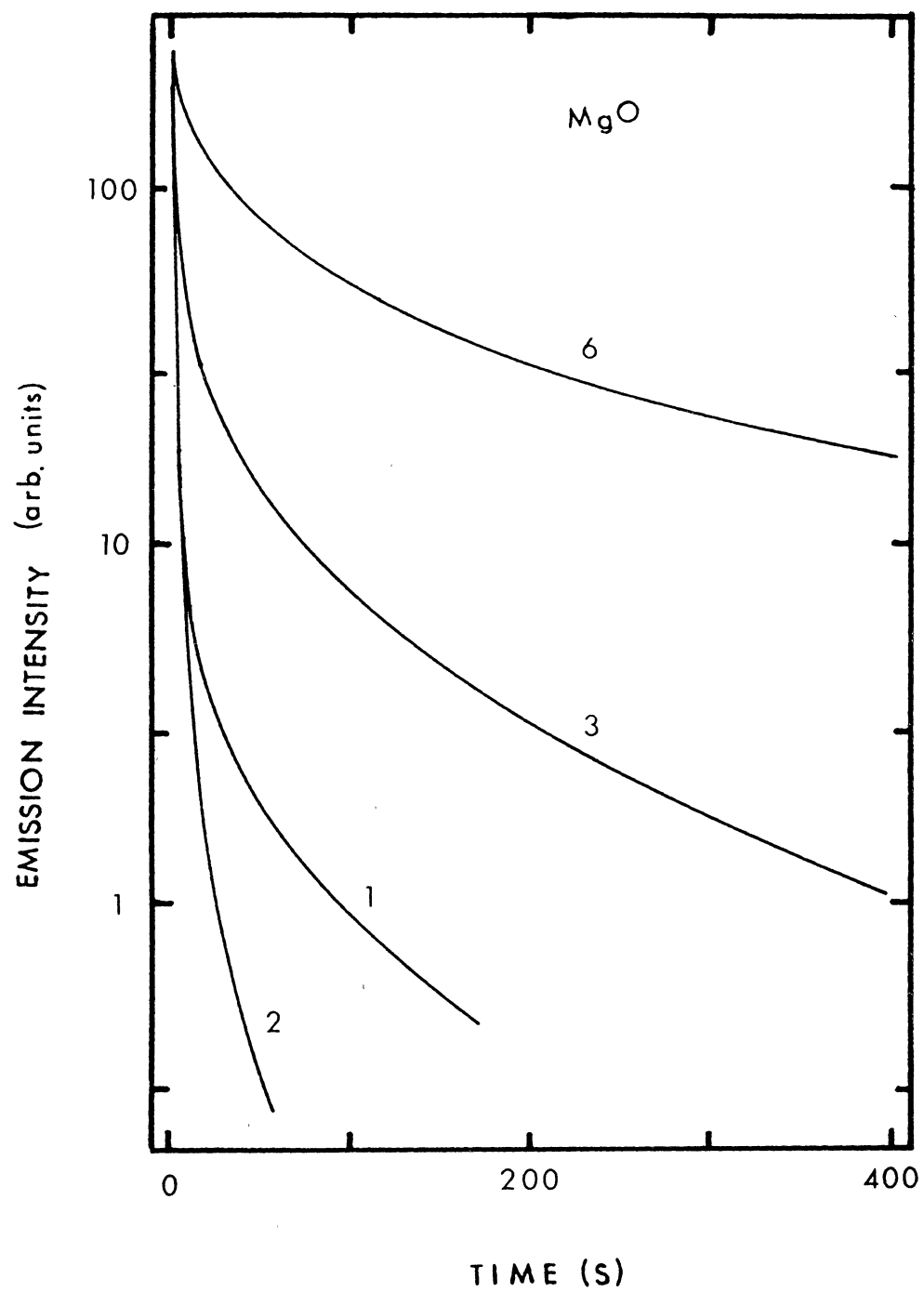


Figure 56. Luminescence Decay

alized at $t=0$ seconds. The actual ratio of intensities at $t=0$ was 0.3:0.5:1.0:0.5 for crystals one, two, three, and six respectively. Plotting the data as the inverse square root of the intensity versus the time is shown in Figures 57 through 60. These plots show that after an initial decrease the decay becomes approximately second order. If the inverse of the slope of this second order decay is taken as a reasonable lifetime for the second order decay, then the lifetimes are 51, 11, 350, and 1070 seconds respectively for the crystals as listed in the above order. These lifetimes show, when compared to the values in Table III, that the magnitude of the second order lifetime is related to the concentration of the H^- ions.

Figures 61 through 64 show the intensity minus the second order intensity plotted as a function of time. These figures show that this initial decay component is exponential. The lifetimes are 6.2, 2.8, 16, and 49 seconds respectively as listed in the above order. The relative magnitudes are similar implying that the two lifetimes are related.

Photoluminescence

The temperature dependent photoluminescence of these crystals was measured over the range from approximately 10 K to 300 K using the experimental arrangements described in Chapter III. Except where noted the excitation source was either a 60 watt deuterium lamp or a 150 watt xenon lamp

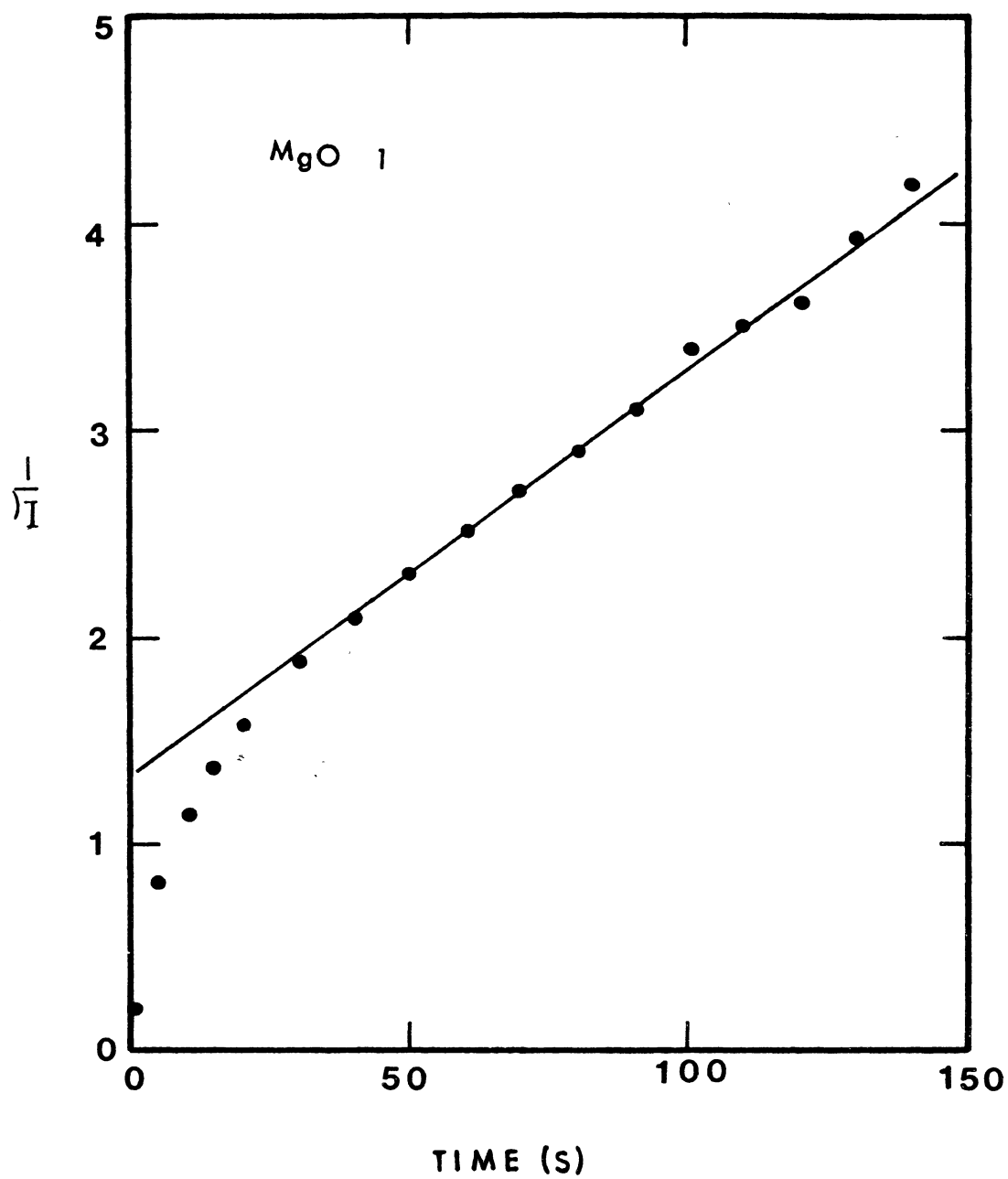


Figure 57. Second Order Lifetime, MgO 1

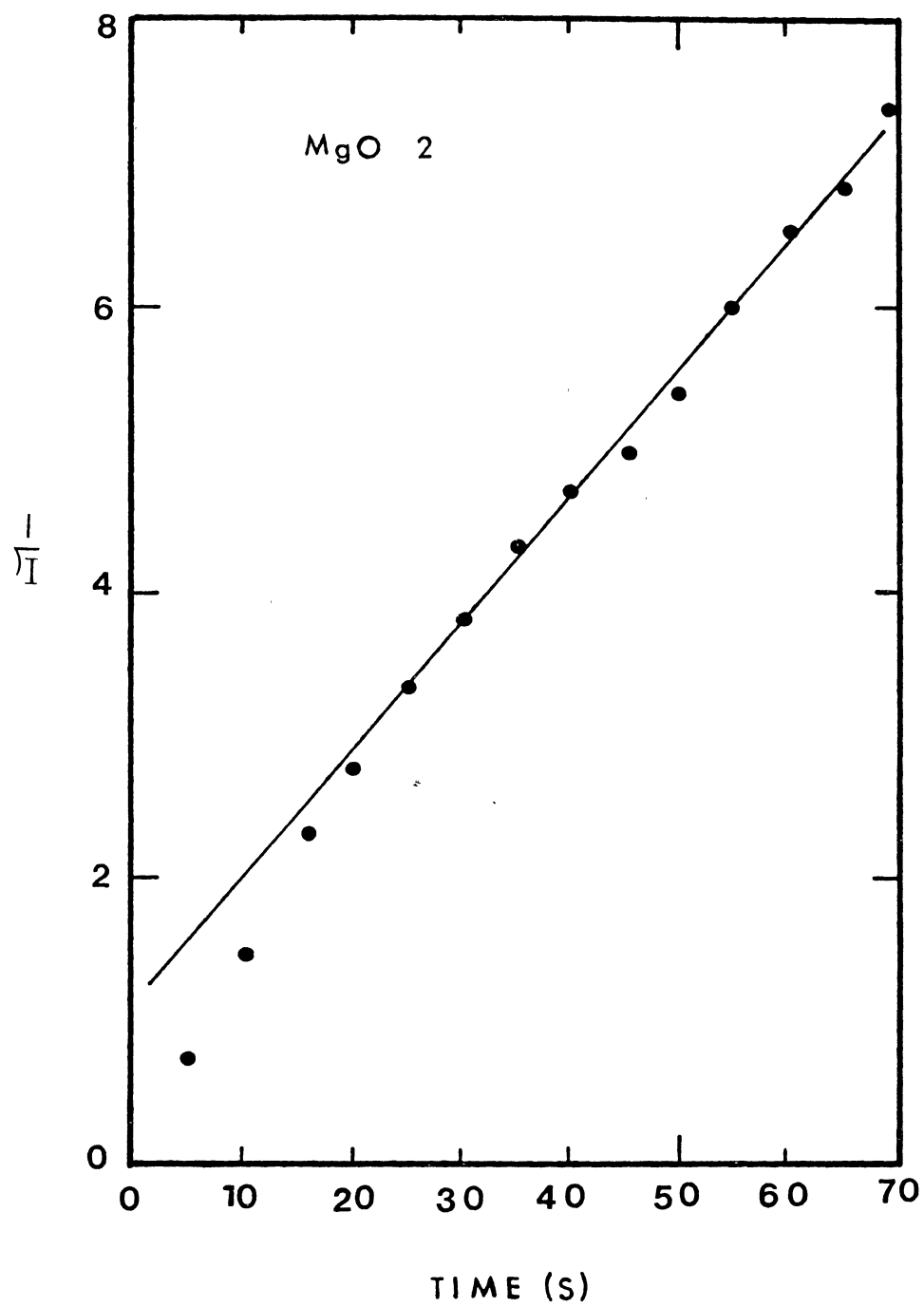


Figure 58. Second Order Lifetime, MgO 2.

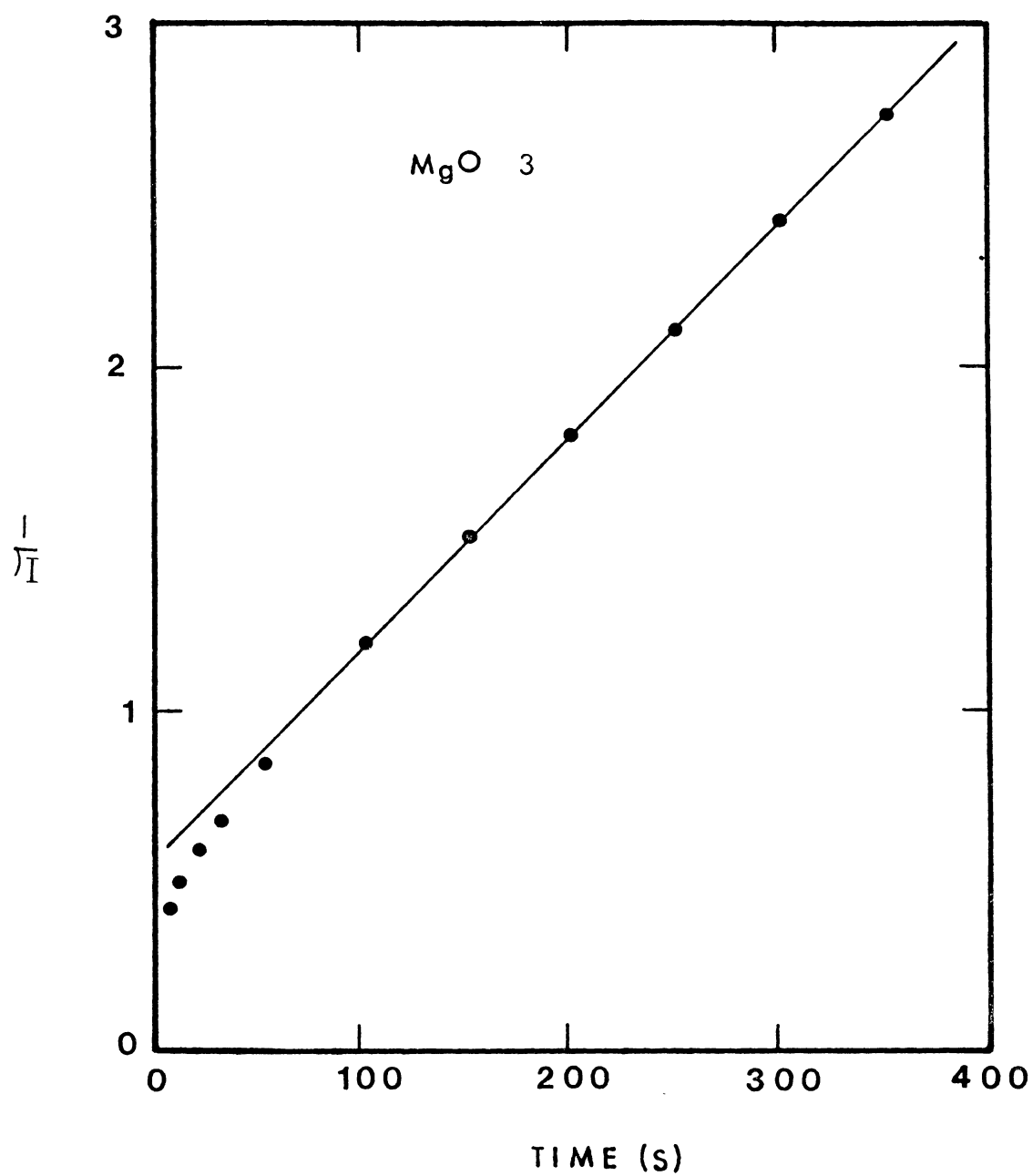


Figure 59. Second Order Lifetime, MgO 3.

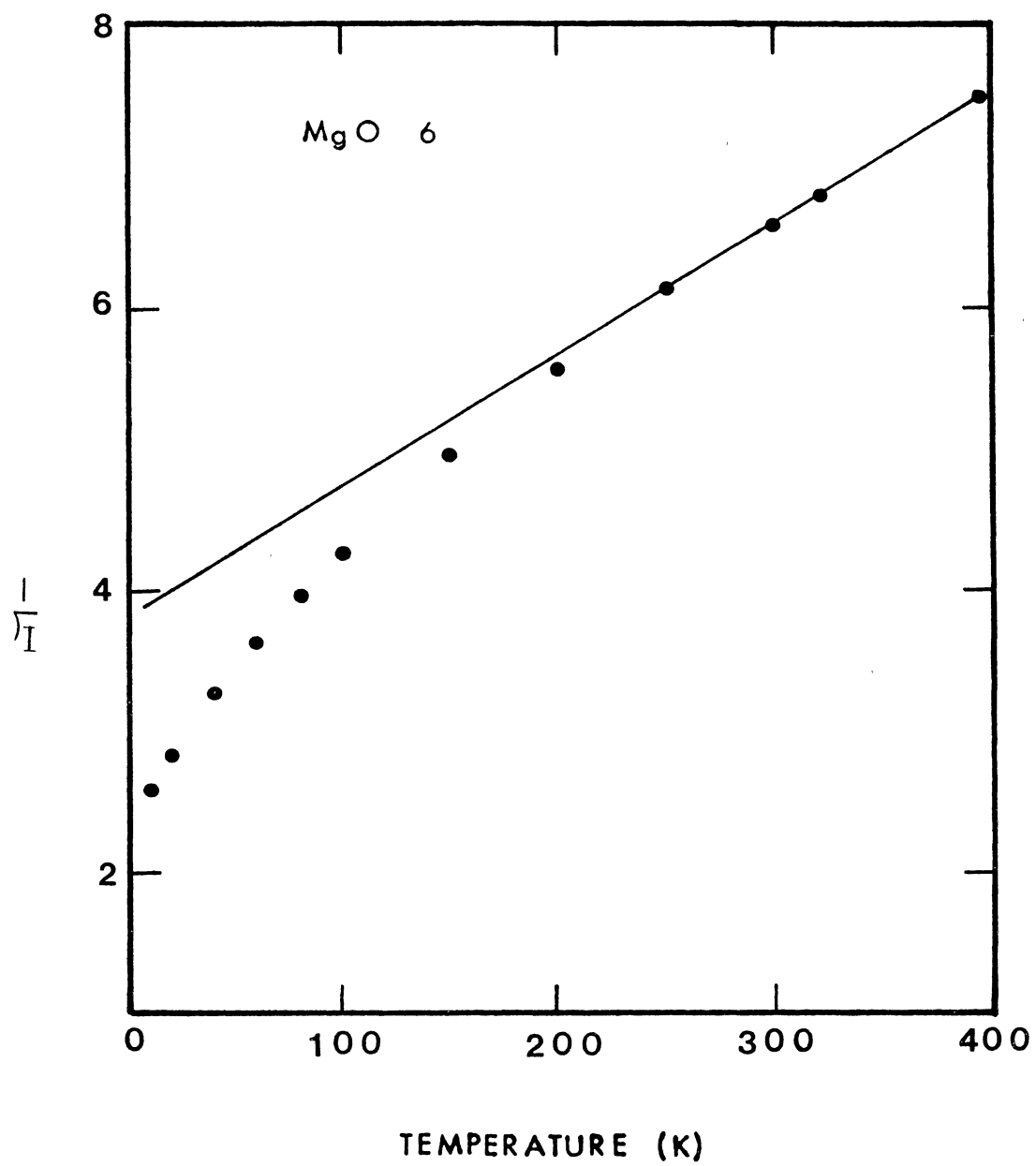


Figure 60. Second Order Lifetime, MgO 6

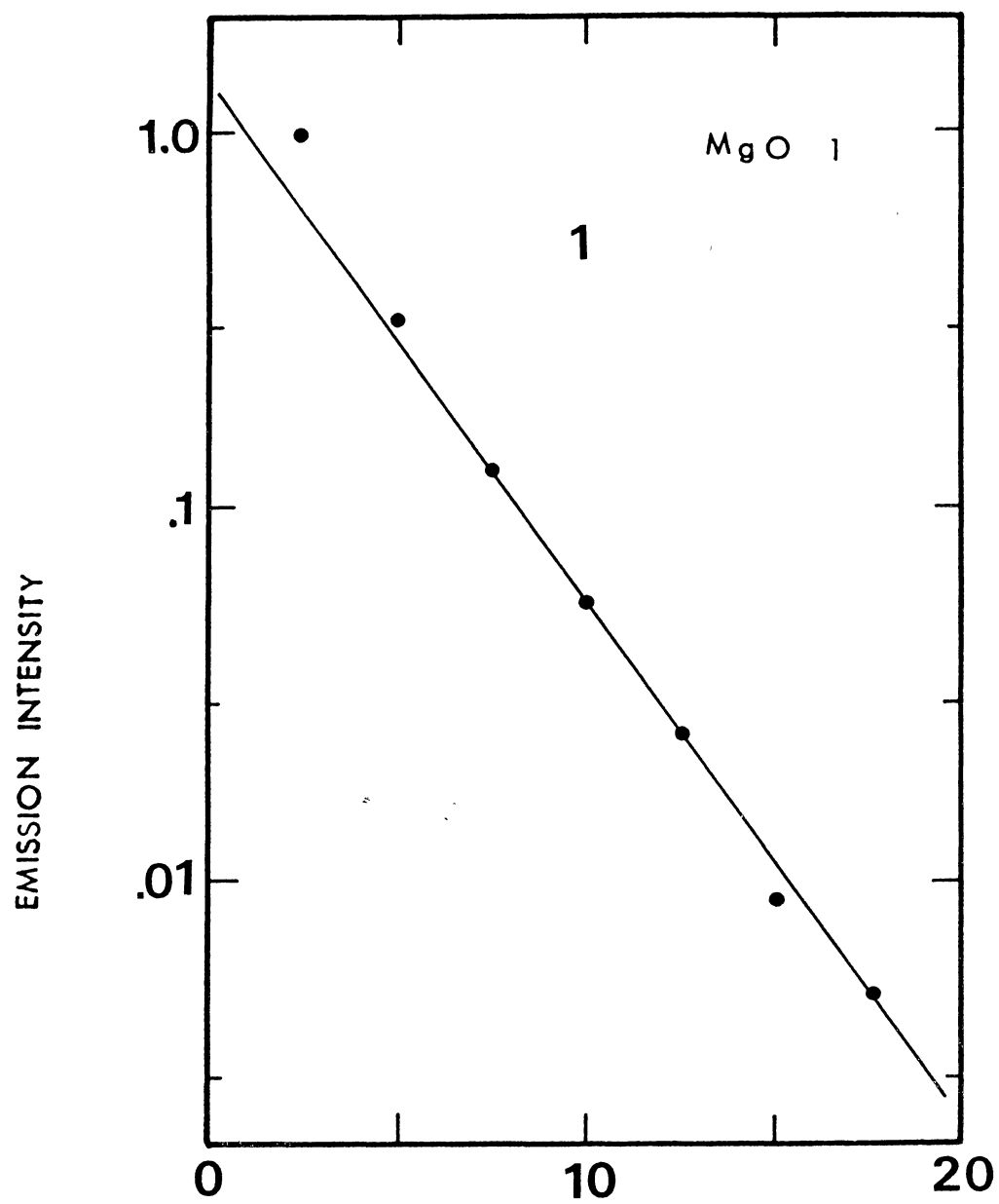


Figure 61. First Order Lifetime, MgO

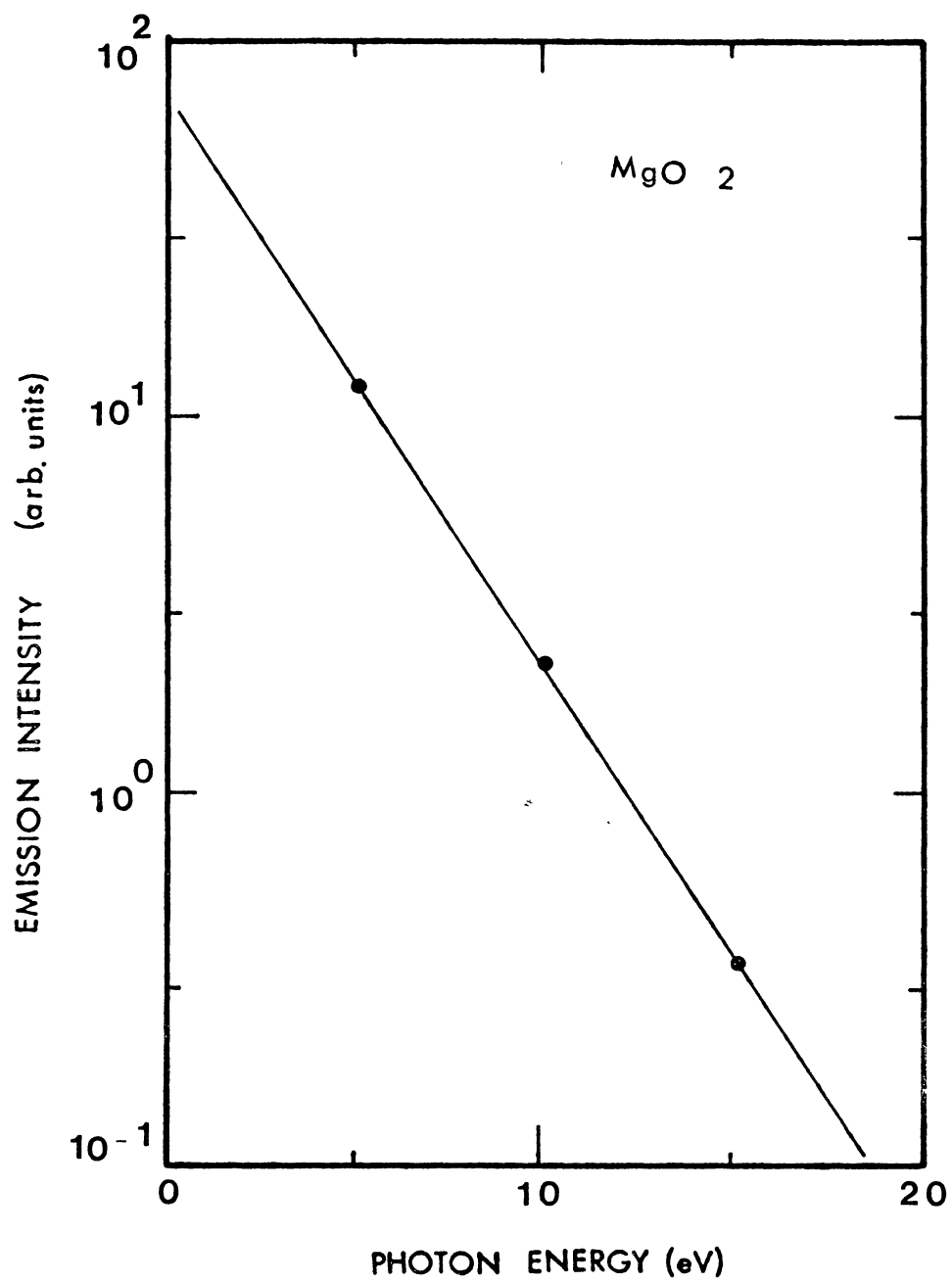


Figure 62. First Order Lifetime, MgO 2

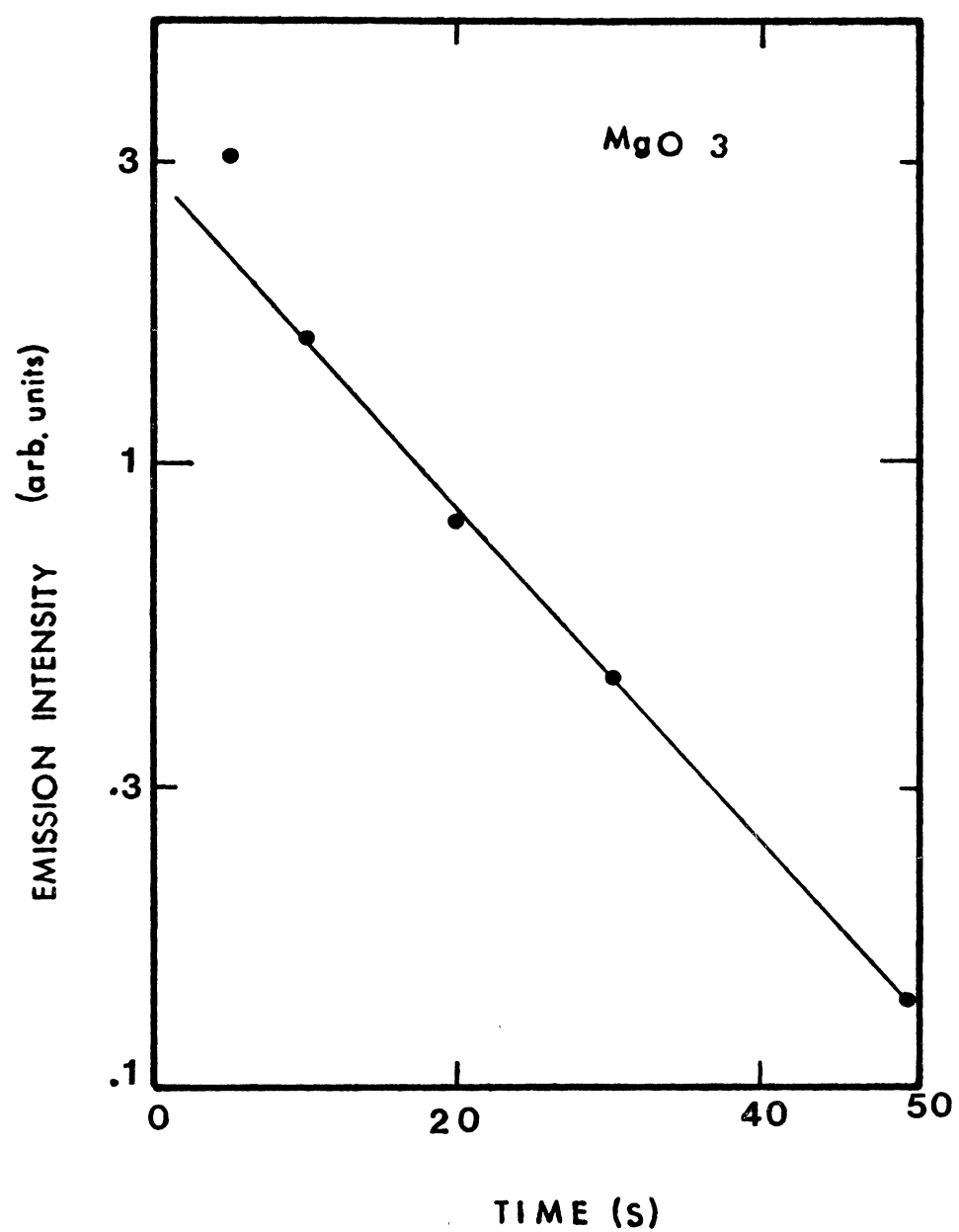


Figure 63. First Order Lifetime, MgO 3

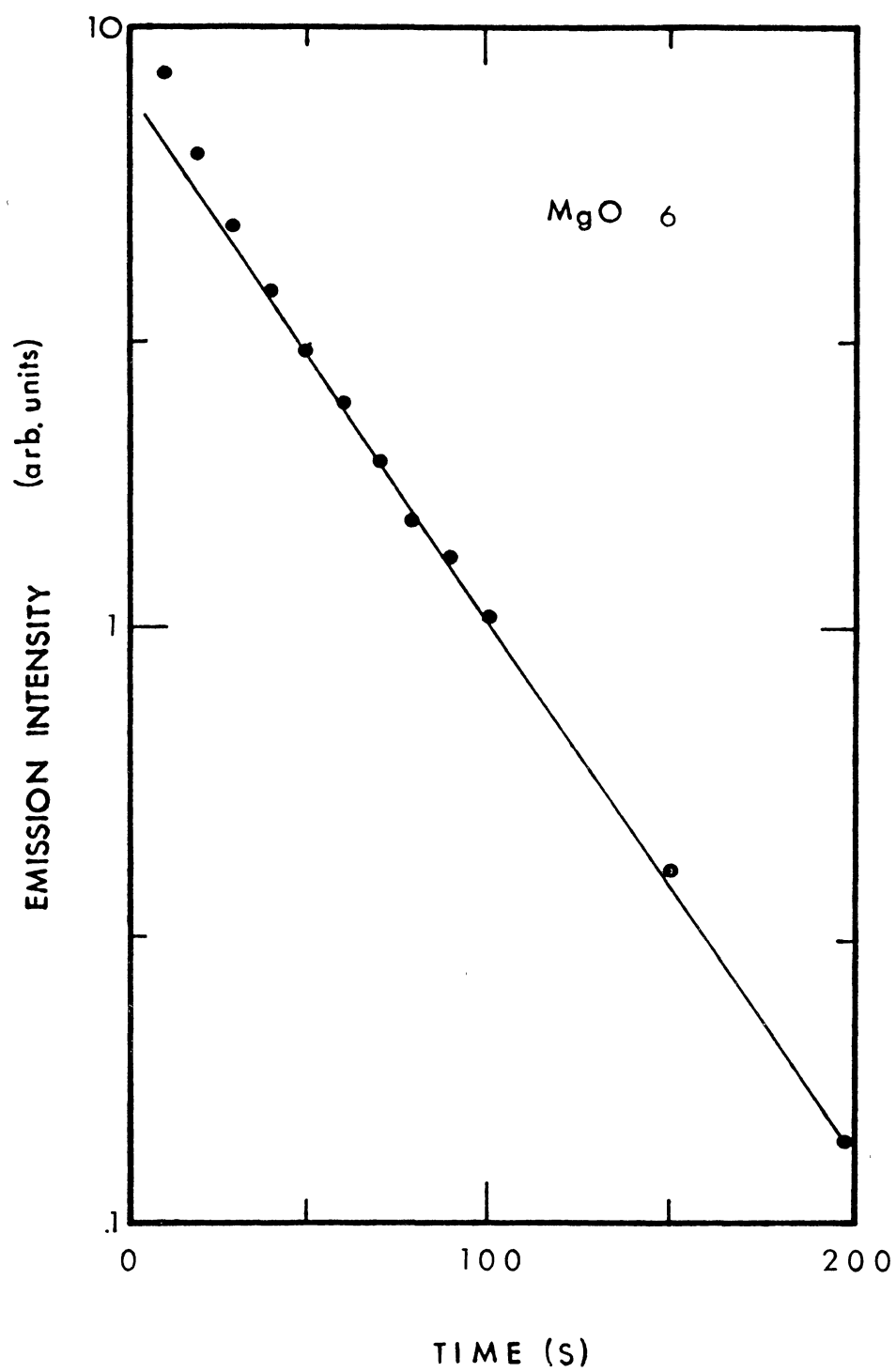


Figure 64. First Order Lifetime, MgO 6

used in series with a 254 nm interference filter. The crystal was illuminated for one minute before the detection system was utilized. The light from the crystal passed through a Corning CS0-53 cut off filter and into the monochromator using either 0.5 or 0.6 mm slits. The size of the slits used was experimentally set to maximize the signal without distorting the band shape. The monochromator scan speed was experimentally set at 1000 angstroms/minute. The intensity scales used on the figures in this section are accurate to about a factor of two.

Figure 65 shows the curves obtained for MgO sample number one. The F peak located at 2.3 eV increases slightly between 9 K and 78 K and then decreases as the temperature increases to 294 K. The intensity at 78 K does not reflect the temperature dependent maximum. The F+ peak located at 3.2 eV decreases as the temperature increases from the starting temperature of 9 K to 294 K. Although the intensity of the F+ center peak is smaller than the intensity of the F center's it is still quite large. Figure 66 shows the curves obtained from crystal number three. For this crystal, the F and F+ center photoluminescence behavior is the same as for sample number one although the F+ photoluminescence is relatively much smaller in magnitude. The curves show in Figure 67 for crystal number six that the intensity of the F center peak increases from a temperature of 84 K to 294 K and that the intensity of the F+ center decreases as the temperature increases.

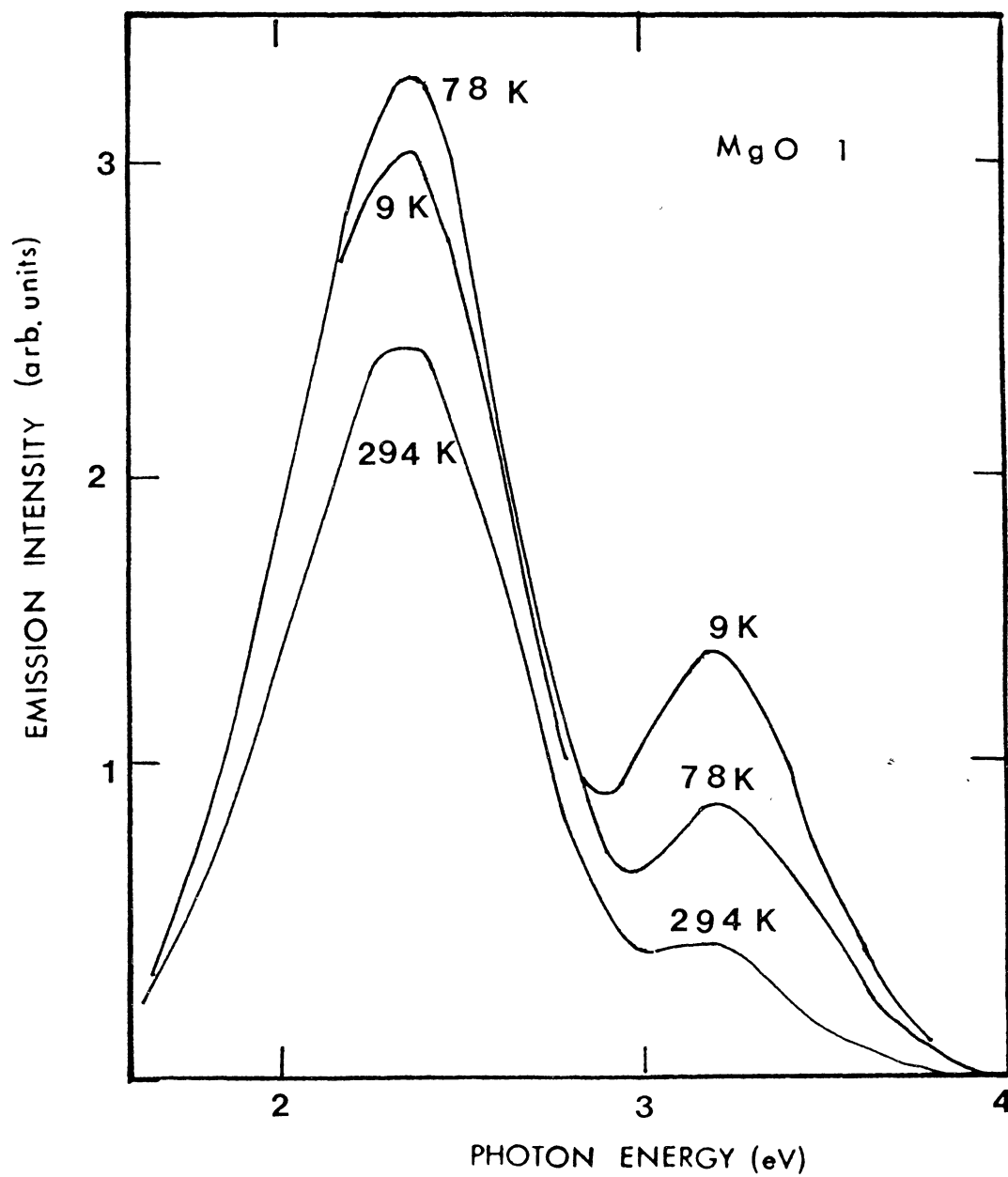


Figure 65. Temperature Dependent
Photoluminescence MgO 1

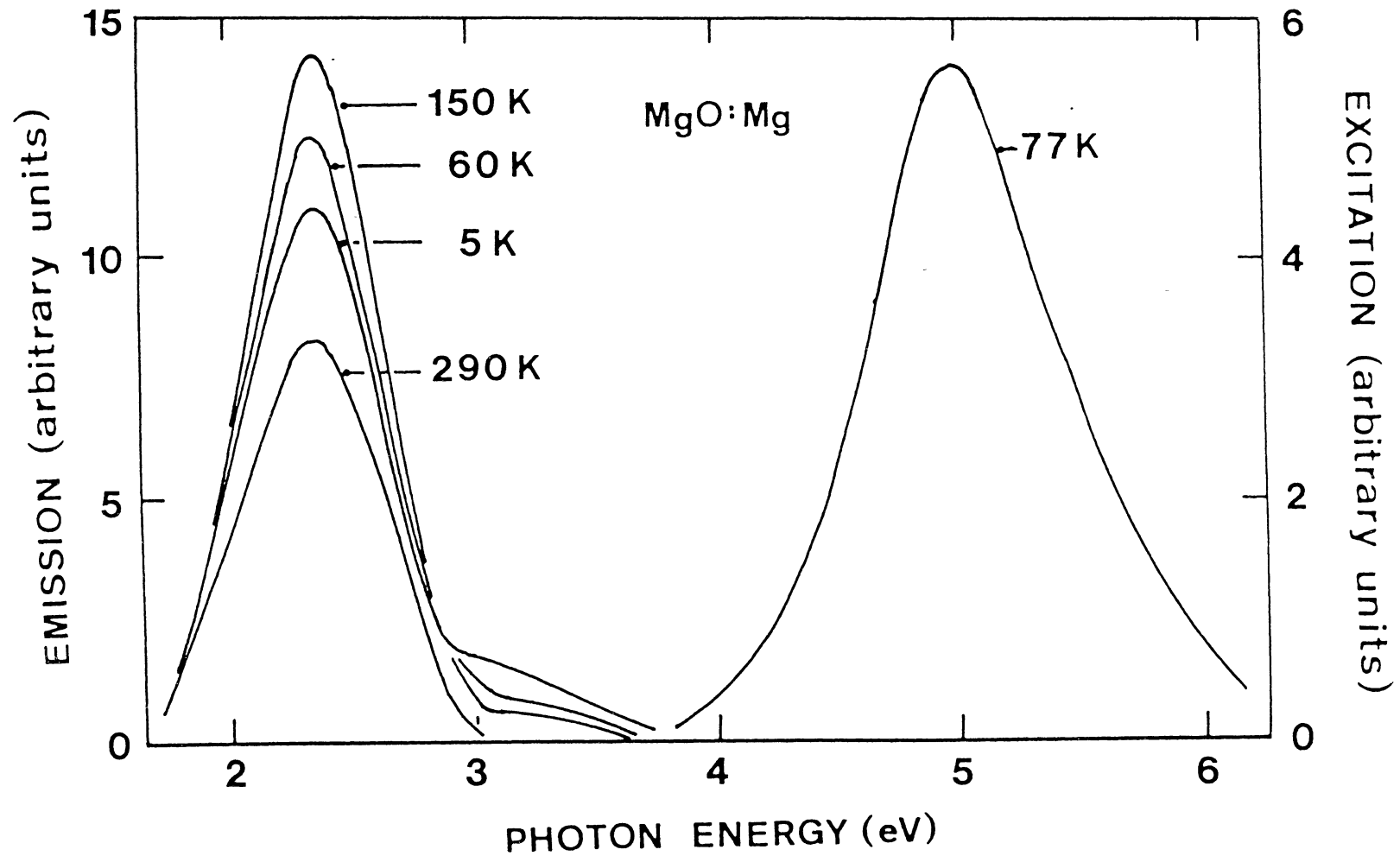


Figure 66. Temperature Dependent
Photoluminescence MgO 3

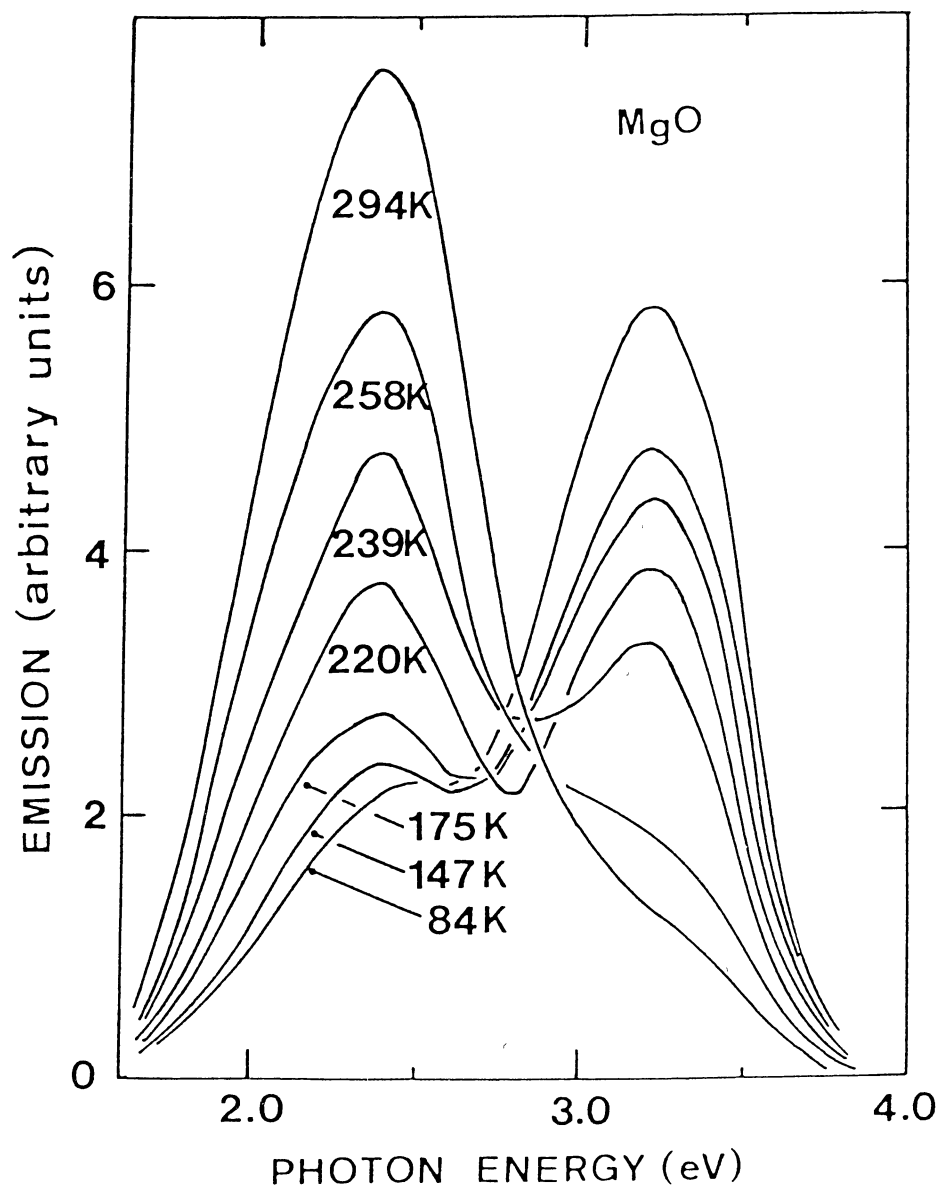


Figure 67. Temperature Dependent
Photoluminescence MgO 6

The peaks positions of the luminescence bands for the above three crystals do not change as the temperature increases. This is evident in all three for the F center luminescence and in number six for the F+ center luminescence. There is a long lived component in the F center emission of each crystal at low temperature. For crystal number three, the shutter in the excitation system was opened and the emission allowed to reach a maximum. The time required for the intensity to reach 90 percent of its maximum was 6, 4.5, 2.2, and 1.4 seconds at the temperatures 30, 60, 90, and 120 K respectively. On sample number one at 9 K, the light was turned off and the monochromator was scanned. This scan showed a small long lived phosphorescence in the F but not detectable in the F+ center emission.

The temperature dependent behavior of crystal number six, which contains the highest concentration of H- ions, shows that as the F+ center emission decreases the F center emission increases in almost the same proportion as the F center emission decreases. The ratio of F center to H- concentrations for this crystal is 2.1:1.0.

For crystal number three the ratio of F center to H- concentration was 27:1.0 and for crystal number one is 9.2:1.0. In crystal number one, with proportionally fewer number of F centers, the F and F+ center emission intensities are more comparable in magnitude than for crystal number three but not as close as for crystal number six. This leads to the conclusion that the relationship between

the relative magnitudes of the F and F+ emission intensities depends upon the ratio of the F center concentration to the H- ion concentration.

Crystal number two grew with predominantly F centers in the inner surface and F+ centers in the outside. Figures 68 and 69 show the curves obtained from the cleaved inner surface over the temperature range from 7 to 280 K. Since the crystal was not cooled down below 80 K in the second figure, the low temperature trap evident in the thermoluminescence data most likely caused the difference in relative magnitudes of the two peaks for the 80 K curves. Two effects are noticeable from these curves. The emission of the F center peak becomes larger relative to that of the F+ peak emission and decreases except at very low temperatures. Secondly, the intensity of the F+ peak decreases as the temperature increases.

Over the 80 to 280 K range the long lived phosphorescence was much more noticeable at 230 K and then only for the F center peak. The data taken at 80 K showed negligible phosphorescence. The shutter was closed while scanning on the F center peak on the 130, 230, and 280 K curves. The time required for the intensity to fall to 30 percent of its maximum was 0.3, 4.5, and 0.8 seconds respectively using the above listed order. The time of 0.3 seconds for 130 K is limited to the response time of the x-t recorder. At 230 and 280 K, the F+ center showed a phosphorescence of approximately 0.4 seconds.

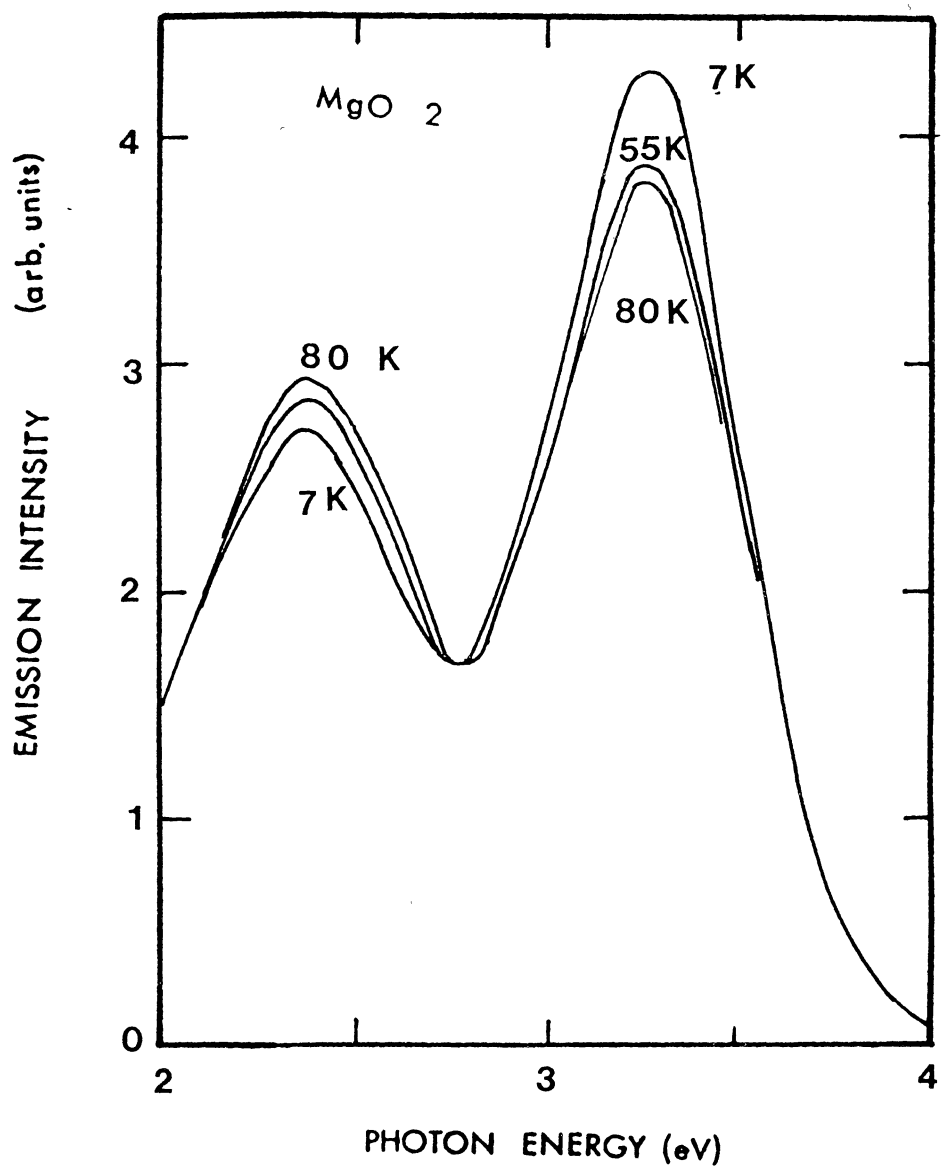


Figure 68. Temperature Dependent
Photoluminescence MgO 2

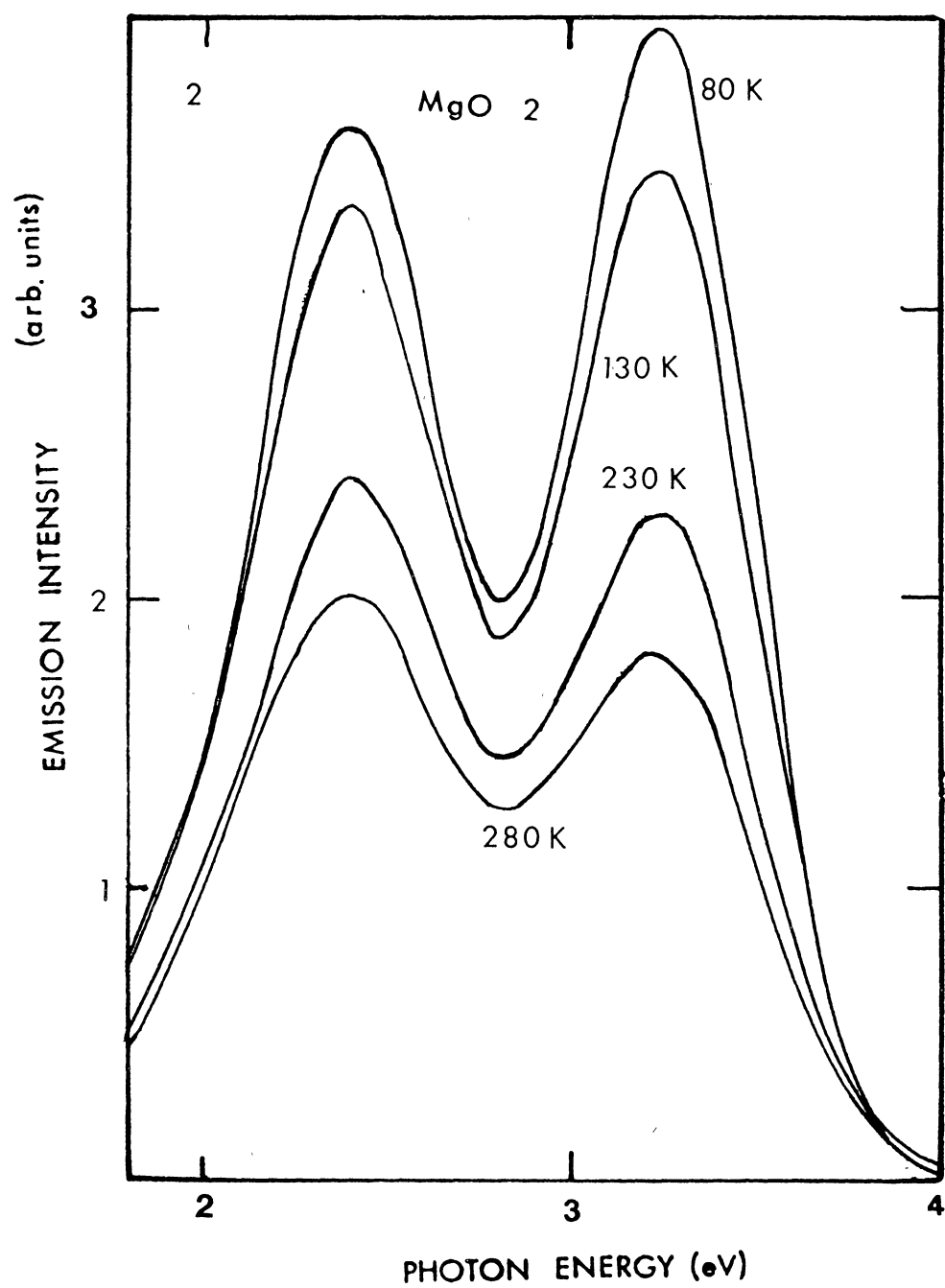


Figure 69. Temperature Dependent
Photoluminescence MgO 2

At 30 K a lock-in amplifier was used which was not sensitive to the long lifetime components of the emission. The light chopper was set at 27 and 169 Hz. Figure 70 shows the results of this experiment. Curve a was obtained using d.c. detection. Curve b shows approximately a 75 percent reduction in the F center peak and curve c 85 percent.

Figure 71 shows curves of data from the F+ center side of crystal number two taken at 20, 77, and 300 K. The F+ center emission is constant at low temperatures while the F center emission decreases. At 300 K both have decreased. At 20 K the F+ center emission is approximately 7.5 times greater than the F center's while at 300 K the F center is negligible.

Crystals number four and five are very similar. At 77 K the ratio of the F to F+ center peak intensities for both is 1:2.1. At room temperature the ratios are 1:3.5 and 1:4.4 for four and five respectively. Figure 72 shows the temperature dependence of the F+ center peak height for crystal number five. The intensity remains large until about 200 K and then falls off. Figure 73 shows number five's photoluminescence at 72 K and room temperature. Curve a is the first scan at room temperature and b is another scan immediately following the first. Each scan takes approximately six minutes. The second scan produced a 130 percent increase in the peak's intensity. Curve c is the first scan at 72 K and d is the second. At this temperature the F+

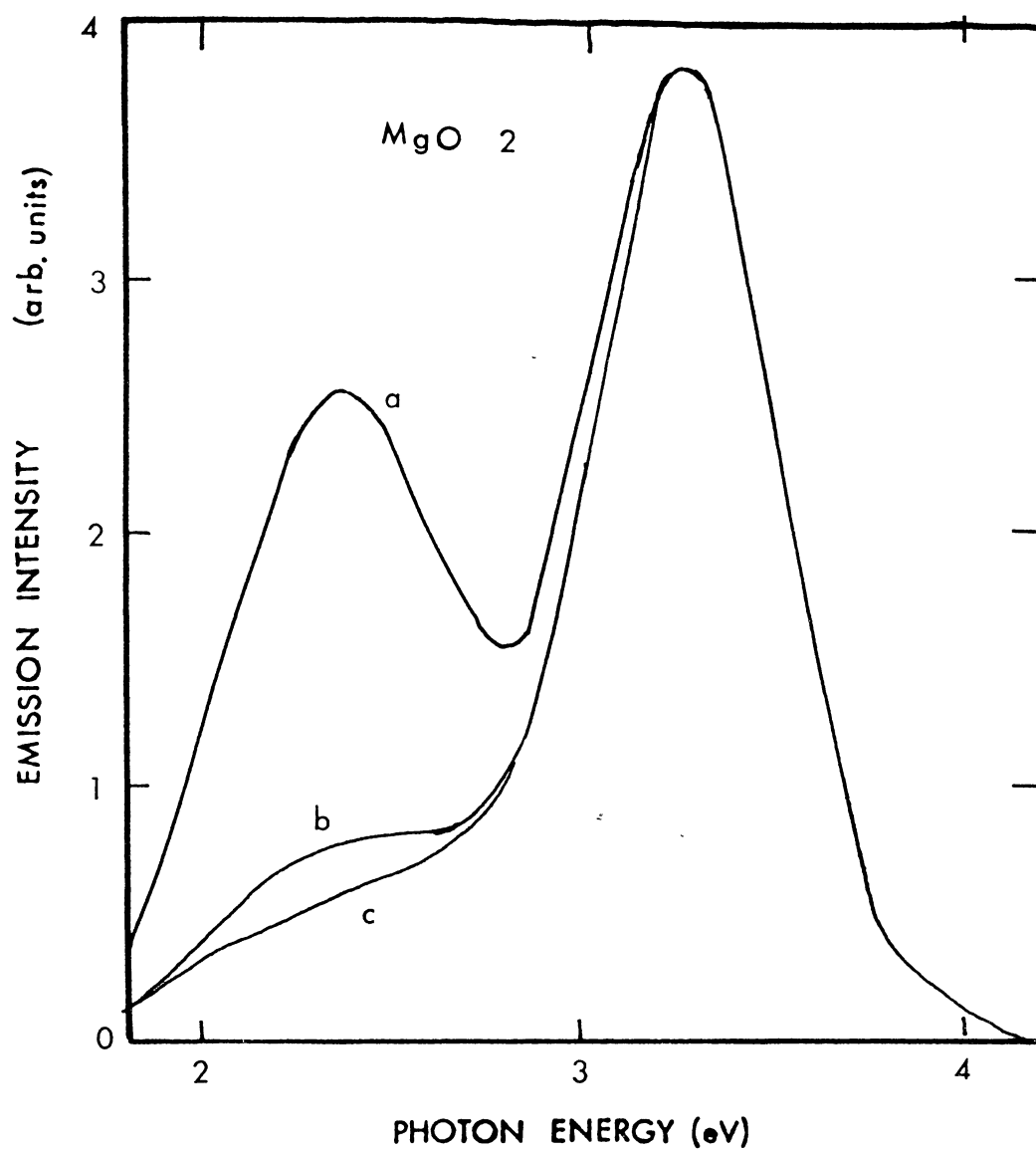


Figure 70. MgO 2, F center Longlived Emission

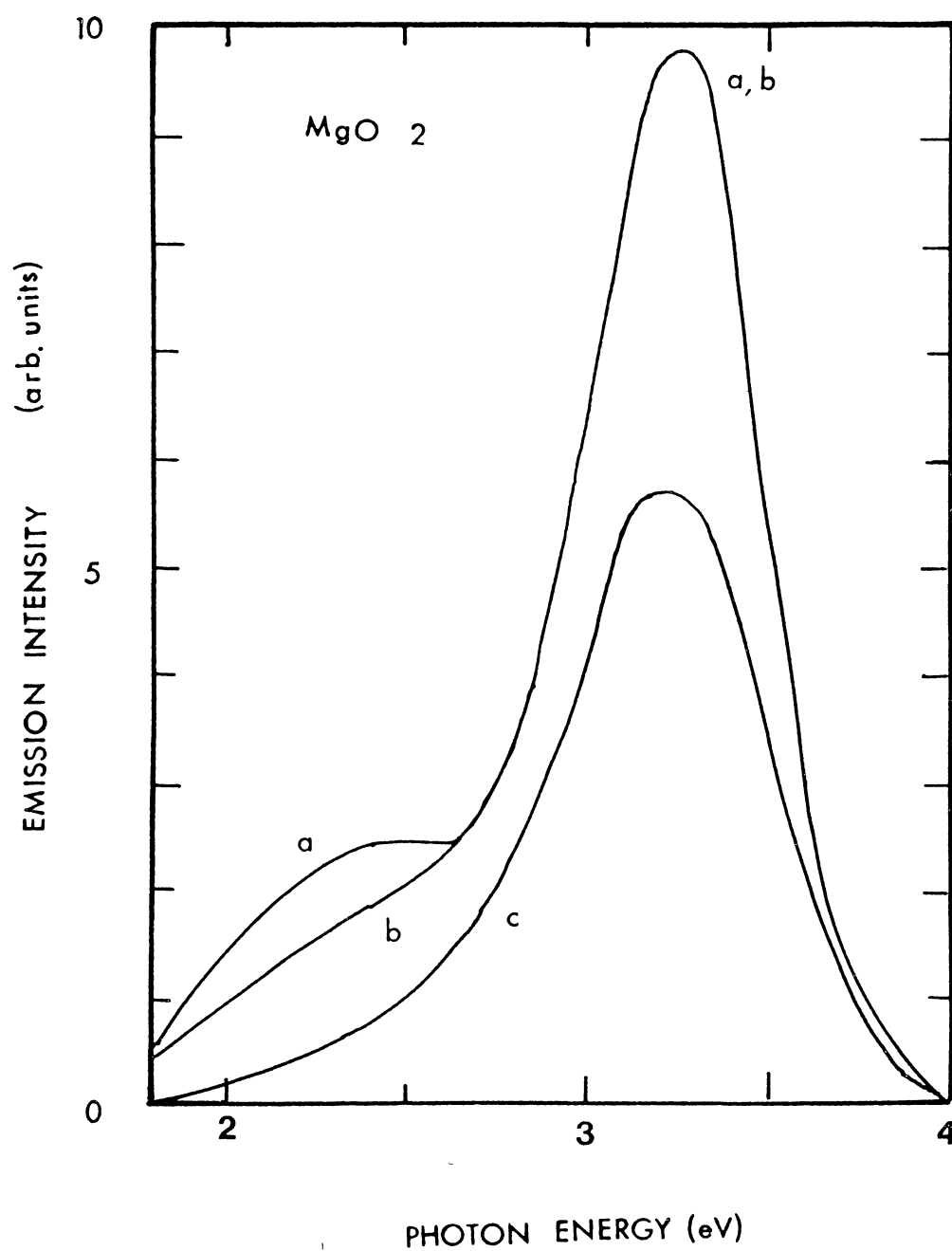


Figure 71. MgO 2, F+ side, Temperature Dependence

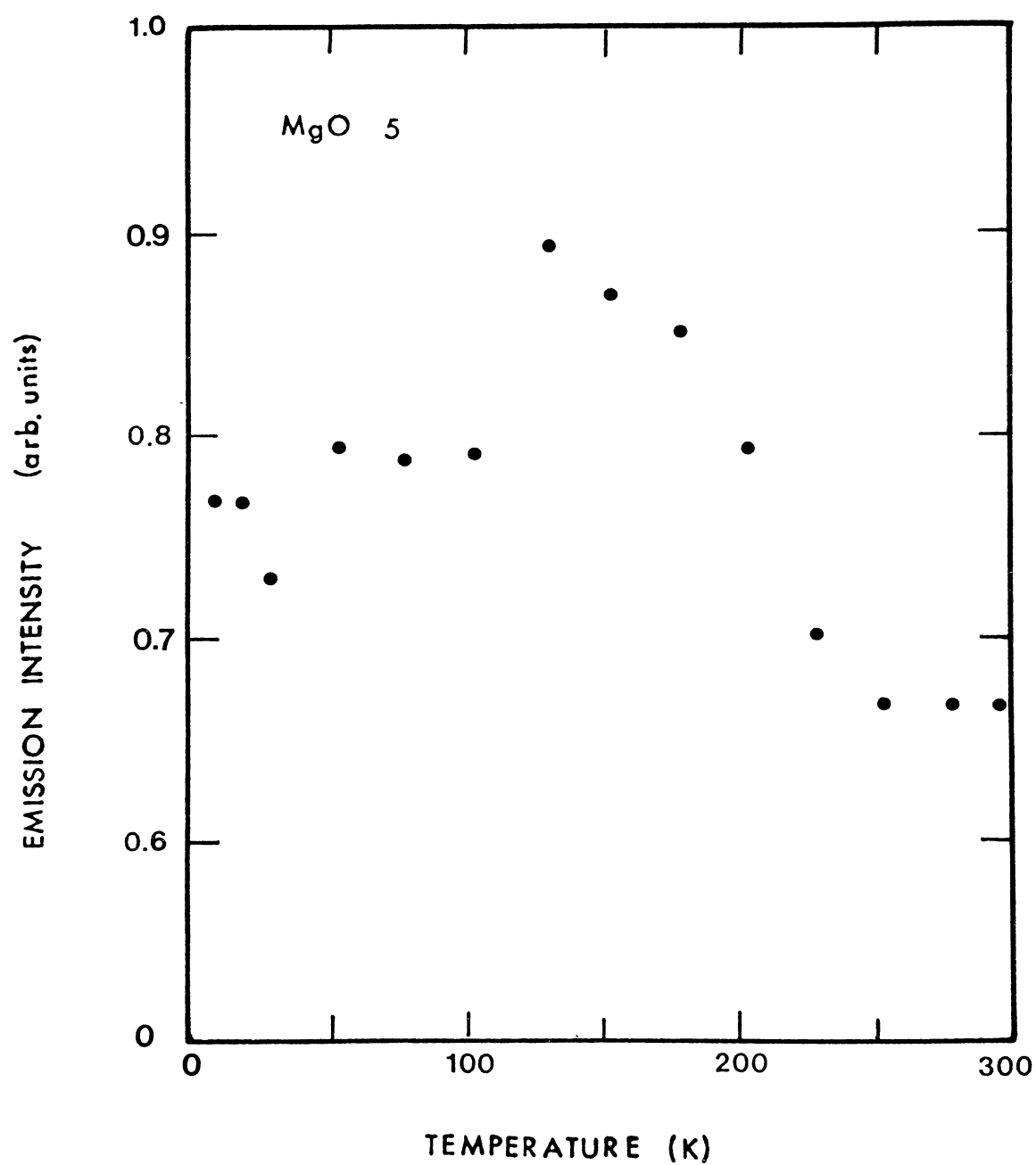


Figure 72. MgO 5, Temperature Dependent Emission

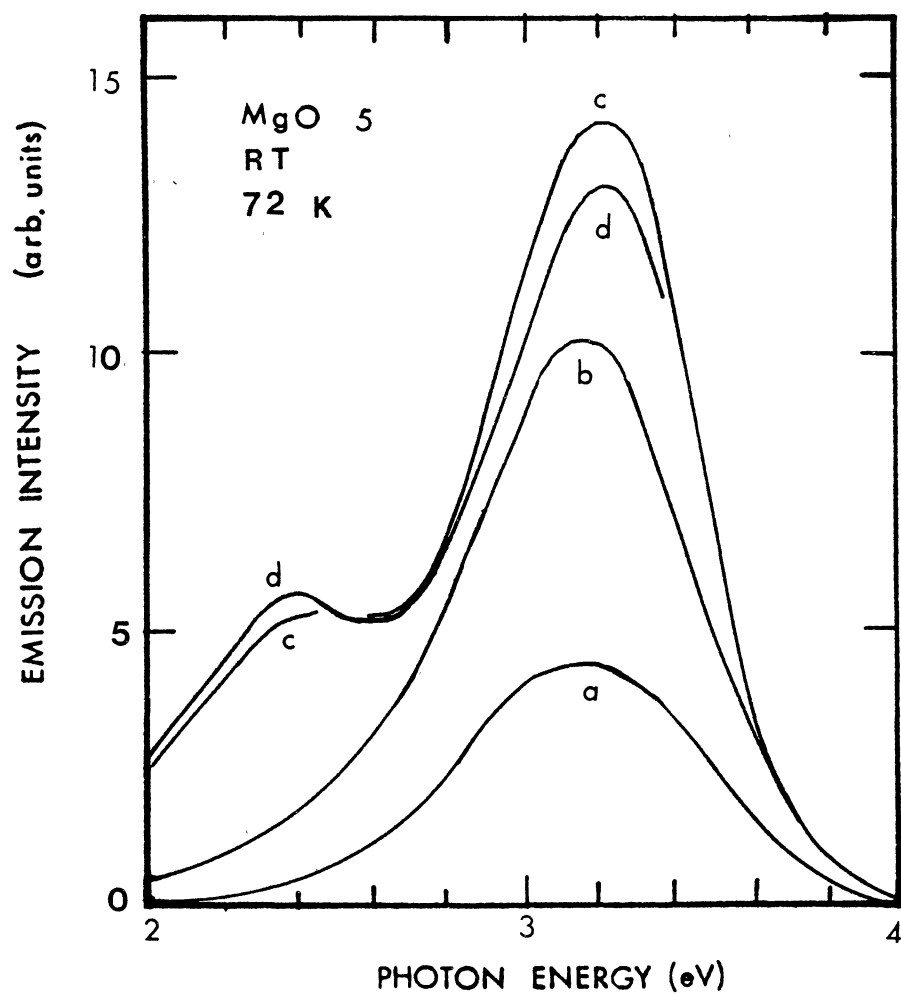


Figure 73. MgO 5, Temperature Dependent Bleaching

center emission is decreased while the F center is increased. This behavior is noted also in crystal numbers two and four also. In contrast, Figure 74 shows the effect of bleaching on crystal number three. The direction of the bleaching effects is the same at 75 K and appears to be of comparable magnitude for each peak. The effect increases the F center emission only a slight amount at room temperature.

Figure 75 shows the photoluminescence of the purple tinted sample number eight from 8 to 230 K. The emission is only from the F⁺ center and shows very little change from 8 to 80 K. As the temperature increases above 80 K it steadily decreases.

Excitation

Several different experimental techniques as given in Chapter III were used in measuring the excitation spectrum of the crystals. In all of the experiments, the excitation system consisted of a 60 watt deuterium lamp shining through a 0.3 m McPherson grating monochromator onto the crystal. Except as mentioned otherwise, the detection system consisted of a PAR 121 Lock-in amplifier with its light chopper set at 27 Hz, a CS3-72 filter for isolating the F center emission, and CS0-52 and CS7-60 filters for isolating the F⁺ center emission.

Figure 76 shows the excitation spectrum for crystal number one with only a Corning CS3-67 filter, a photomulti-

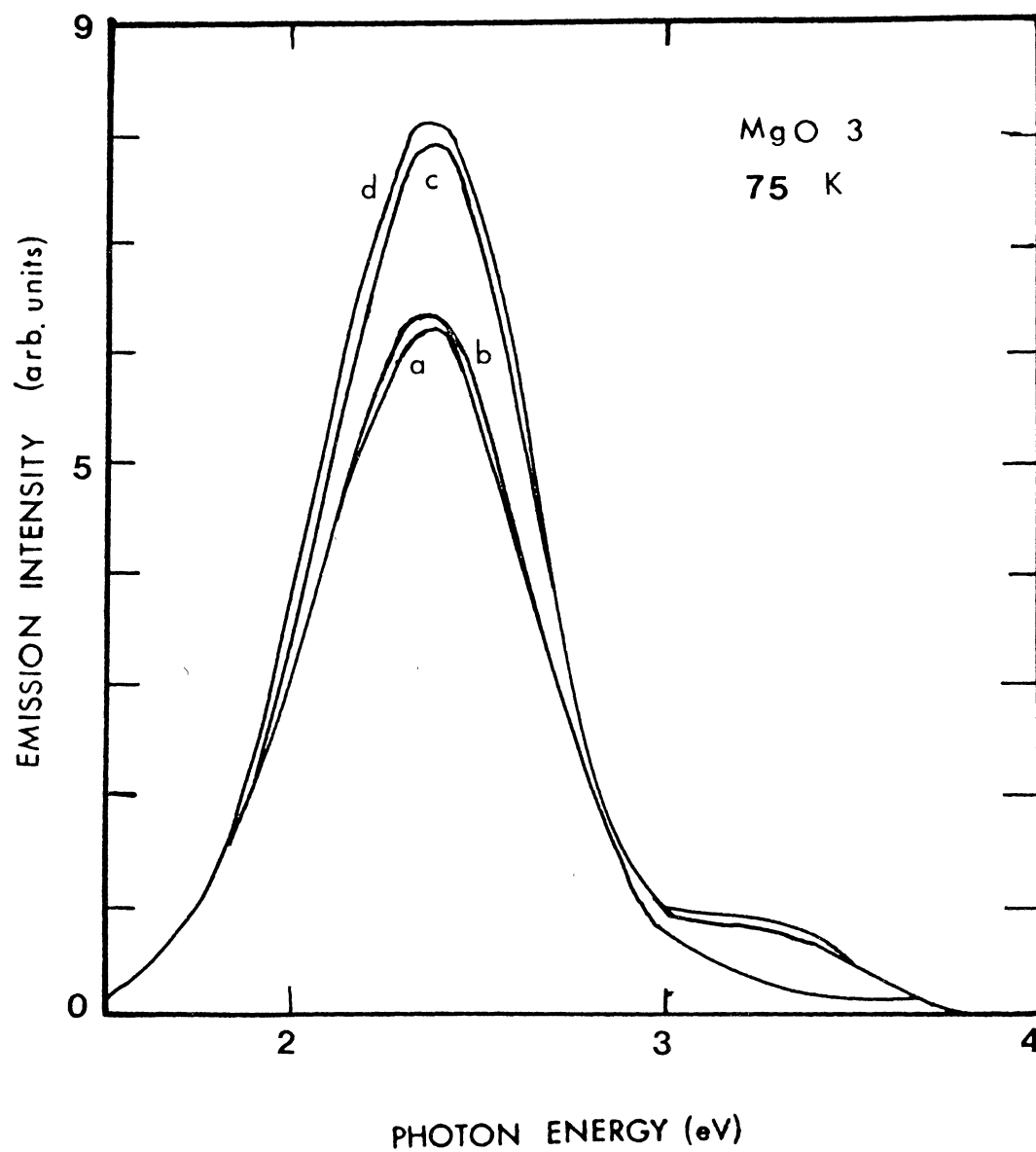


Figure 74. MgO 3, Temperature Dependent Bleaching

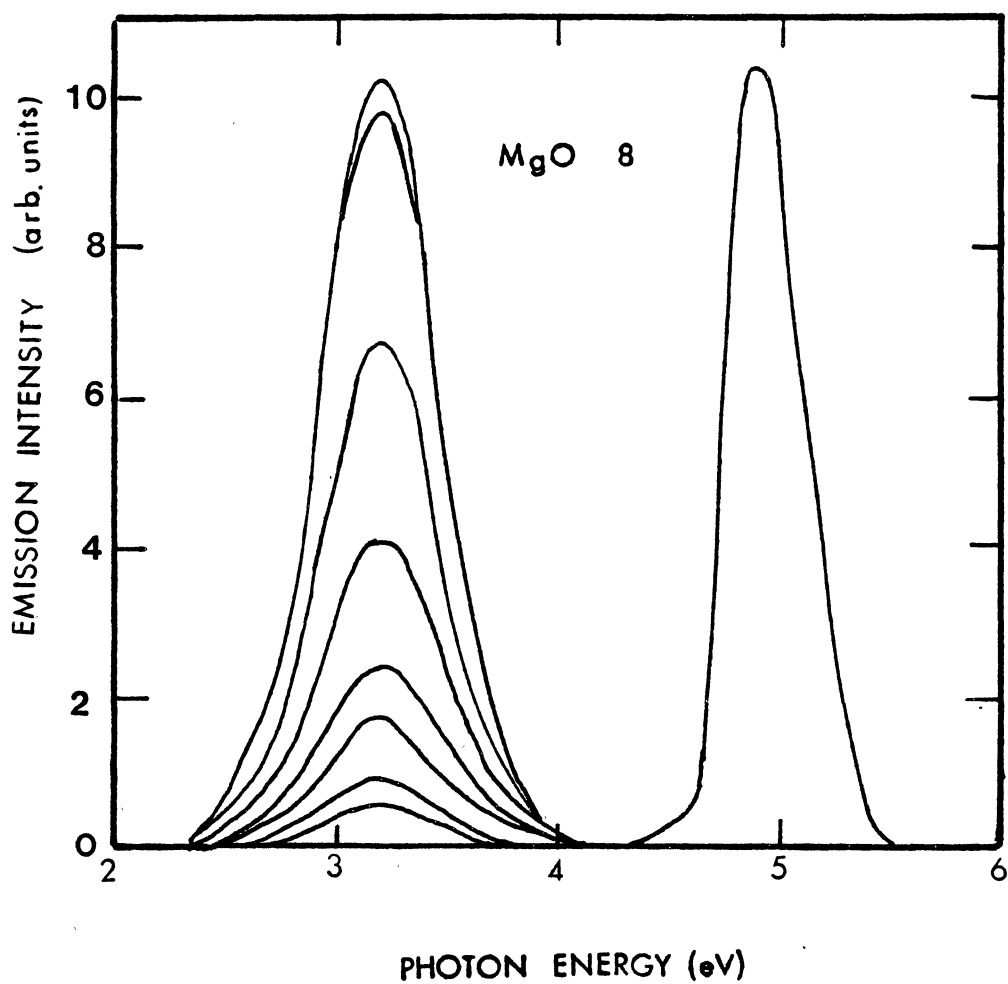


Figure 75. MgO 8, Temperature Dependent Photoluminescence.

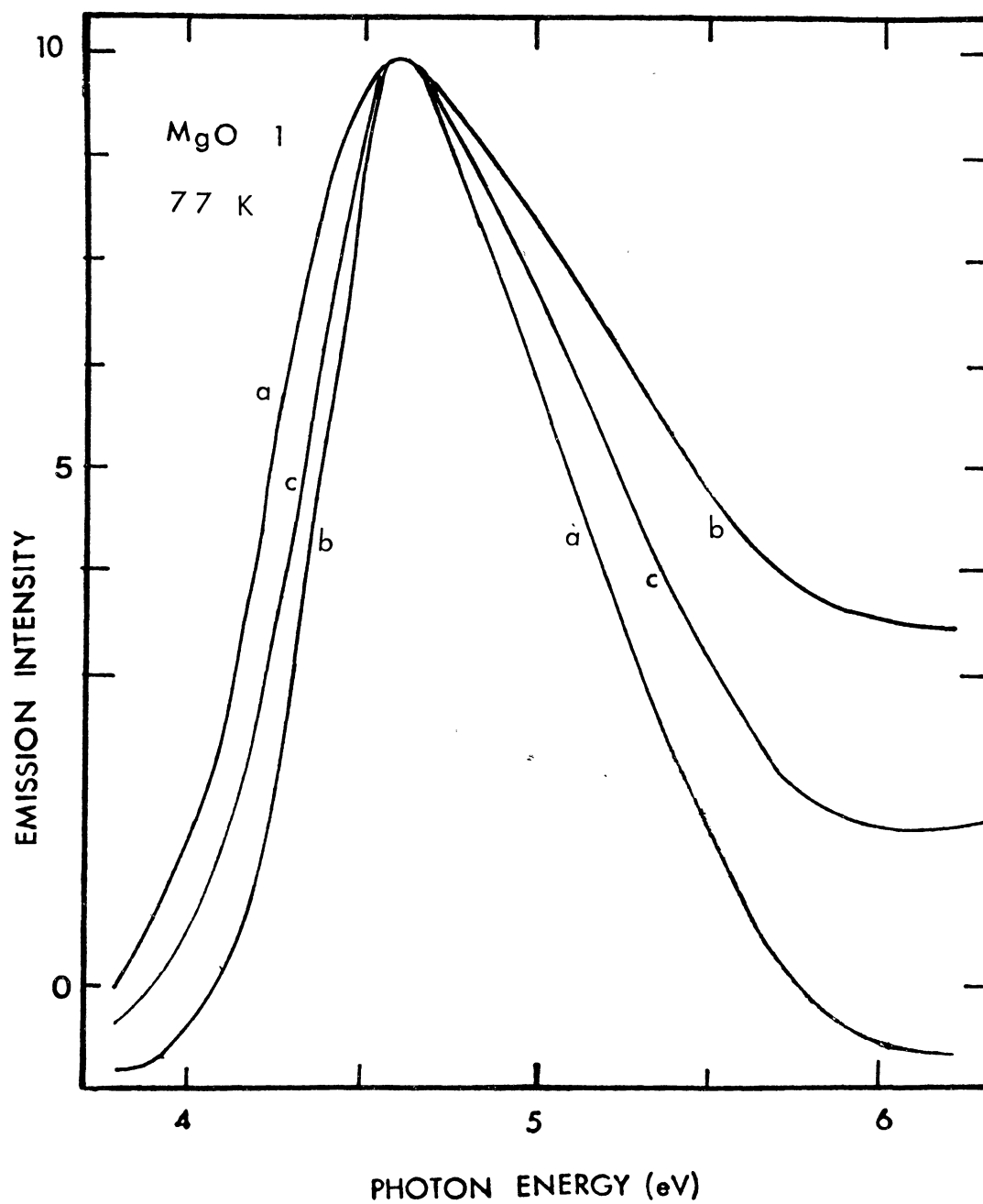


Figure 76. MgO 1, Excitation Spectrum

plier tube, and an ammeter used to detect the emission. The monochromator was scanned at 10 angstroms/minute with its slits set at 0.4 mm. The 77 K phosphorescence distorted the curves so the crystal was scanned from both the high and low energy sides. Curve c is the average of the two scans. Notice that the curve is skewed in the low energy direction with the peak at 4.6 eV.

Figure 77 shows the spectrum for crystal number one using a waveform educator signal averager and a oscilloscope in the detection system. The excitation was chopped at either 1 kHz or Hz using either a CS3-67 or CS3-72 filter respectively which allowed the fast component of the emission spectrum to be measured. In this figure the peak of the spectrum is at 4.4 eV. Figure 78 shows the spectrum measured using a PAR Lock-in amplifier with a light chopper set at 27 Hz. Curve a is of the F center and b is of the F+ center emission. Curve a is identical to the curve in Figure 77 except for the small peak at 5.8 eV. Curve b shows peaks at 4.2, 4.8, and 5.8 eV respectively. The 4.8 eV peak is the most prominent although the 4.2 eV peak was also intense.

The spectrum curves obtained for the outside surface of crystal number two are shown in Figure 79. They are similar to the curves obtained for crystal number one except that the F center emission shows only one peak centered at 4.8 eV. In this case the low energy peak of the F+ center is not as prominent. The curves for the inner cleaved surface

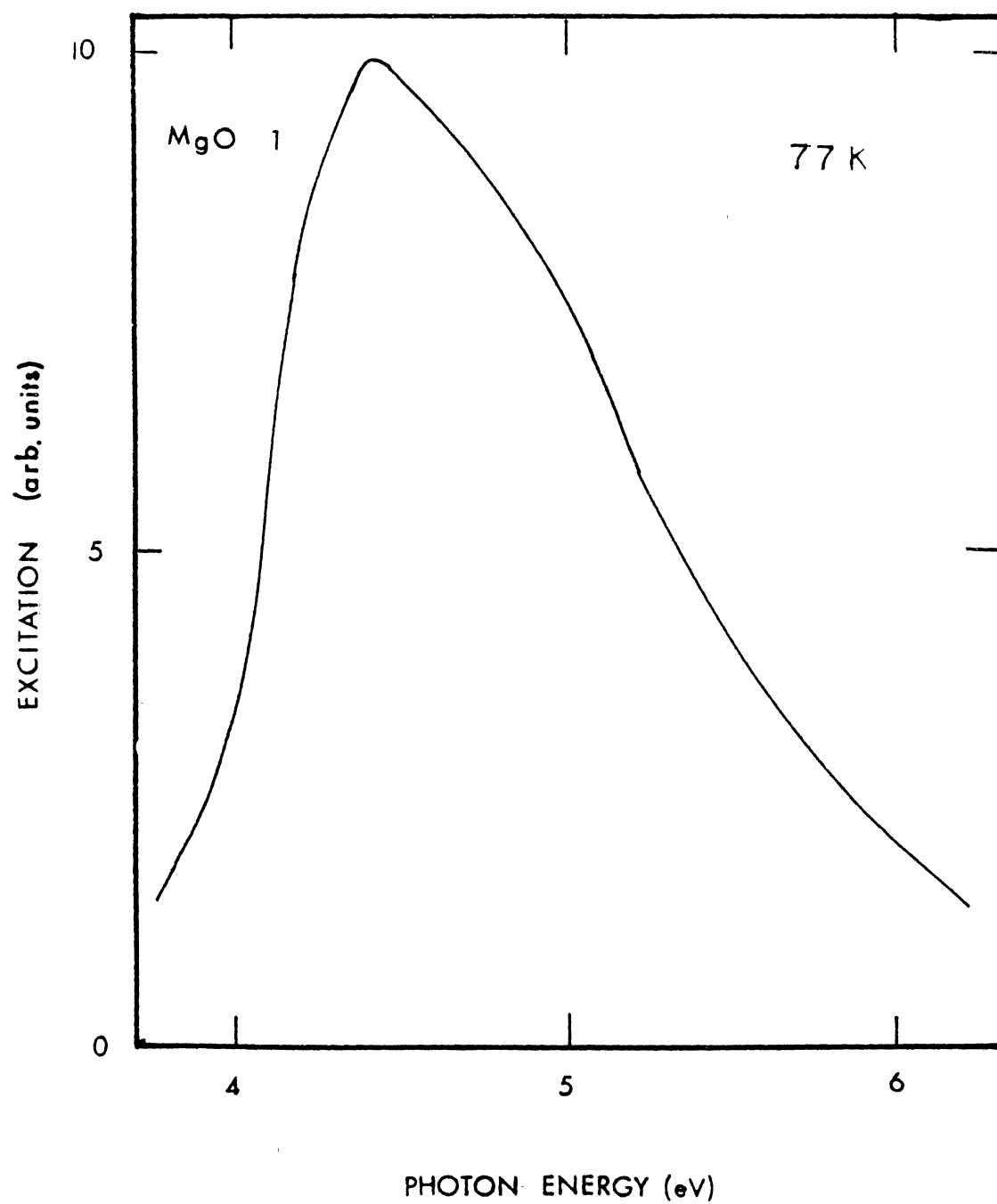


Figure 77. MgO 1, Fast Component
Excitation Spectrum

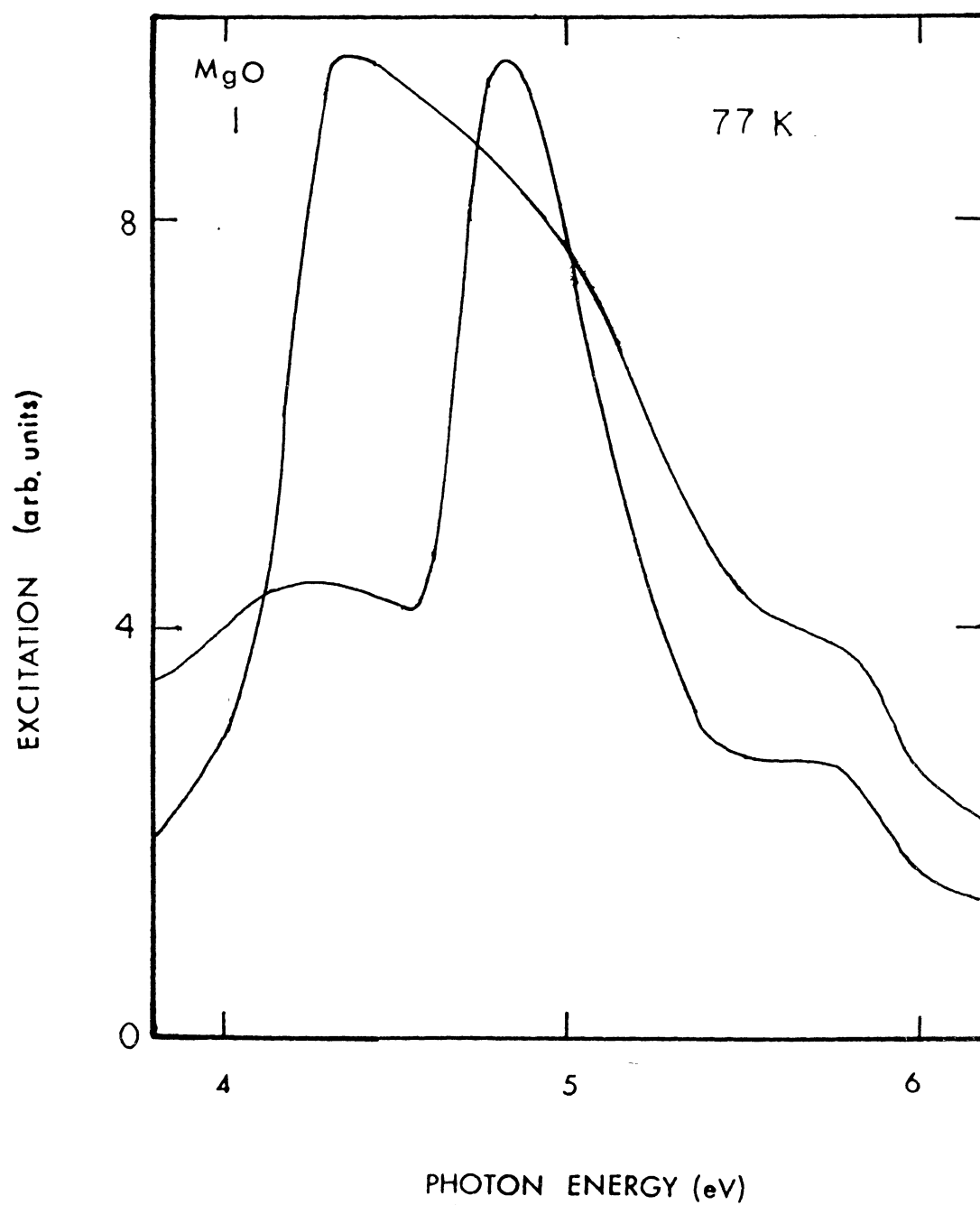


Figure 78. MgO 1, F and F+ Fast
Component Excitation

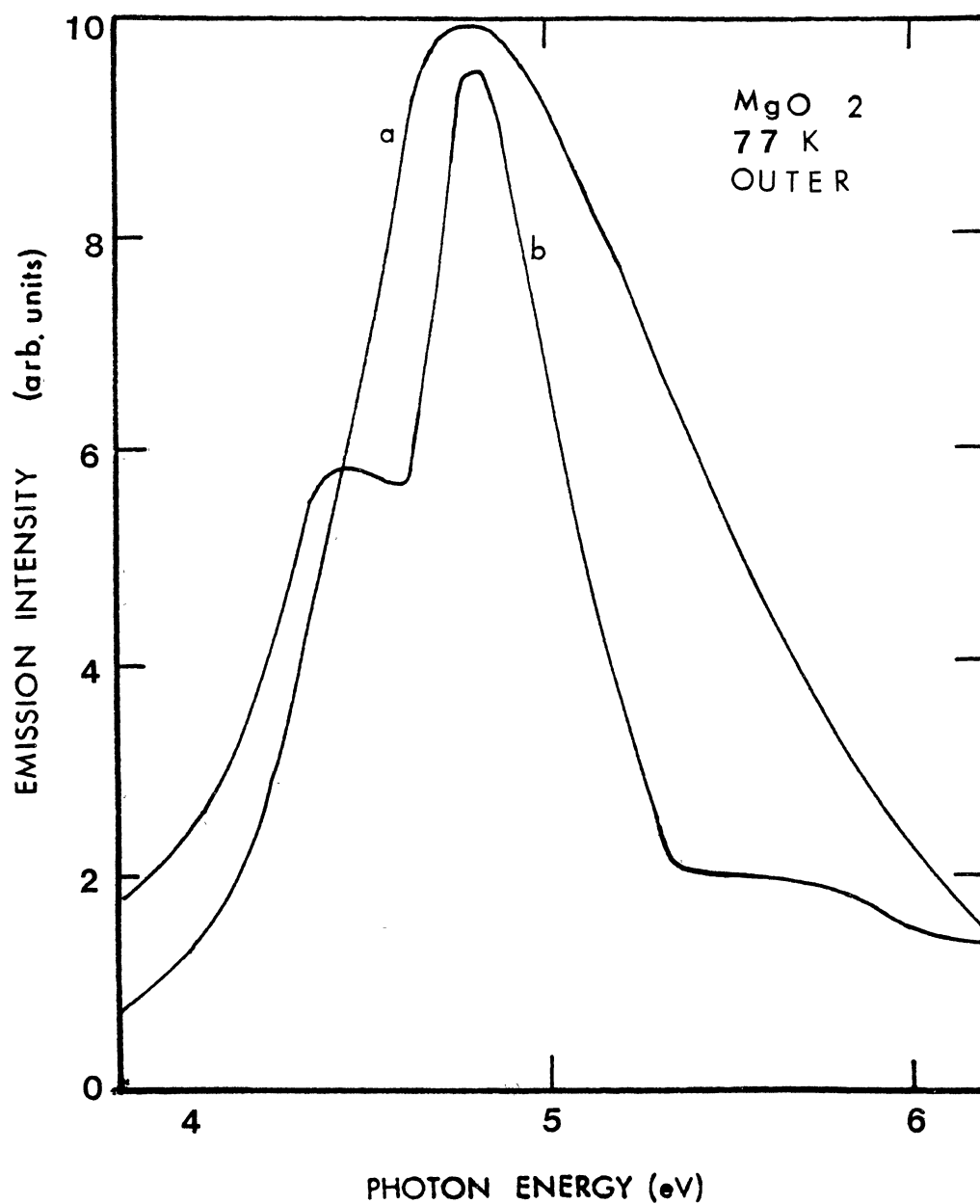


Figure 79. MgO 2, F+ Side Fast Component
Excitation. F emission, a.
F+ emission, b.

of crystal number two are shown in Figure 80. The F center emission curve is skewed with its peak at 4.6 eV and the F+ center shows only one peak with its center at 4.8 eV.

Figure 81 shows the spectrum for crystal number three. The detection system used a picoammeter and the monochromator's scan rate was set at 10 angstroms/minute. The single peak is centered at 5.0 eV and the phosphorescence caused a high energy tail. Its curve is not as skewed as that of number one. This the same excitation curve which is shown along with the photoluminescence curves for this crystal. Figure 82 shows the spectrum with lock-in detection at one kHz. The peak is shifted from 5.0 to 4.8 eV and a shoulder is present on the low energy side.

Figure 83 shows the curves for crystal number five. Both curves peak near 4.8 eV and are slightly skewed towards the low energy side. Figure 84 shows the Curves for the neutron irradiated crystal number seven. Both are also slightly skewed towards the low energy side and peak near 4.8 eV. Both show the presence of a peak at 5.8 eV and the F+ center emission curve shows the presence of a low energy peak. The curve for crystal number eight is shown in Figure 75 along with the photoluminescence. The peak is at 4.9 eV and is slightly skewed to the low energy side.

The low energy shoulder on the F+ center emission is relatively larger for the crystals with a large concentration of H⁻ ions. This is shown by looking at the relative magnitudes of the fluorescent lifetimes and at Table III.

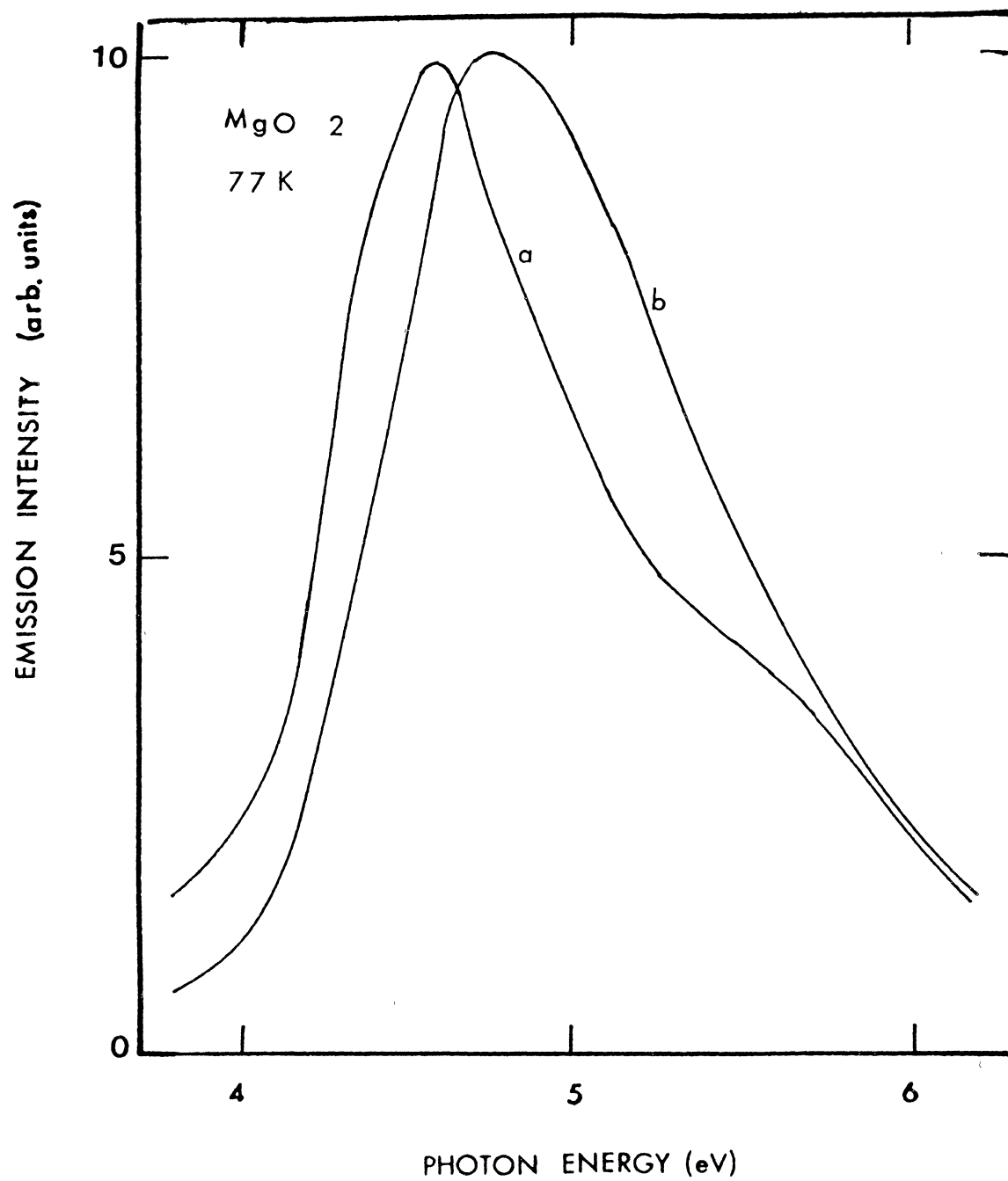


Figure 80. MgO 2, F Side Fast
Component Excitation

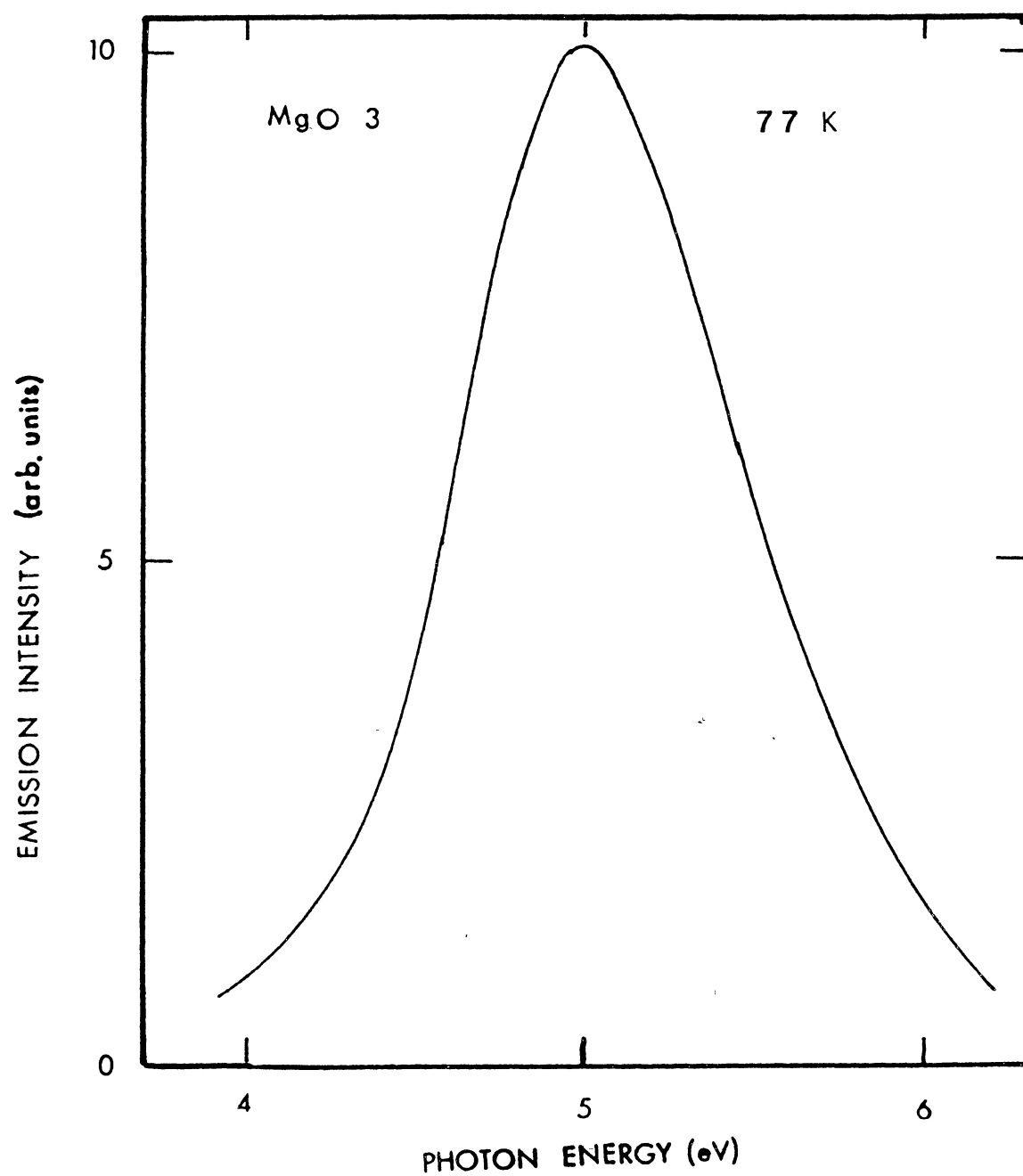


Figure 81. MgO 3 Total Excitation Spectrum

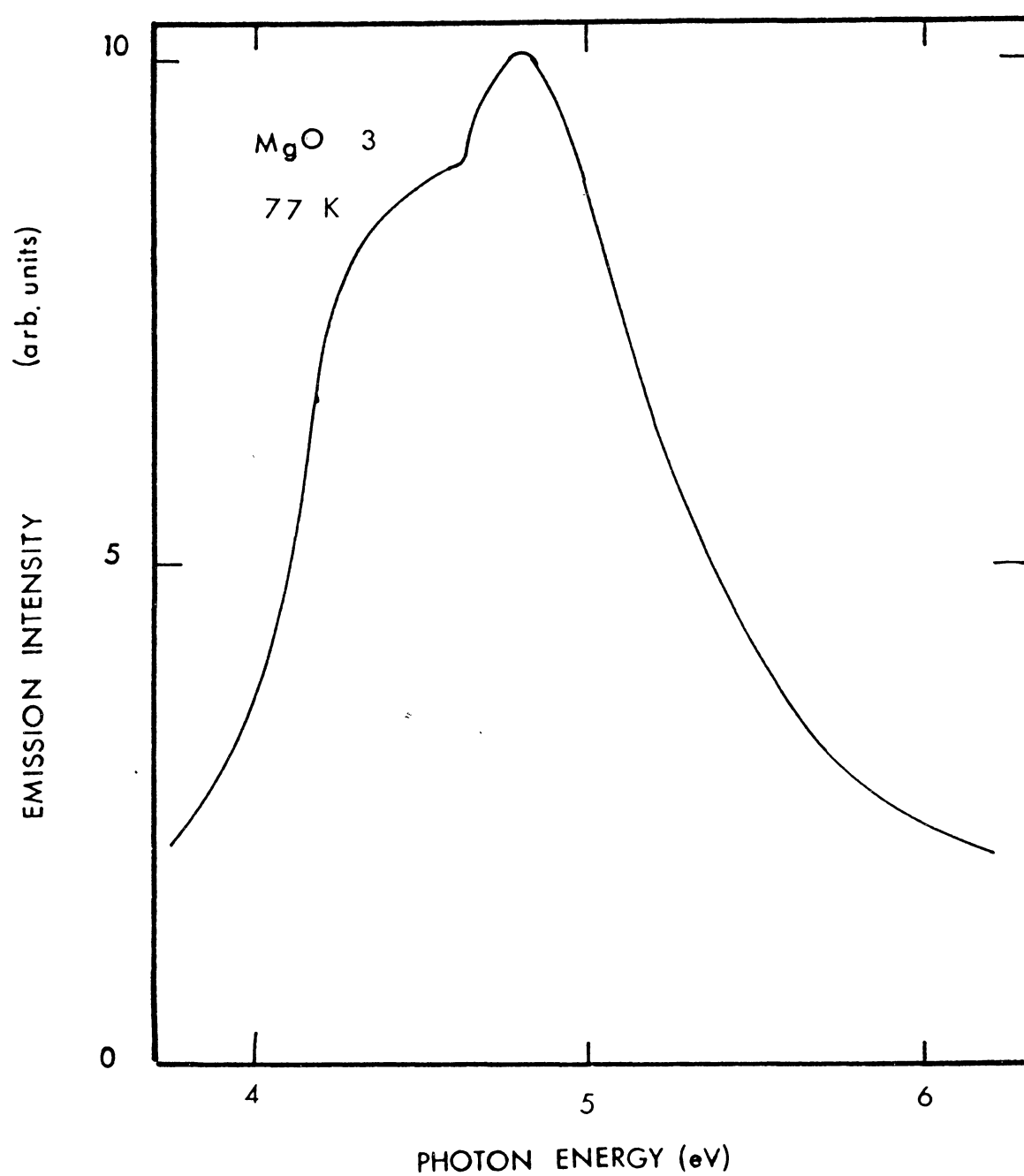


Figure 82. MgO 3 Total Fast
Component Excitation

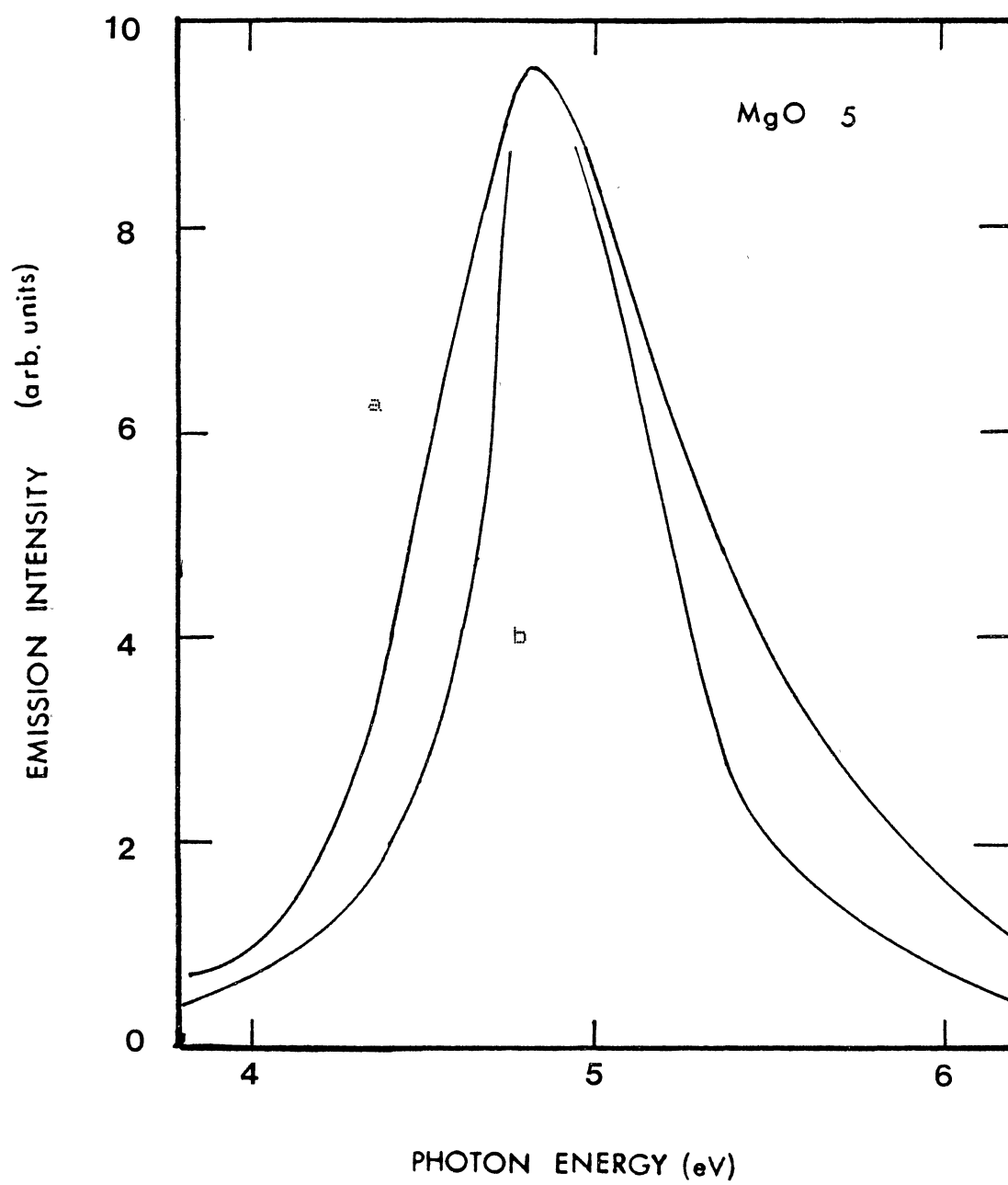


Figure 83. MgO 5 Fast Component Excitation

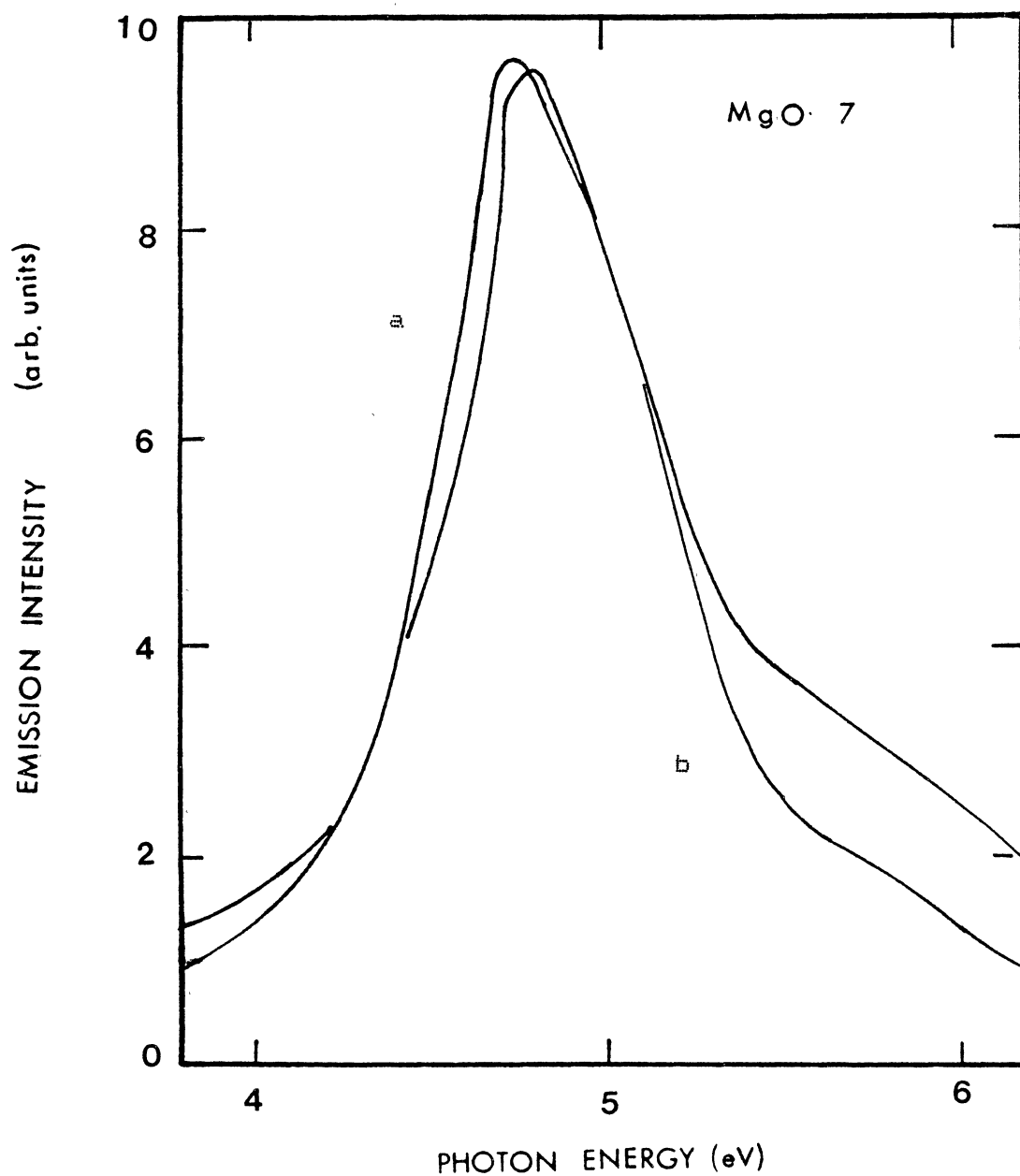


Figure 84. MgO 7 Fast Component
Excitation

The peak may cause the long lived lifetime seen in some of the crystals. The larger the peak the larger the number of electrons that will be released when the 254 nm interference filter is used to excite the F and F⁺ centers.

Photoconductivity

The photoconductivity was measured for crystals number seven and eight using the experimental set up detailed in Chapter III. A 300 volt battery was used making the electric field across the sample approximately 3000 volts/cm depending upon the thickness of the crystal. The crystal was always scanned from low to high energy.

Figure 85 shows the photoconductivity curves for the neutron irradiated crystal number seven after it had been irradiated for one minute with 1.0 MeV electrons at a current of 15 microamperes. At the initial temperature of 75 K the photoresponse curve shows a peak at 6.0 eV and a broad peak centered at approximately 5.0 eV. The photoresponse of the 6.0 eV peak decreased as the temperature increased while that of the 5.0 eV peak increased. The energy of the 5.0 peak decreased to approximately 4.7 eV at 180 K. The reading at 200 K showed a dramatic change as the photoresponse of the curve around 5.0 eV decreased while at 4.6 eV it increased. An identical experiment performed on this crystal before it was electron irradiated did not show this effect. Instead, the photoresponse increased over the range from 4.0 to 6.0 eV and a long lived photocurrent was evident

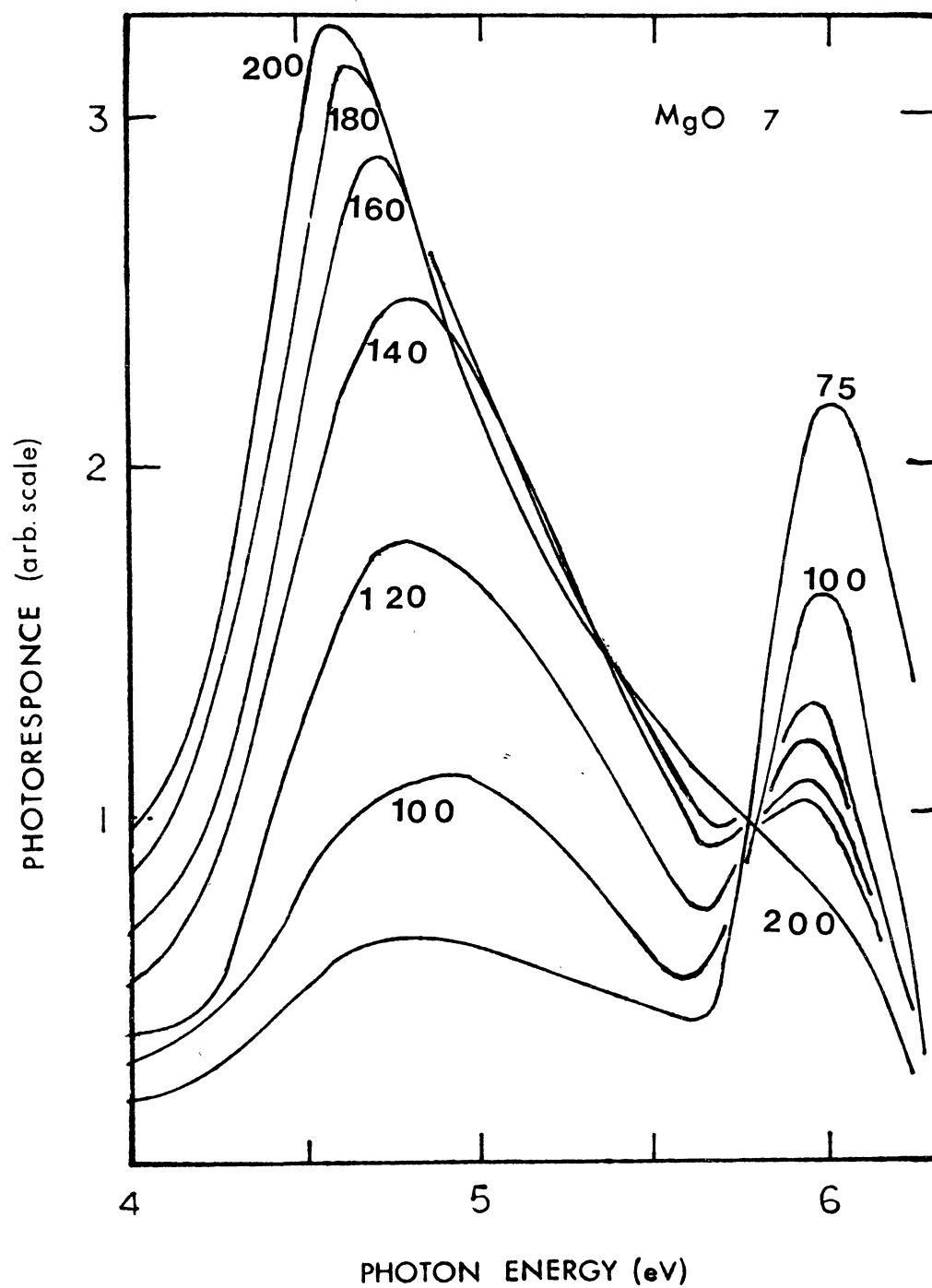


Figure 85. Temperature Dependent
Photoresponce, MgO 7

above 230 K. Also the electron irradiation increased the magnitude of the photoresponse in the crystal by a factor of approximately 3.5.

The crystal was electron irradiated again and the effect of bleaching on the photoresponse was checked at room temperature. Figure 86 shows the results. Curve a is the initial scan, b is the third, and c is the seventh. Each scan took three minutes and the electric field was applied between scans. Figure 87 shows the difference between curves a and c. It was found that bleaching with 5.4 eV light restores the original curve shape and subsequent bleaching with 4.6 eV light slightly decreases the 5.0 eV peak and increases the 4.6 eV peak.

It appears some interconversion may occur between the center responsible for the 4.6 eV peak and the F type centers at 5.0 eV, but they are not directly responsible for all of the effects seen above. The 4.6 eV peak may be contributing to the room temperature long lifetime effects seen in several of the crystals.

During the initial experiments on crystal number seven before it was electron irradiated, an increase in the dark current was noticed at high temperatures when the voltage across the crystal was turned on. This current rose immediately to a peak and then slowly decayed. At 295 K two percent of this long lived current was still evident after two hours. Figure 88 is the temperature dependent plot of this current versus the initial peak intensity and Figure 89

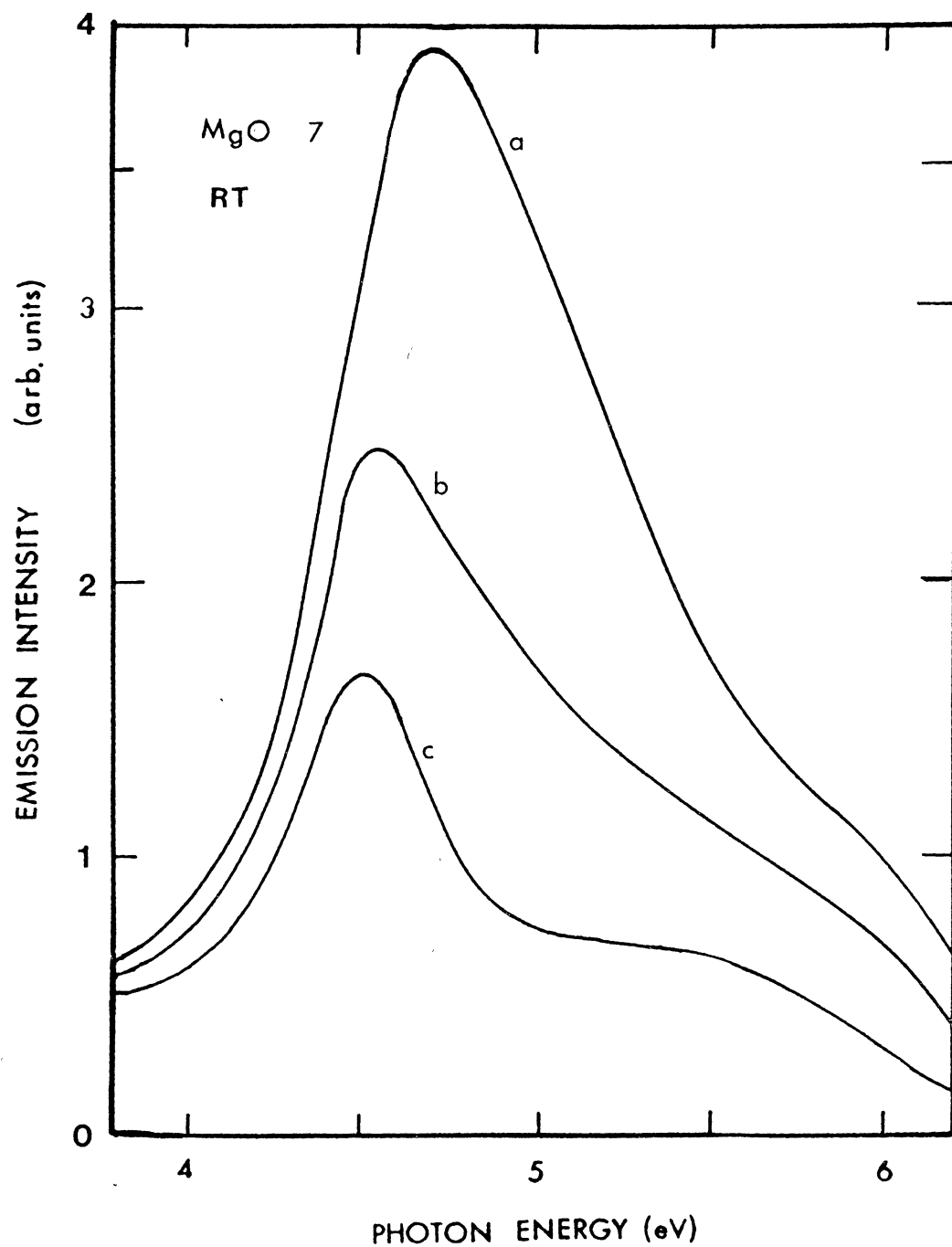


Figure 86. MgO 7 5.0 eV Photoresponce Bleach

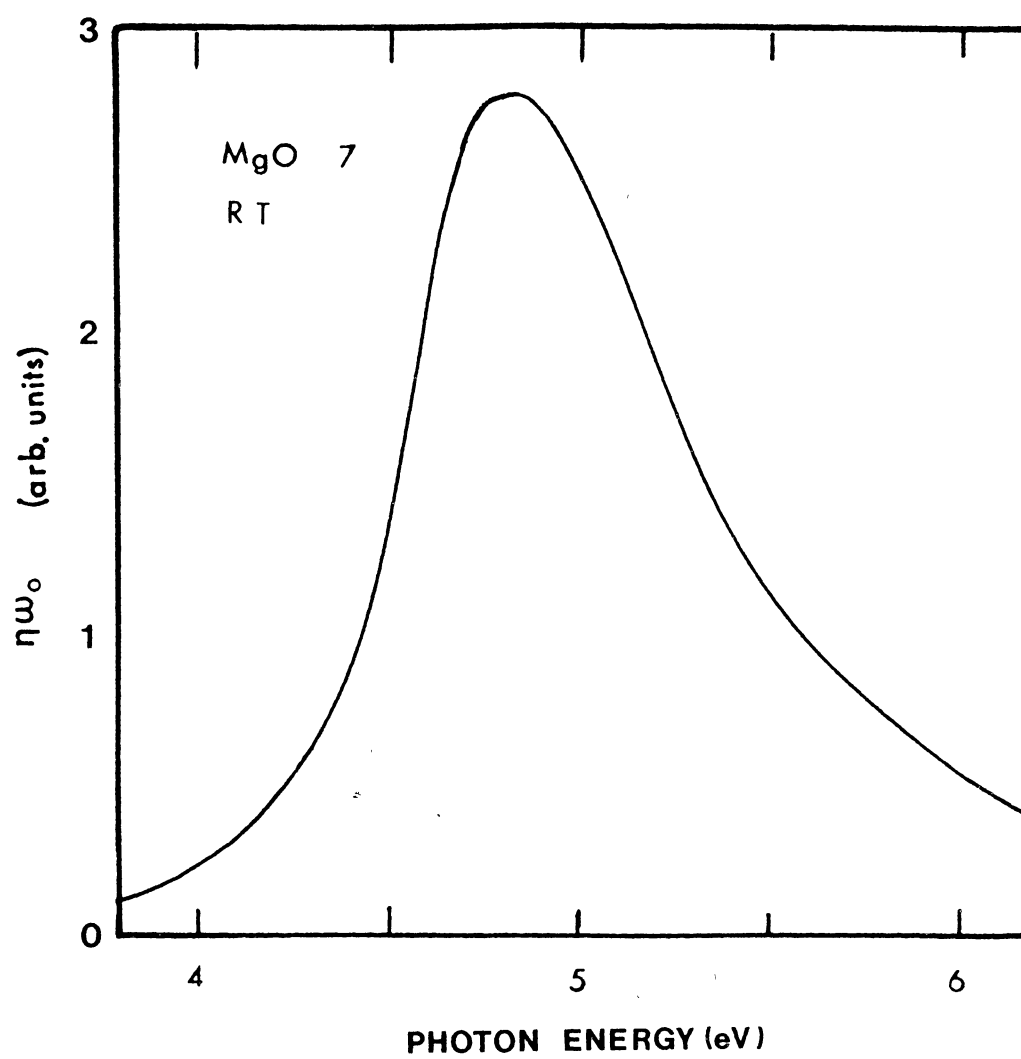


Figure 87. MgO 7 Bleached Component

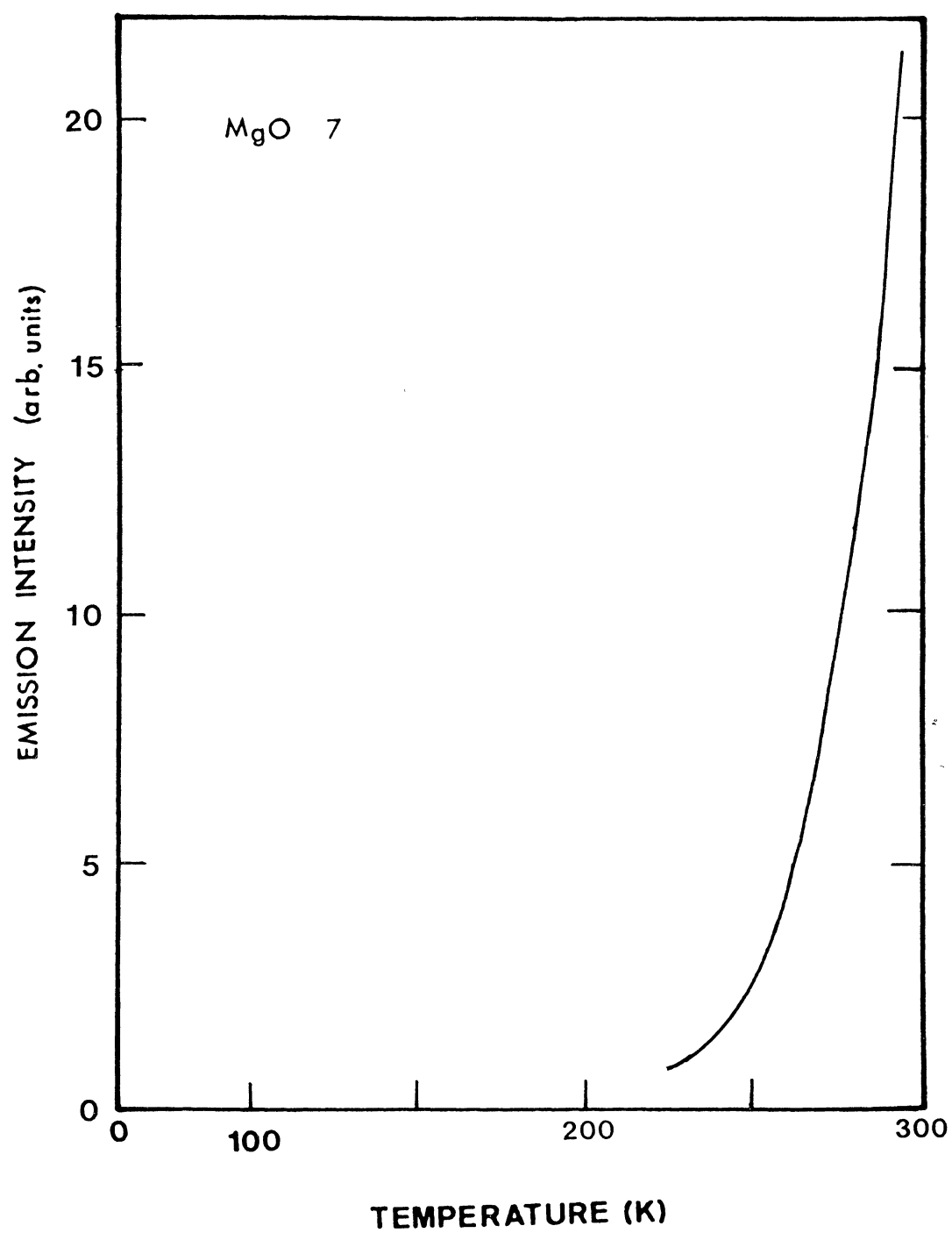


Figure 88. Dark Current, MgO 7

is a plot showing an associated thermal trap depth of approximately 0.30 eV. A check of this at 230 K after the crystal had been electron irradiated showed the effect was greatly enhanced. This effect is most likely a different trapping mechanism than the ones discussed above and may be responsible for the greatly enhanced photoresponse seen after the electron irradiation.

Figures 90 and 91 show the photoresponse curves for crystal number eight after it had been irradiated for one minute with 1.5 MeV electrons in a beam current of 15 microamperes. The 5.0 eV peak increases from 6 K to 140 K. It then decreases until 200 K and then increases. The only other peak is a 6.0 peak evident only up to 80 K. The initial dark current seen was comparable to that seen in the unirradiated crystal number seven. This experiment was repeated but the measurement at each temperature consisted of turning the voltage and light on until the photocurrent reached a maximum and then turning them off. The excitation system was set at 5.0 eV. The results are seen in Figure 92. The curve is a computer fit of the equation

$$\eta = \frac{1}{\tau_0 E + \tau_r \exp(-E/kT)} \quad (5.1)$$

The F⁺ centers vibrational frequency (1/ τ_0) was assumed to be 10^{12} Hz. This gave a radiative lifetime τ_r of 0.76×10^{-9} seconds and 0.076 eV as the depth of the excited state below the conduction band.

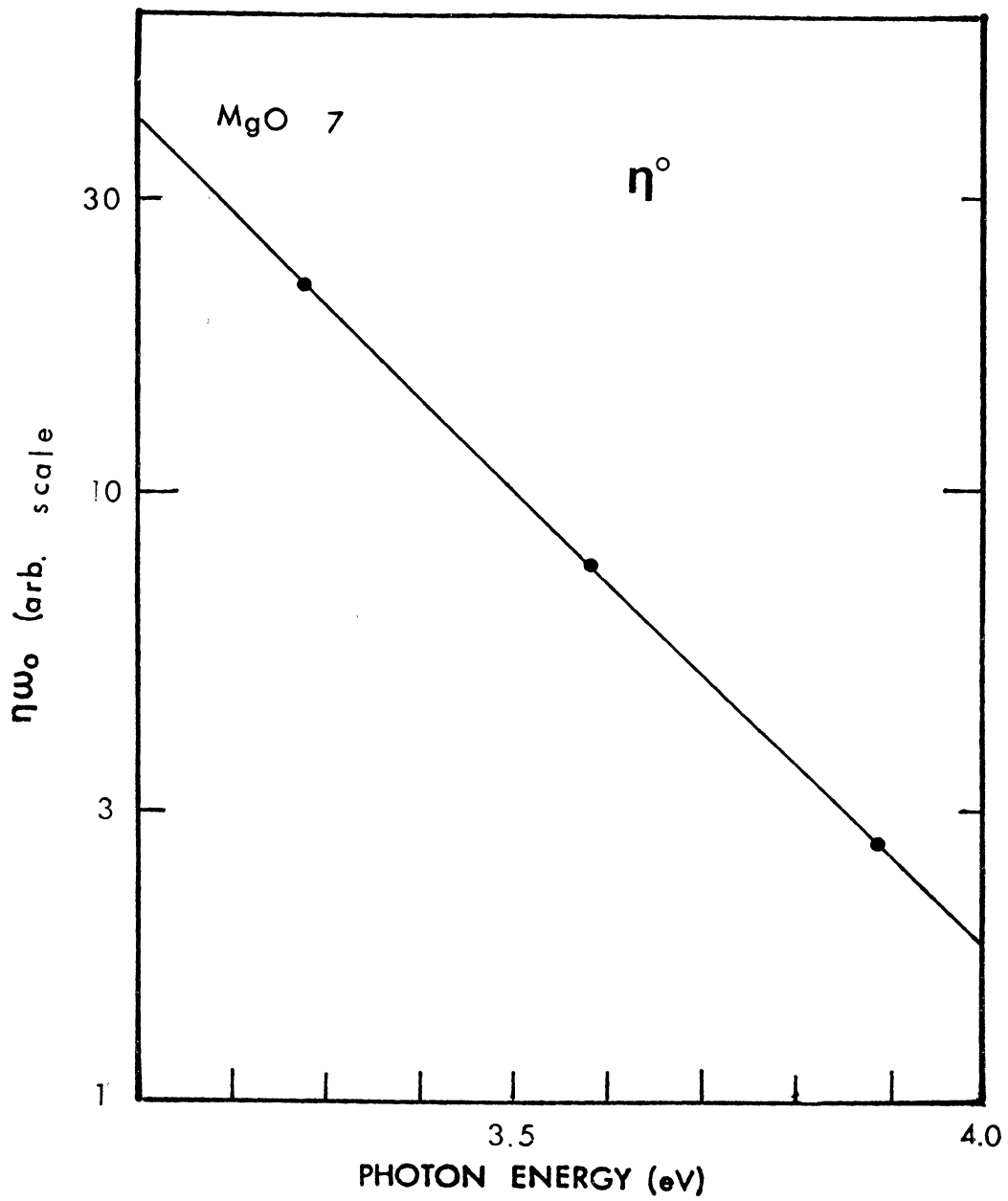


Figure 89. Dark Current Lifetime Plot

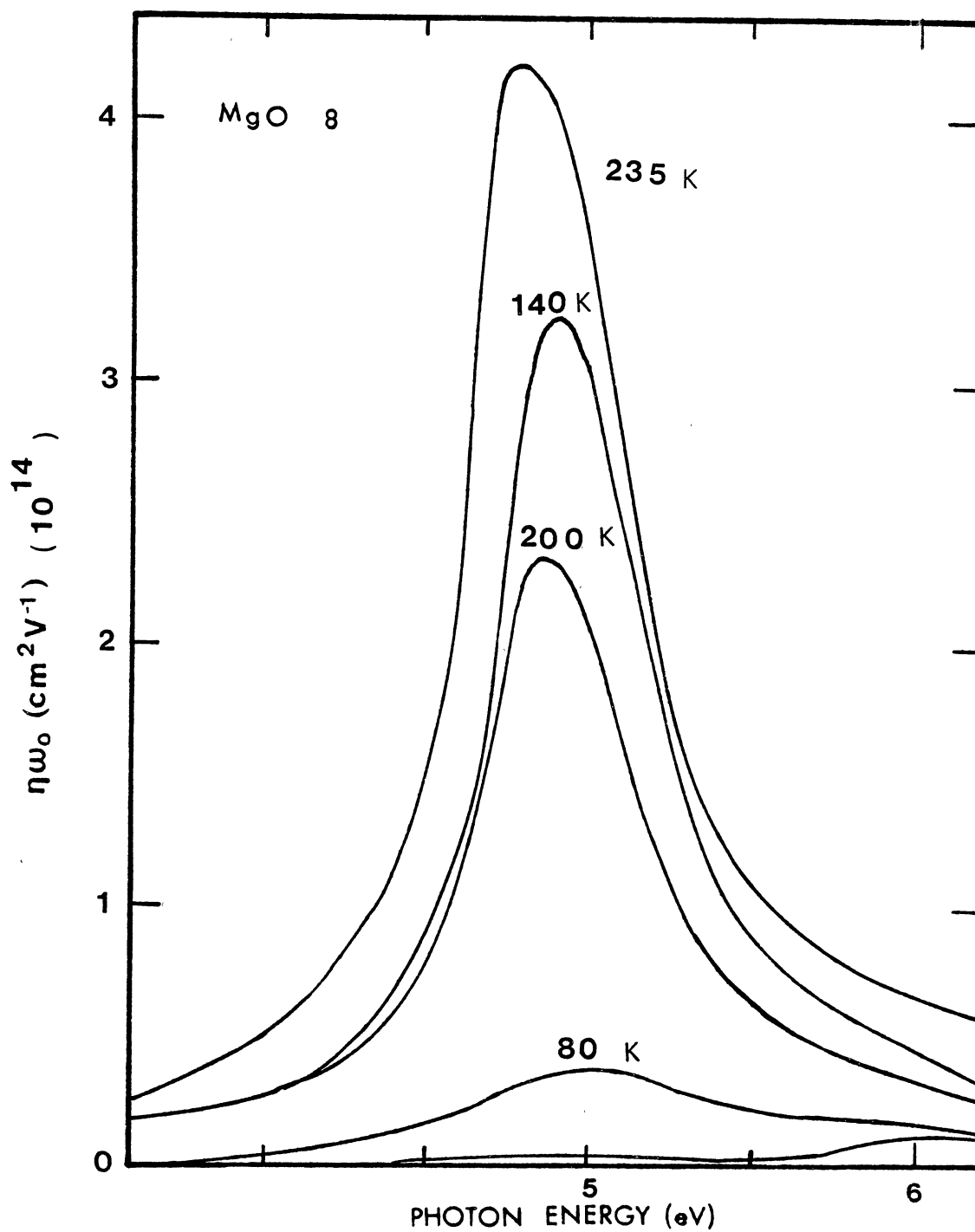


Figure 90. MgO 8, Temperature
Dependent Photoresponse

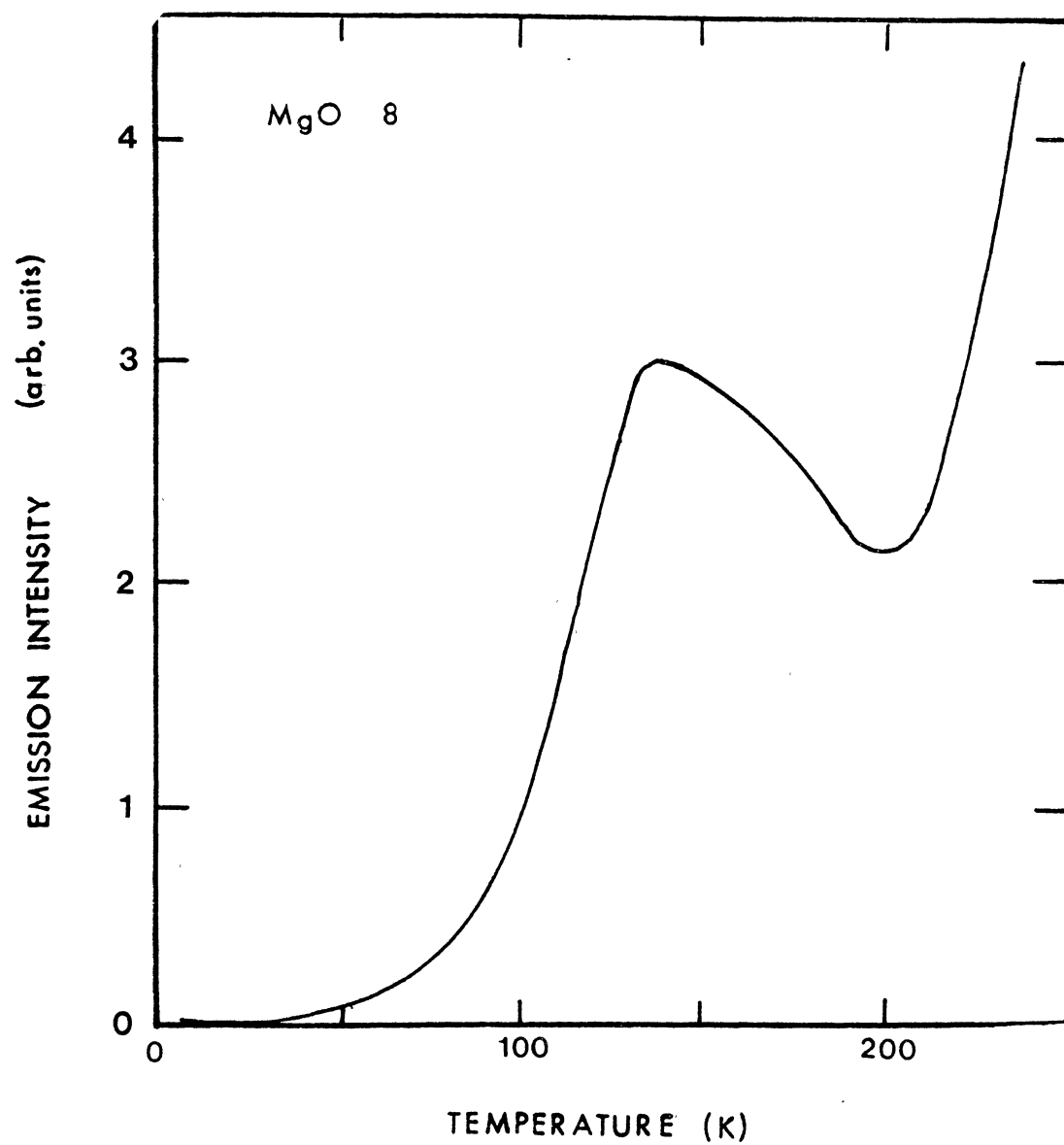


Figure 91. MgO 8, Temperature
Dependent Peak Height

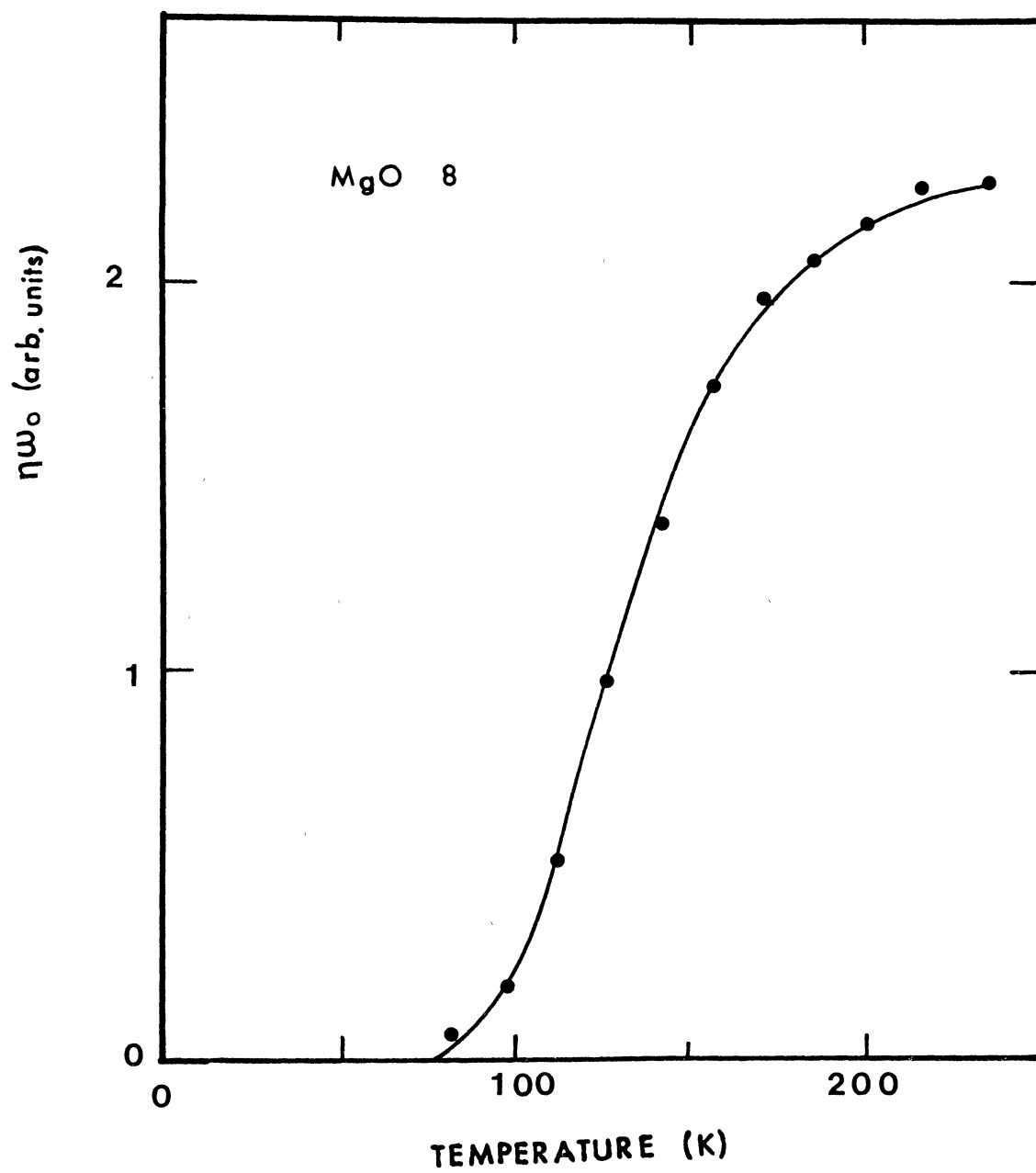


Figure 92. MgO 8, Temperature

Analysis and Discussion

The following section discusses the affect of the H^- ions upon the experimental results shown above and the current theoretical results.

The concentration of H^- ions located at oxygen vacancies is directly responsible for the long lived fluorescence lifetime of the F center near room temperature. This is shown by comparing the relative magnitudes of the H^- ions with the lifetimes for crystals one, three, and six. A like comparison of the concentration of the F centers with the lifetimes also shows that the these two properties are not related.

In crystals number one, three, and six the thermoluminescence peak at 260 K is more pronounced than in the other crystals and is responsible for the long lived phosphorescence seen at or near room temperature in these crystals.

A comparison of the H^- ion and F center concentrations with the fluorescence lifetimes for crystals one, three, and six shows that the longlifetime of the 2.3 eV emission at room temperature is due primarily to the concentration of H^- ions relative to the concentration of F centers and not to that of the F centers. This result is in contradiction to models involving interacting pairs of F centers as the cause of the long lifetime for F centers (17).

In three crystals the thermoluminescence peak at 260 K is also responsible for the phosphorescence seen at or

near room temperature. Thus, the traps causing this long lived phosphorescence are H^- ions. Since the magnitude of the thermoluminescence is not directly related to the concentration of the H^- ions but that of the F centers, it is caused by a combination of both. H^- ions alone cannot cause the 2.3 eV emission but F centers are required (17). This was found out from a crystal which had H^- ions present but no detectable F centers that showed no 2.3 emission.

The crystals with high concentrations of H^- ions, which showed the 260 K thermoluminescence peak, showed a different emission spectrum than those without the peak. Crystals one and three had predominately the 2.3 eV F center emission band. The intensity of both of these bands started increasing from the initial starting temperature of around 5 K. The F center band for crystal six started with a minimum intensity at the initial temperature of 84 K and increased until the final temperature of 294 K. Its comparable F^+ band intensity decreased over the same range. The above behavior along with the relatively large thermoluminescence at low temperatures for all three crystals implies that the electron in the relaxed optically accessible excited state can fairly easily be released into the conduction band. The one minute bleach of the crystal before the photoluminescence was measured at the initial temperature most likely produced the effect. The thermoluminescence peaked rapidly at 40 K and then decreased at least up to 150 K.

The theoretical model for MgO discussed in Chapter II

1
 predicts that the T_{1u} relaxed excited state from which the
 2.3 emission occurs lies very close to the bottom of the
 conduction band. The corresponding T_{1u} to A_{1g} transition
 from the excited state to the ground state should have a
 relatively short life time. There was some evidence from
 the emission caused by fast, approximately 10 ns, pulsed
 excitation that a short lived component with a lifetime of
 approximately 1 microsecond was present. This could be the
 intrinsic lifetime of the F center, ie. the lifetime of
 electrons that remain on the same F center. The observed
 phosphorescence at low temperatures, especially the emis-
 sion lasting several seconds in crystal three, plus the
 above mentioned photoluminescence and thermoluminescence
 results are not fully explained by the short lifetime but
 imply some other process is also involved.

Recent work by J. Tombrello et al. (30) more fully
 explains what is happening. They have shown that the H⁻ ion
 makes a very effective low temperature trap in MgO. It is
 doubly negatively charged and is very effectively formed by
 shining 400 nm light on the crystal. They also found that
 shining UV light on the crystal will destroy the traps.

The intensities of the low temperature thermolumines-
 cence peaks are not directly related to the magnitudes of
 the H⁻ ion or F center concentrations except that the two
 most intense peaks belong to crystals one and three. Also
 the intensity of the crystal six peak at 80 K places
 it above the others except for one and three. This informa-

tion plus that in the above paragraph implies that the H^- ion is most likely the trap responsible for the observed low temperature phosphorescence.

The low temperature thermoluminescence of crystals four, two, and five and the low temperature dependence of the photoluminescence of crystal five show that H^- ions are most likely present though in small amounts.

The interaction of the F centers with the H^- ions can be described using the model shown in Figure 93. An electron is excited from the A_{1g}^1 state to the T_{1u}^1 state by the absorption of a photon. There is then a high probability that the electron is released into the conduction band where it can then be trapped. In this figure we consider either trapping by an F center or by a H^- ion. Trapping by the H^- ion leaves an F^+ center and an H^{-2} ion (15). The activation energy of this trap is approximately 0.6 eV and is thermally stable up to a temperature of approximately 240 K. At low temperatures there are two possible ways to describe how the electrons get from the hydrogen trap to the F center. The first method comes from the description of the excited state orbitals of the F center and the H^- ion. Recent calculations have shown that for reasonably close F center- H^- ion pairs, an overlap exists between the excited state of the F center and an extended relaxed excited state of a H^{-2} ion (29). The electron is then able to tunnel from the H^{-2} ion to the empty excited state of the F center.

The second explanation is that the release of the

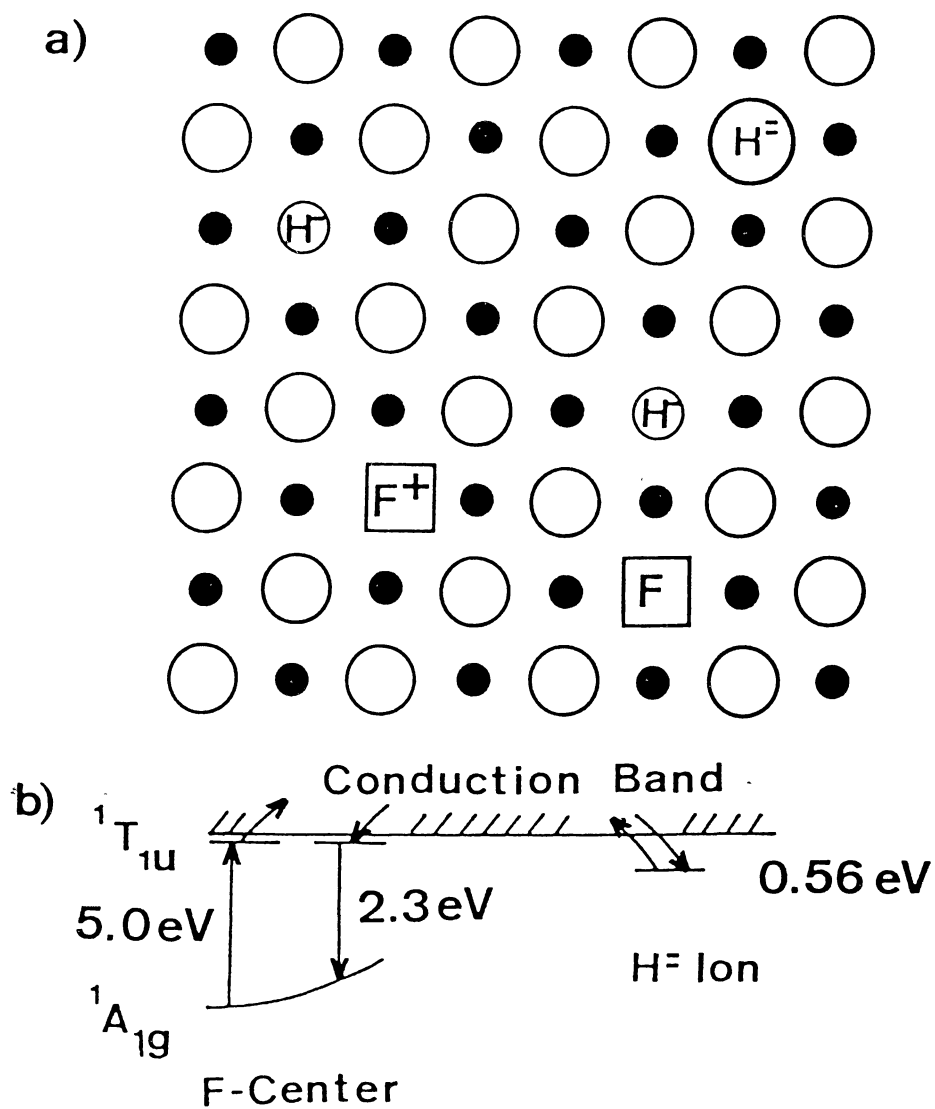


Figure 93. Model of F center and H^- ion Interaction

electron is from H^{-2} ions with a different configuration. There is evidence that the intensity of the three lines of the infrared spectrum of the H^{-} ion are not correlated (30) and that point group symmetries lower than O_h may be involved. This may be due to a local charge compensation effect and result in lower activation energies for release of the electron.

Neither of the two explanations can be shown to be preferable using our data. It appears that a relatively small phosphorescence near 80 K is present at 3.2 eV in crystals three and six but this may come from the high energy tip of the F center band being slightly measured at this energy.

The excitation spectrum for the fast component of the F center exhibits a low energy skew that is present in crystals one, two, and three. These are the samples with the the highest H^{-} ion concentration. For those samples with low H^{-} ion concentration as determined from their glow curves, the excitation spectrum are narrower though still slightly skewed. The shape of the F and F+ center curves also become nearly the same. For the F+ center excitation spectrum the 4.5 eV band is evident in only three crystals. They are crystal one, the F+ center side of crystal two, and crystal seven.

The only other occurrence of this is the 4.5 eV photoconductivity peak of crystal seven. The increase in photo-response of both peaks in this crystal most likely is caused

by the rapid increase of their quantum efficiency. The only occurrence of interaction between the 4.5 and 5.0 eV bands is when at room temperature, the crystal was bleached with 4.6 eV light and the 4.5 band's photoresponse increased while the 5.0 eV band's decreased. In contrast to this, bleaching by scanning the spectrum at room temperature showed no change in the 4.5 eV peak but partially bleached out the 5.0 eV peak. The 4.5 peak has not been identified but the dark current seen may be caused by the presence of the H^- ion because of its initial increase around 250 K. Why electron irradiation caused it to start at a lower temperature and why the activation energy was no larger than 0.3 eV is not understood if it is due to the H^- ion.

The experimental data collected on crystal eight shows only the F^+ center luminescence. The electron in the relaxed excited state can be thermally excited into the conduction band at approximately 80 K. This is shown in both the photoluminescence and photoconductivity experiments. The photoresponse curve in Figure 91 shows bleaching out of the 5.0 eV band occurs above 140 K. From Figure 92, the radiative lifetime is calculated to be 0.8 nanoseconds and the thermal activation energy is found to be 0.0756 eV. This calculation assumes an F center local vibrational frequency of 10^{12} Hz. According to Choi and Takeuchi (24) hole motion would be measured during photoconductivity.

BIBLIOGRAPHY

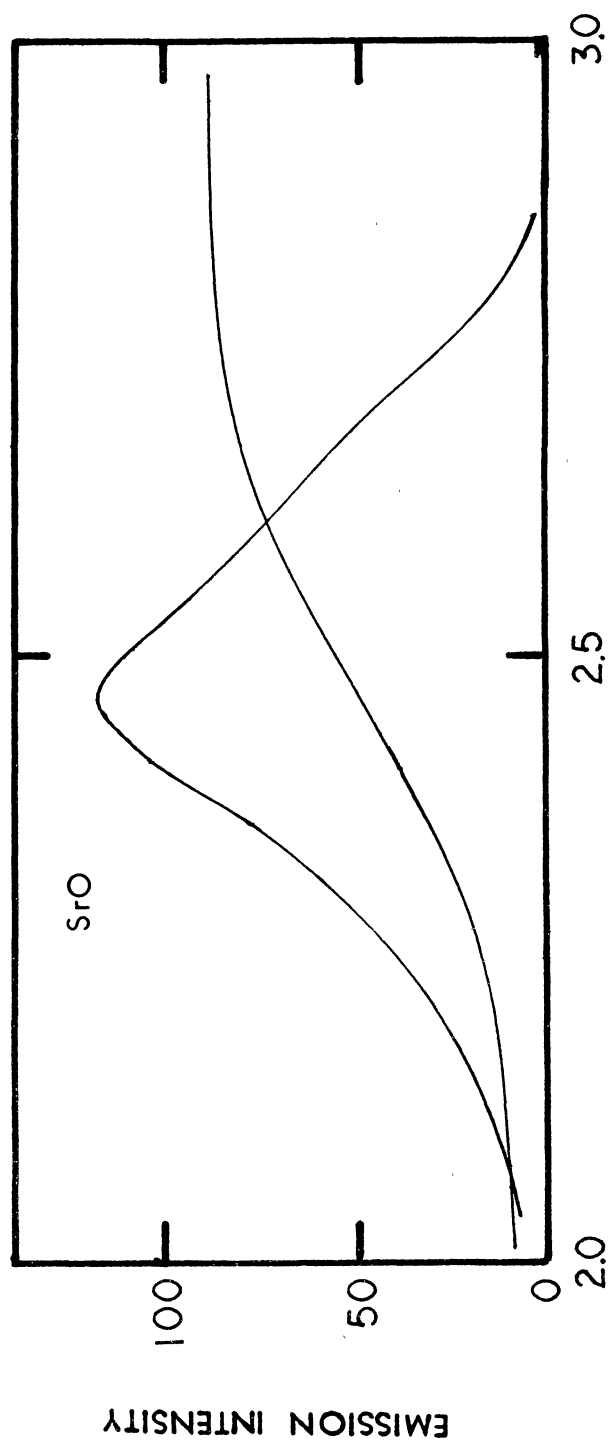
1. Arnold, G. W., and W. D. Compton, Phys. Rev. Lett. 4, 66 (1960).
2. Pells, G. P., U.K.A.E.A. Harwell Publication, AERE-R 9359 (1979).
3. Turner, T. J., and J. H. Crawford, Solid State Comm. 17, 167 (1975).
4. Turner, T. J., and J. H. Crawford, Phys. Rev. B 13, 1736 (1976).
5. Lee, K. H., and J. H. Crawford, Jr., Phys. Rev. B 15, 4065 (1977).
6. Draeger, B. G., and G. P. Summers, Phys. Rev. B 19, 1172 (1979).
7. La, S. V., R. H. Bartram, and R. T. Cox, J. Phys. Chem. Solids 34, 1079 (1973).
8. Evans, B. D., and M. Stapelbroek, Phys. Rev. B 18, 7089 (1978).
9. Lehman, H. W., and H. H. Gunthard, J. Phys. Chem. Solids 25, 941 (1964).
10. Brewer, J. D., B. T. Jeffries, and G. P. Summers, Phys. Rev. B 19, 4900 (1980).
11. Henderson, B. and R. D. King, Phil. Mag. 13, 1149 (1966).
12. Chen, Y., W. A. Sibley, F. D. Srygley, R. A. Weeks, E. B. Hensley and R. L. Dries, J. Phys. Chem. Solids 29, 863 (1968).
13. Wertz, J. E., P. Auzins, R. A. Weeks and R. H. Selsbee, Phys. Rev. 107, 1535 (1957).
14. Hughes, A. E. and B. Henderson, In Point Defects in Solids, edited by J. H. Crawford and L. M. Slifkin (Plenum, New York, 1972).

15. Summers, G. P., T. M. Wilson, B. T. Jeffries, H. T. Tover, Y. Chen and M. M. Abraham, Phys. Rev. B 27, 1283 (1983).
16. Wilson, T. M. and R. F. Wood, J. Phys. (Paris) Colloq. 37, C7-190 (1976).
17. Edel, P., B. Henderson, Y. Merle d'Aubigne, R. Romenstain and L. Kappers, J. Phys. C 12, 5245 (1979).
18. Gonzalez, R., Y. Chen and Mark Mostoller, Phys. Rev. B 24, 6862 (1981).
19. Fowler, W. B., In Physics of Color Centers, edited by W. B. Fowler (Academic Press, New York, 1968).
20. Fitchen, D. B., In Physics of Color Centers, edited by W. B. Fowler (Academic Press, New York, 1968).
21. Brown, F. C., The Physics of Solids, (W. A. Benjamin, Inc., New York, 1967).
22. Van Heyingen, R. S. and F. C. Brown, Phys. Rev. 121, 1303 (1961).
23. Edel, B. Henderson, and R. Romestain, J. Phys. C 15, 1569 (1982).
24. Choi, S. and T. Takeuchi, Phys. Rev. Lett. 50, 1474 (1983).
25. Kellan, M., private communication (1985).
26. Brewer, J. D., "An Experimental Investigation of Low Temperature Fluorescence in Sapphire" (Unpublished M.S. Thesis, Oklahoma State University, 1978).
27. Summers, G. P., private communication (1985).
28. Jeffries, B. T., J. D. Brewer and G. P. Summers. Phys. Rev. B 24, 6074 (1981).
29. Engston, H., J. B. Bates, J. C. Wang and M. M. Abraham, Phys. Rev. B 21, 1520 (1980).
30. Tombrello, J., H. T. Tover, Y. Chen and T. M. Wilson, Phys. Rev. B 30, 7374 (1984).

APPENDIX

SrO

A thermoluminescence peak at 90 K was measured for neutron irradiated SrO. Figure 89 shows the result of measuring the spectral dependence of the peak. Curve a is the photoluminescence curve for the F+ center. Curve b shows the percent of light passed by several different cut-off filters which were inserted between the crystal and the photomultiplier tube. Curve b is a plot of the energy of the light the filters would pass at 45 percent of their transmittance. The curve definitely shows that the emission is from an F+ center. This could mean that the bare oxygen vacancy does exist in SrO if the trap responsible for the TL frees electrons.



PHOTON ENERGY (eV)

Figure 94. SrO TL Peak Spectral Dependence

VITA 2

Bryce Todd Jeffries

Candidate for the Degree of

Doctor of Philosophy

Thesis: AN EXPERIMENTAL INVESTIGATION OF POINT DEFECTS AND
MOTION OF CHARGE IN Al_2O_3 , MgO , and SrO .

2 3

Major Field: Physics

Biographical:

Personal Data: Born in Wichita, Kansas, May 20, 1948,
the son of Mr. and Mrs. Milo Jeffries.

Education: Graduated from Cheney High School, Cheney,
Kansas, May 1966; attended Kansas University,
Lawrence, Kansas, September, 1966, to May, 1969;
Central State University, Edmond, Oklahoma, Sep-
tember, 1974, to December, 1976, Bachelor of
Science, Physics; Oklahoma State University,
Stillwater, Oklahoma, January, 1977, to December,
1979, Master of Science, Physics; January, 1980,
to May, 1985, Doctor of Philosophy, Physics.

Professional Experience: Graduate teaching assistant
spring semester of 1977; maintained Model AN2000
van de Graaf Accelerator, June, 1977, to June,
1978; graduate research assistant, July, 1978, to
August, 1981; teaching assistant, September, 1981,
to December, 1981; flow measurement specialist,
Conoco, Ponca City, Oklahoma, February, 1982, to
present.